Universidade de Lisboa

Faculdade de Ciências

Departamento de Engenharia Geográfica, Geofísica e Energia

Global land-atmosphere coupling associated with cold climate processes

Emanuel Dutra

Doutoramento em Ciências Geofísicas e da Geoinformação
(Meteorologia)

Tese Orientada por:
Prof. Doutor Pedro Miranda
Prof. Doutor Christoph Schär

2011

Contents

Acknowledgments

I am deeply grateful to all the people who accompanied me in these last years for their support, encouragement, sympathy, friendship, love, drinks, parties and other exotics matters.

I would like to acknowledge my doctoral advisors Pedro Miranda, Pedro Viterbo and Christoph Schär for their scientific advice and support throughout my doctoral work. I am in debt to Pedro Miranda and Pedro Viterbo for the opportunity to progress with my scientific work, since my time as undergraduate student, and also for their constant scientific inspiration and friendship. I thank Christoph Schär for the warm welcome into his research group and for his scientific guidance. A special thank you goes to Gianpaolo Balsamo for all his support and for receiving me at ECMWF in two periods during my thesis development. I also thank Anton Beljaars, Victor Stepanenko, Dmitrii Mironov, and Sven Kotlarski, for the collaborative work and encouragement.

The work hereby presented was carried out at the Centro de Geofísica da Universidade de Lisboa in the Faculty of Sciences of the University of Lisbon and at the Institute for Atmospheric and Climate Science at ETH Zurich. In both institutions I received all the administrative, technical and financial support I could possibly need. Most importantly, my friends and colleagues in both institutes were fundamental both scientifically and personally. I am grateful to all of them, including Ricado Tomé, João Martins, Maria João Rocha, Sandra Gomes, José Alves, Rita Cardoso, Pedro Soares, Ricardo Trigo, Martin Wild, Paulo Oliveira and many other former and present colleagues.

This work was supported by the Portuguese Foundation for Science and Technology (FCT) under grant SFRH/BD/35789/2007 and Fundação Calouste Gulbenkian.

Apenas foi possível chegar aqui graças ao apoio constante, mesmo à distância, da minha família. Aos meus pais, irmão, Gracinda, e Daniela, que desde sempre me apoiaram, mesmo quando isso implicou a minha ida para Lisboa. Estiveram e estarão sempre presentes. Aos pais da Carina, Celeste e António pela forma com me receberam na família e por todo o apoio. Dedico este trabalho à Carina pelo seu amor e compreensão.

Abstract

This dissertation constitutes an assessment of the role of cold processes, associated with snow cover, in controlling the land-atmosphere coupling. The work was based on model simulations, including offline simulations with the land surface model HTESSEL, and coupled atmosphere simulations with the EC-EARTH climate model. A revised snow scheme was developed and tested in HTESSEL and EC-EARTH. The snow scheme is currently operational at the European Centre for Medium-Range Weather Forecasts integrated forecast system, and in the default configuration of EC-EARTH. The improved representation of the snowpack dynamics in HTESSEL resulted in improvements in the near surface temperature simulations of EC-EARTH. The new snow scheme development was complemented with the option of multi-layer version that showed its potential in modeling thick snowpacks. A key process was the snow thermal insulation that led to significant improvements of the surface water and energy balance components. Similar findings were observed when coupling the snow scheme to lake ice, where lake ice duration was significantly improved. An assessment on the snow cover sensitivity to horizontal resolution, parameterizations and atmospheric forcing within HTESSEL highlighted the role of the atmospheric forcing accuracy and snowpack parameterizations in detriment of horizontal resolution over flat regions. A set of experiments with and without free snow evolution was carried out with EC-EARTH to assess the impact of the interannual variability of snow cover on near surface and soil temperatures. It was found that snow cover interannual variability explained up to 60% of the total interannual variability of near surface temperature over snow covered regions. Although these findings are model dependent, the results showed consistency with previously published work. Furthermore, the detailed validation of the snow dynamics simulations in HTESSEL and EC-EARTH guarantees consistency of the results.

KEYWORDS: snow, lakes, land surface, climate model, Land-atmosphere coupling,

Resumo

A criosfera representa todas as formas de água no estado sólido sobre a superfície terrestre. Estas incluem a cobertura de neve sazonal, solo gelado, glaciares, calotes polares, lagos e rios gelados e gelo oceânico. Devido às suas particularidades térmicas e ampla cobertura da superfície terrestre, os processos físicos associados à criosfera desempenham um papel fundamental no sistema climático. Por outro lado, espera-se que o aumento da concentração de gases com efeito de estufa tenha um impacto significativo na criosfera. Um destes impactos está relacionado com a possível amplificação do sinal das mudanças climáticas devido a processos de realimentação positivos (Flanner et al. 2011). Estas mudanças influenciam o sistema climático, com implicações na sociedade, em especial nos recursos hídricos (Immerzeel et al. 2010; Molini et al. 2011).

O papel da cobertura de neve no sistema climático é um tópico de investigação com um longo percurso. Uma das primeiras campanhas observacionais remonta a 1935, tendo sido conduzida por Sverdrup. No domínio da modelação numérica da atmosfera, Williams (1975) realizou um dos estudos pioneiros sobre a influência da cobertura de neve na circulação atmosférica. A cobertura de neve sazonal é caracterizada por uma elevada variabilidade espacial e temporal. A importância da cobertura de neve sazonal para os sistemas de previsão numérica do tempo e clima é justificada pela sua extensão, variabilidade, bem como pelo papel no controlo dos fluxos de energia e água junto à superfície terrestre. Este controlo justifica também a relação entre a temperatura do ar junto à superfície e a presença ou ausência de cobertura de neve (Armstrong and Brun 2008). Por exemplo, a cobertura de neve sobre a Eurásia foi associada à variabilidade da Monção na Índia (Douville and Royer 1996; Peings and Douville 2010; Robock et al. 2003), bem como a alterações na circulação atmosférica em todo o Hemisfério Norte (Fletcher et al. 2009b; Gong et al. 2007). É de notar que a cobertura de neve também constitui um importante reservatório de água doce que, ao ser libertado durante a Primavera, influencia o escoamento à superfície, a humidade do solo, a evaporação e por conseguinte todo o ciclo da água à superfície (Douville et al. 2002; Groisman et al. 2004). É, portanto, crucial que os modelos numéricos de previsão do tempo e clima incluam uma formulação correcta da massa e densidade do manto de neve. Estes dois parâmetros governam a forma como o isolamento térmico da superfície é representado nos modelos (Cook et al. 2008). Este processo tem um papel importante em cenários de mudanças climáticas, com consequências directas na evolução das características hidrológicas e térmicas da superfície terrestre (Bartlett et al. 2004, 2005; Stieglitz and Smerdon 2007). O isolamento térmico da cobertura de neve influencia ainda a camada limite atmosférica (Viterbo et al. 1999), bem como a evolução do gelo sob os lagos (Dutra et al. 2010b).

Esta dissertação procura avaliar o papel dos processos físicos à superfície associados à cobertura de neve no controlo do acoplamento terra-atmosfera. Este trabalho foi baseado maioritariamente em simulações numéricas, incluindo simulações com o modelo de superfície HTESSEL (Balsamo et al. 2009) em modo offline, e simulações atmosféricas com o modelo de clima EC-EARTH (Hazeleger et al. 2010). Numa fase inicial do trabalho, foram encontradas algumas limitações na representação da cobertura de neve pelos modelos. Uma vez que a avaliação do controlo da cobertura de neve no acoplamento terra-atmosfera está dependente da representação realista dos seus processos físicos nos modelos numéricos, procedeu-se a uma revisão prévia das parametrizações associadas à cobertura de neve nos modelos. A partir desta revisão desenvolveu-se uma nova formulação para a representação

da cobertura de neve, tendo esta sido testada nos modelos HTESSEL e EC-EARTH e mais tarde incorporada no modelo de previsão numérica do tempo operacional do Centro Europeu de previsão do tempo a médio prazo (ECMWF), bem como na configuração padrão do EC-EARTH. A nova formulação revelou-se especialmente eficaz na representação do isolamento térmico da superfície pela neve, resultando em melhorias significativas nas simulações dos vários componentes dos balanços de energia e água à superfície (em particular a radiação solar absorvida e escoamento superficial). Nas simulações climáticas com o modelo EC-EARTH, o isolamento térmico da cobertura de neve resultou no aumento das temperaturas do solo durante o Inverno e Primavera. Consequentemente, observou-se uma redução da fracção de solo congelado, acompanhada por um aumento da infiltração de água no solo em detrimento do escoamento superficial. O aumento da quantidade de água no solo durante o final da Primavera e Verão resultou por sua vez no aumento da taxa de evaporação, da humidade relativa na troposfera e consequentemente da precipitação. Observou-se ainda que esta sequência de processos é desencadeada durante o Inverno com impactos no Verão. Estes resultados revelam a importância da cobertura de neve, e da sua representação, em modelos de clima. A formulação desenvolvida conduziu também ao aumento da eficácia do isolamento térmico da superfície pelo manto de neve, reduzindo, nas simulações climáticas efectuadas, o viés positivo da temperatura do ar sobre regiões cobertas de neve. Por último, desenvolveu-se ainda uma formulação mais detalhada para o manto de neve. Esta nova formulação, incluindo várias camadas, veio colmatar os problemas da representação do manto de neve com apenas uma camada, tendo as simulações efectuadas mostrado o seu potencial na representação de mantos de neve espessos. Simulações climáticas com esta nova parametrização realçaram o isolamento térmico da superfície pelo manto de neve, mais eficiente quando várias camadas são representadas.

Foi também estudada a importância do isolamento térmico da cobertura de neve sobre os lagos gelados também foi estudada. Para tal, foi implementado e validado um modelo de lagos no HTESSEL em modo offline, numa escala global. Apesar das limitações decorrentes do uso de simulações offline (os fluxos de superfície não alteram os campos atmosféricos), o modelo teve um bom desempenho, quando comparado com observações. Uma das vantagens da implementação técnica do modelo de lagos no HTESSEL consistiu na representação dos lagos de subescala. Esta reveste-se de particular importância para as aplicações de clima, onde a resolução horizontal típica (cerca de 100 km), não permite a representação da maioria dos lagos. Nas latitudes elevadas, a introdução da representação dos lagos de subescala modificou o ciclo anual médio de armazenamento de energia na superfície, com um aumento durante o Verão e posterior libertação durante o Outono. Por outro lado, nas regiões equatoriais, observou-se uma alteração na partição dos fluxos de energia para a atmosfera, traduzida por um aumento dos fluxos de calor latente e redução dos fluxos de calor sensível. Estes resultados comprovam a importância das massas de água continentais no controlo do balanço energético da superfície terrestre, amplamente negligenciadas na maioria dos modelos de superfície. A parametrização da cobertura de neve no HTESSEL foi acoplada à evolução do gelo nos lados. Este acoplamento levou a uma melhoria das simulações da duração do gelo nos lagos, bem como a uma evolução semelhante do gelo nos lagos e do gelo nos solos, em regiões próximas. Estes resultados, semelhantes ao impacto do manto de neve na evolução da temperatura do solo, demonstram a importância do isolamento térmico da superfície terrestre pela cobertura de neve.

Na sequência do desenvolvimento da nova parametrização para o manto de neve, procurou-se avaliar a sensibilidade das simulações em relação à resolução horizontal, parametrizações e campos

atmosféricos prescritos. Foram assim efectuadas simulações offline com o modelo HTESSEL forçado pelas previsões meteorológicas do ECMWF de Março de 2006 a Junho de 2010. Estas simulações foram validadas com recurso a quatro conjuntos de dados observacionais independentes. A resolução horizontal provou desempenhar um papel importante na simulação da cobertura de neve em regiões com uma topografia complexa, embora o seu impacto em regiões planas seja reduzido. Em regiões planas, as simulações da cobertura de neve mostraram-se mais sensíveis à qualidade dos campos atmosféricos prescritos e às parametrizações do modelo. A abordagem utilizada poderá ser aplicada na investigação de outros processos de superfície, em especial novas formas para descrever a variabilidade de subescala, um tópico muito relevante para os modelos climáticos.

Após os avanços alcançados na representação da cobertura de neve no HTESSEL e EC-EARTH, foi abordada a relação entre a cobertura de neve e o acoplamento terra-atmosfera. Para este efeito, realizaram-se simulações atmosféricas globais com o modelo climático EC-EARTH, com e sem evolução interactiva da cobertura de neve. Nas simulações sem neve interactiva, a evolução temporal da cobertura de neve foi substituída por uma climatologia, obtida através de uma simulação de controlo. A variabilidade interanual da cobertura de neve permite explicar quase 60% da variabilidade interanual da temperatura do ar, observada durante o inverno, no Norte da Eurásia e América, regiões que estão predominantemente cobertas de neve. Este controlo da cobertura de neve sobre a variabilidade da temperatura do ar é mais reduzido durante a primavera. Observou-se também que a variabilidade interanual da temperatura do solo é afectada ao substituir-se a evolução da cobertura de neve pela climatologia. Verificou-se ainda que os padrões espaciais do impacto nas temperaturas do solo são semelhantes aos da temperatura do ar. No entanto, existem regiões com um sinal pronunciado na temperatura do solo, sem contrapartida na temperatura do ar. Estas regiões distinguem-se por uma elevada variabilidade interanual da massa de neve à superfície, apresentando uma cobertura de neve constante durante o Inverno. Estes resultados mostram que além da presença de neve à superfície, a sua quantidade também desempenha um papel importante no controlo do acoplamento terra-atmosfera.

PALAVRAS CHAVE: neve, lagos, superfície, modelo de clima, acoplamento terra-atmosfera

List of acronyms and abbreviations

AGCM	Atmosphere General Circulation Model
AL	Alps (see Table 4.1)
AMIP	Atmospheric Model Intercomparison Project
BSWB	Basin Scale Water Balance dataset
CdP	Col de Porte
CE	Central Eurasia (see Table 4.1)
COUP	Simulation with free evolving snow (chapter 6)
CRU	Climate Research Unit
CTR	Simulations with snow scheme described in section 3.7 (old snow scheme)
DENS	See Table 3.2
DU10	Acronym for (Dutra et al. 2010a)
DWD	German Meteorological Service
ECMWF	European Centre for Medium-Range Weather Forecasts
EE	Eastern-Europe (see Table 4.1)
ERA-40	ECMWF 40-years reanalysis
ERAI	ECMWF Interim reanalysis
Flake	Freshwater Lake model
GCM	General Circulation Model
GLCC	Global Land Cover Characterization
GPCP	Global Precipitation Climatology Project
GRDC	Global Runoff Data Centre
GSWP2	Global Soil Wetness Project-2
GTS	Global Telecommunication System
HIG	High resolution simulation 25 km (chapter 4)
HQ06	Acronym for (Hall and Qu 2006)
HTESSEL	Hydrology Tiled ECMWF Scheme for Surface Exchanges over Land
HY	Himalaya (see Table 4.1)
IFS	Integrated Forecast System
IGBP	International Geosphere-Biosphere Program
IMS	Interactive Multisensor Snow and Ice Mapping System
ISCCP	International Satellite Cloud Climatology Project
LOW	Low resolution simulations – 200 km (chapter 4)
LSM	Land Surface Model
LSWT	Lake Surface Water Temperature
LWD	See Table 3.2
LWDR	See Table 3.2
LWDR_A	See Table 3.2
LWDR_AFA	See Table 3.2
LWDR_FA	See Table 3.2
LWDR_SC	See Table 3.2
LWnet	Net Longwave Radiation (or STR, surface thermal radiation)
LWPR	See Table 3.2
ME	Mid-Europe (see Table 4.1)
MED	Medium resolution simulations 80 km (chapter 4)
MFEI	As MED, but forced by ERAI
ML3	Simulation / snow scheme described in section 5.6 (multi-layer)

MODIS	Moderate-Resolution Imaging Spectroradiometer, Lake water surface temperature in chapter 2, and land surface albedo in chapters 3, 4, and 5
MOSN	As MED, but using the CTR snow scheme (chapter 4)
NASA	National Aeronautics and Space Administration
NDVI	Normalized Difference Vegetation Index
NESDIS	National Environmental Satellite, Data, and Information Service
NEW	Simulation with snow scheme described in section 3.2.2 (new snow scheme)
NEW_PR	See Table 3.2
NH	Northern Hemisphere
NL	Simulations with lake model switched off (chapter 2)
NOAA	National Oceanic and Atmospheric Administration
NSIDC	National Snow and Ice Data Center
NWP	Numerical Weather Prediction
OPER	Simulation / snow scheme described in section 3.2.2 (same as NEW)
RK	Rockies (see Table 4.1)
RMSE	Root Mean Square Error
SC	Scandinavia (see Table 4.1)
SCA	Snow-covered area (km^2, or fraction of total area)
SCD	Snow-covered duration (days)
SCF	Snow-covered fraction (0-1, fraction of a region)
SLF	Switzerland snow mass dataset
SLW	Snow Liquid Water
SNOWCLIM	Snow cover duration dataset
SnowMIP2	Snow Models Intercomparison Project-2
SSR	Surface solar radiation (or SWnet)
STR	Surface thermal radiation (or LWnet)
SWE	Snow Water Equivalent, also referred as snow mass
SWnet	Net shortwave radiation (or SSR, surface solar radiation)
T2M	2-meter temperature
TESSEL	Tiled ECMWF Scheme for Surface Exchanges over Land
TWSV	Terrestrial Water Storage Variation
UNCOUP	Simulation with prescribed snow evolution (chapter 6)
USGS	U.S. Geological Survey
WFC	ECMWF deterministic weather forecast (chapter 4)
WL	Simulations with lake activated and overlying snow depth (chapter 2)
WLns	Simulations with lake activated - no snow on top of lake ice (chapter 2)
WMO	World Meteorological Organization

List of symbols

$(\rho C)_{sn^*}$	Snow volumetric heat capacity (J m^{-3} K^{-1})
c_{sn}	Snow cover fraction (0-1)
d	Characteristic temperature difference in respect to T_f(-)
D_{sn^*}	Snowpack depth (m)
E_{sn}	Snow sublimation (kg m^{-2} s^{-1})
F	Snowfall (kg m^{-2} s^{-1})
F_l	Rainfall (kg m^{-2} s^{-1})
G_{sn^*}	Heat flux (W m^{-2})
G_{sn}^{B}	Snow basal heat flux (W m^{-2})
H_{sn}	Sensible heat flux (W m^{-2})
I_t	Incoming solar radiation at the top of the atmosphere (W m^{-2})
L_f	Latent heat of fusion for ice at T_f (3.335x 10^5 J kg^{-1})
L_s	Latent heat of sublimation for ice at T_f (2.838x10^5 J kg^{-1})
M_{sn}	Snow melt (kg m^{-2} s^{-1})
N	Number of snow layers
Q	Net incoming shortwave radiation at the top of the atmosphere (W m^{-2})
Q_{sn^*}	Snowpack heat changes associated with phase changes (W m^{-2})
Q_{sn}^{INT}	Snowpack heat changes associated with internal phase changes (W m^{-2})
R_{sn^*}	Runoff (kg m^{-2} s^{-1})
R_{sn}^{N}	Surface net Radiation (W m^{-2})
S	Snow water equivalent (sum of liquid and solid, SWE) (kg m^{-2})
S_{l^*}	Snow liquid water content (kg m^{-2})
S_l^c	Snow liquid water capacity (kg m^{-2})
T_{air}	Near surface air temperature (K)
T_f	Melting temperature (273.15 K)
T_{ice}	Lake ice temperature (K)
T_{sn^*}	Snow temperature (K)
V_{air}	Near surface wind speed (m s^{-1})
$w_{i,j}$	Intersection area of $y_j \cap x_i$
x_i	Grid-point value to be interpolated
y_i	Grid-point value after interpolation
α_b	Blue ice albedo (0-1)
α_{Lice}	Lake ice albedo (0-1)
α_p	Planetary albedo (0-1)
α_s	Surface albedo (0-1)
α_{sn}	Snow albedo (0-1)
α_w	White ice albedo (0-1)
β	Empirical exponential decay lake ice albedo (-)
Δt	Time step (s)
$\Delta\sigma$	Fraction of interannual variance explained by land-atmosphere coupling (chapter 6)
η_{sn}	Snow viscosity (Pa s)
ρ_{sn}	Snow density (kg m^{-3})
σ	Sample standard deviation (chapter 6)
σ_{sn}	Pressure of overlying snow (Pa)

* the subscript ",i", when present, stands for the variable in the i^{th} snow layer, or the flux between the i^{th} and $(i+1)^{th}$ snow layer (chapter 5).

1 Introduction

The cryosphere is formed by all the forms of water in the solid phase covering the Earth's surface. It includes the seasonal snow, frozen ground (including permafrost), glaciers, ice caps and ice sheets, river ice, lake ice and sea ice. Due to its particular characteristics and large coverage of the Earth's surface, the cold processes associated with the cryosphere play an important role in the climate system. Furthermore, the increasing greenhouse gas concentrations are expected to impact significantly on its characteristics, with possible amplifications of the climate change signal associated with positive feedback processes (Flanner et al. 2011). These changes will impact on the Earth system, with implications in society, such as water resources (Immerzeel et al. 2010; Molini et al. 2011). The study of the several components of the cryosphere, and their interactions with the climate system, covers various disciplines and is recognized as a priority by the international community. The International Polar Year is an example of a collaborative effort, on an international scale, to study the Polar Regions in 1957-58 and 2007-09 under the auspices of the International Council for Scientific Union the World Meteorological Organization.

The role of snow cover in the climate system has been a topic of research for a long time, including early field observations reported by Sverdrup (1935). On a modeling framework, Williams (1975) was one of the first to explore the influence of snow cover on atmospheric circulation and climate change. Snow cover is characterized by high spatial and temporal variability, represented in Figure 1.1. The extent and variability of snow cover are important parameters in weather and climate prediction systems due to their effects on the surface energy and water fluxes, justifying the strong dependency of surface temperature on the presence or absence of snow cover (Armstrong and Brun 2008). Eurasian snow cover has been linked with the variability of the Indian summer monsoon (Douville and Royer 1996; Peings and Douville 2010; Robock et al. 2003) and with significant changes in the hemispheric circulation (Fletcher et al. 2009b; Gong et al. 2007). Snow cover also acts as a water reservoir, which is released by snowmelt in spring, influencing runoff, soil moisture, evaporation, and thus precipitation and the entire hydrological cycle (Douville et al. 2002; Groisman et al. 2004). Therefore, a correct representation of snow water equivalent (SWE) and density is crucial for predicting the snow thermal insulation (Cook et al. 2008), especially in climate change conditions, with direct consequences for soil hydrology and ground temperature (Bartlett et al. 2004, 2005; Stieglitz and Smerdon 2007). This thermal process also plays an important role in controlling soil moisture freezing, with impact on the stable boundary layer (Viterbo et al. 1999), and lake ice evolution (Dutra et al. 2010b). Moreover, on a modeling framework, the assessment of the role of snow cover in the land-atmosphere coupling is hampered by a realistic representation of the cold processes associated with snow in the models.

The land-atmosphere coupling and its associated feedbacks are an open research topic on process oriented studies, climate change diagnostics and predictability exploration. One important focus of research is the role of soil moisture in controlling near surface temperature, with particular interest on extremes (Fischer et al. 2007; Hirschi et al. 2011), or precipitation (Koster et al. 2004; Schar et al. 1999). Seasonal snow cover is known to have an important role on surface albedo (Flanner et al. 2011;

Qu and Hall 2006), whereas the land surface hydrology, and its coupling with the atmosphere, is a potential source for long-range atmospheric predictability (Dirmeyer 2005; Douville 2010; Peings et al. 2010).

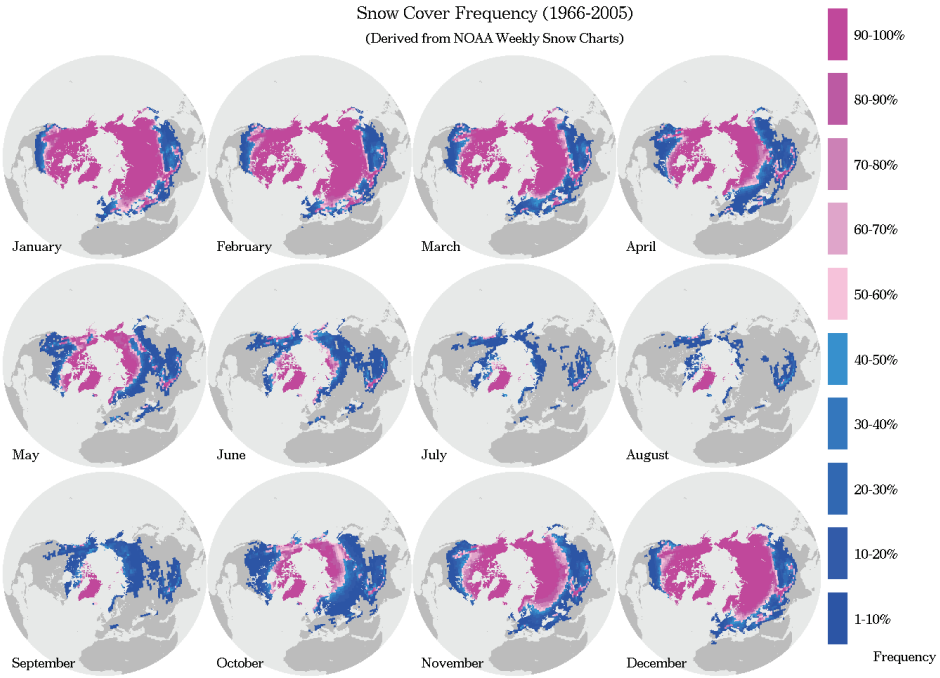

Figure 1.1. 12-month average probability of occurrence of snow cover derived from NOAA Weekly snow charts. Source: National Snow and Ice Data Center - Weekly Snow Cover and Sea Ice Extent[*].*

In most of the above mentioned studies, the land surface component of the atmospheric models plays a fundamental role. The different treatment of snow processes in land surface models (LSM) has been demonstrated in several offline LSM intercomparison experiments (Etchevers et al. 2004; Nijssen et al. 2003; Rutter et al. 2009). The snow schemes designed for atmospheric models (both global and regional) and applied in numerical weather prediction and climate modeling share a similar principle: provide boundary conditions to the atmosphere over snow covered regions. Boone and Etchevers (2001) divided snow schemes in three general categories according to their complexity: 1) simple force-restore or single explicit snow layer schemes (Douville et al. 1995; Slater et al. 1998; Verseghy 1991; Yang et al. 1997); 2) detailed internal-snowprocess schemes (Anderson 1976; Brun et al. 1989; Jordan 1991); and 3) intermediate-complexity schemes based on class 2 but using simplified versions of the physical parameterizations (Boone and Etchevers 2001; Loth et al. 1993; Lynch-Stieglitz 1994; Sun et al. 1999).

This dissertation focus on the cold processes associated with the terrestrial branch of the cryosphere with a seasonal cycle, namely snow cover and lake ice. The problem is approached from the land surface point of view, on a global modeling framework, with special attention to the role of snow and ice in controlling the land-atmosphere coupling, impacting on its upper (atmosphere) and bottom (soil) boundaries. The LSM HTESSEL (Balsamo et al. 2009), the land surface component of the European Centre for Medium-Range Weather Forecasts (ECWMF) integrated forecast system (IFS) and of the

[*] http://nsidc.org/data/docs/daac/nsidc0046_nh_ease_snow_seaice.gd.html

EC-EARTH climate model (Hazeleger et al. 2010), is explored in this work in offline simulations, along with coupled simulations with EC-EARTH. A previous version of HTESSEL, TESSEL (with the same snow scheme as HTESSEL), participated in the Snow Models Intercomparison Project-2 (SNOWMIP2) (Essery et al. 2009; Rutter et al. 2009). As an outcome of the project, several limitations of TESSEL in simulating the snowpack evolution were found (see Figure 1.2). Moreover, initial EC-EARTH climate experiments revealed a significant warm bias of near surface temperature during winter over snow-covered regions (see Figure 1.3). These two independent assessments of HTESSEL and EC-EARTH, in offline and coupled mode, indicated that the representation of cold processes associated with seasonal snow cover in HTESSEL and EC-EARTH had some deficiencies. These results motivated the initial work presented in this dissertation, to assess and improve the snow representation in HTESSEL and EC-EARTH. Further analysis on the sensitivity of snow cover evolution to the atmospheric forcing, horizontal resolution and model physics were performed. Atmospheric simulations with the EC-EARTH model were carried out to (i) assess how the complexity of snowpack representation impacts on model performance, (ii) and to investigate the role of interannual snow cover variability in controlling the land-atmosphere coupling. An assessment of the potential impact of lakes included in HTESSEL was also addressed, including the role of the snow thermal insulation in controlling the evolution of lake ice.

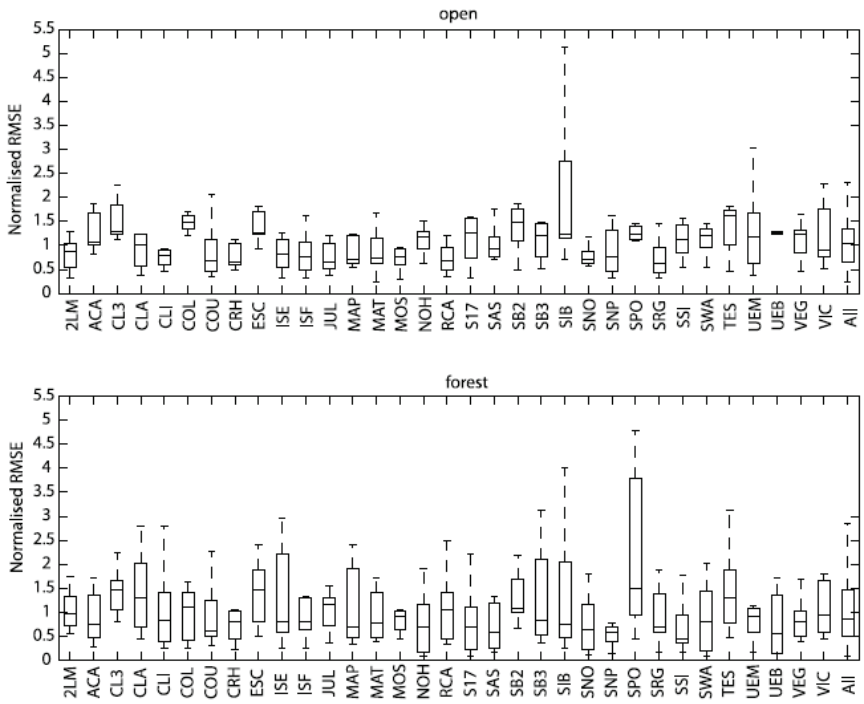

Figure 1.2 Box plot summaries describing the performance of individual models (TESSEL is noted as TES in the horizontal axis) and all models, combined at all SnowMip2 locations and years at open and forest sites. The model's performance is assessed by the root mean square error of simulated snow water equivalent, normalized by the standard deviation of the observations (vertical axis). Each box has horizontal lines (solid) at lower quartile, median and upper quartile values; whiskers (dashed lines) extend from the end of the each box to 1.5 times the interquartile range. Source: Rutter et al. (2009) figure 6.

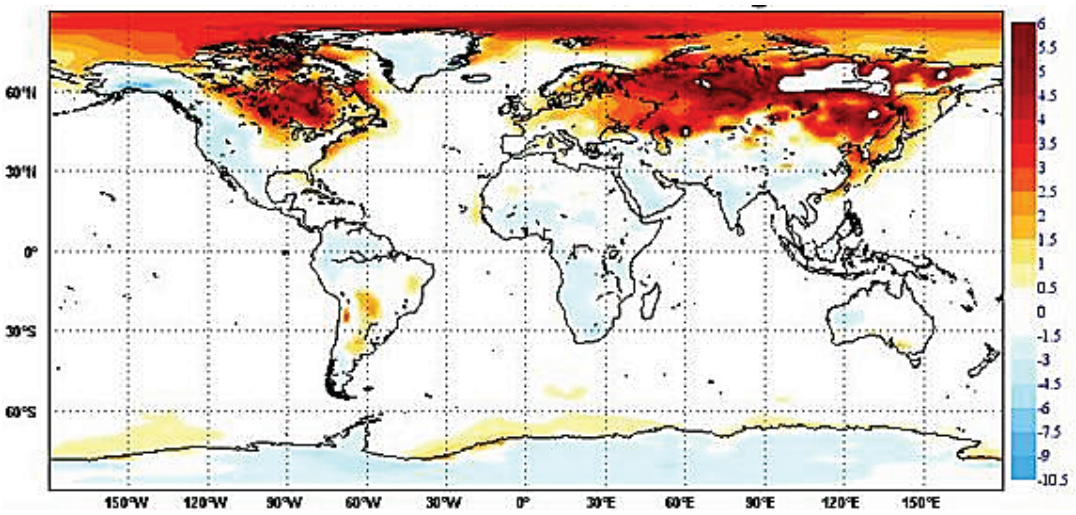

Figure 1.3 Mean winter near surface temperature differences (K) between EC-EARTH climate model simulations version 0 and ECMWF reanalysis ERA-40. Source: EC-EARTH wiki page accessed March 2011: http://ecearth.knmi.nl/CY31R1_T159L62Control.html.

This dissertation is organized in 7 chapters, where 5 of them (chapters 2-6) are presented as self-contained scientific papers, as they have been already published or submitted for publication. While allowing the reading of each chapter by itself, there can be some duplication in the description of methods, namely model description and observations. However, each chapter presents the methods differently, focusing on the particular application. The last chapter (7) summarizes the overall conclusions of the dissertation and an outlook on future research topics, addressing open questions discussed during the dissertation. In the following paragraphs an overview of each chapter is presented.

Chapter 2 presents the incorporation of the lake model Flake into HTESSEL. Global offline simulations were carried out and validated against remote sensing lake surface water temperature, and lake ice duration. The impact of snow insulation on lake ice duration is discussed, as well as the sensitivity of the results to the prescribed lake depth. General aspects concerning the incorporation, and possible impacts, of lake models into general circulation models for weather and climate modeling are discussed.

Chapter 3 describes the development and validation of a new snow scheme for HTESSEL. The validation includes offline simulations for several observations sites from SnowMIP2 and global simulations driven by the meteorological forcing from the Global Soil Wetness Project-2 (GSWP2) and from the ECMWF ERA-Interim Re-analysis. The simulations are validated against local site observations, and remote sensing snow cover and surface albedo.

Chapter 4 presents an assessment of the relative impacts of horizontal resolution, snow physics and atmospheric forcing in snow cover simulations by HTESSEL. Similarly to chapters 2, and 3, offline simulations were carried out in a set of experiments, including different horizontal resolutions, different model physics activated and different atmospheric forcing. The experiments are then compared with four independent observational datasets.

Chapter 5 presents an intercomparison of three snow schemes of different complexity, coupled to the EC-EARTH climate model. The snow schemes include the original HTESSEL snow scheme, the snow

scheme described in chapter 3, and a multi-layer version of the latter. Coupled atmosphere simulations performed by EC-EARTH are validated against remote sensing snow cover and surface albedo. Special attention is given to the role of snow thermal insulation in controlling the heat exchanges between the underlying soil and the overlying atmosphere.

Chapter 6 describes an assessment of the role of snow cover interannual variability in controlling the land-atmosphere coupling, and its relation with near surface and soil temperatures. Global atmospheric simulations are carried out with the EC-EARTH climate model. Snow climatology, derived from a control run, is used to replace snow evolution in the snow-uncoupled simulation. As in chapters 2, 3, and 5 the role of the snow thermal insulation in decoupling the atmosphere from the underlying surface is highlighted.

2

An offline study of the impact of lakes on the performance of the ECMWF surface scheme*

Abstract

The lake model FLake was incorporated into the European Centre for Medium-Range Weather Forecasts (ECMWF) land-surface scheme HTESSEL. Results from global offline simulations are presented in order to evaluate the model performance in different climates and assess the impact of lake representation on the surface energy balance. The model was forced by ECMWF reanalysis ERA-Interim (1989–2005) near surface meteorology and surface radiation fluxes for the entire globe. Model validation includes lake surface temperatures and lake ice duration. The impact of the snow insulation on lake ice cover duration is discussed, as well as the sensitivity of results to the lake depth. Results show changes in the variation of surface energy storage, and changes in the partition of surface energy fluxes in high latitude and equatorial regions, respectively. General aspects concerning the incorporation of lake models into General Circulation Models for weather forecast and climate modeling are discussed.

* Dutra, E.[1,2], V. M. Stepanenko[3], G. Balsamo[4], P. Viterbo[1,5], P. M. A. Miranda[1], D. Mironov[6], and C. Schär[2], 2010: An offline study of the impact of lakes on the performance of the ECMWF surface scheme, *Boreal Environ. Res.*, **15**(2), 100-112.

Also available as ECMWF *technical memorandum N. 608.*

[1] Centro de Geofísica da Universidade de Lisboa, Instituto Dom Luiz, University of Lisbon, Lisbon, Portugal.

[2] Institute for Atmospheric and Climate Science, ETH, Zurich, Switzerland.

[3] Moscow State University, Research Computing Center, Faculty of Geography, Moscow, Russia.

[4] European Centre for Medium-Range Weather Forecasts, Reading, United Kingdom.

[5] Institute of Meteorology, Lisbon, Portugal.

[6] German Weather Service, Offenbach am Main, Germany.

2.1 Introduction

Lakes and other inland waterbodies can, in certain areas, constitute a large fraction of the land surface. As compared with vegetated land surfaces, inland waters play an important role in determining local and regional climates, primarily because of large differences in albedo, heat capacity, roughness, and energy exchange. Despite the radically different physical characteristics of inland waters as compared with their surrounding, most land surface models (LSMs) put more emphasis on the comparatively weaker differences within continental surface types (such as various types of vegetation and bare soil). Thus, so far sub-grid lakes have been largely neglected.

It has been shown that inland waterbodies can have important impacts on climate on various spatial scales (Bonan 1995; Hostetler et al. 1994; Krinner 2003; Lofgren 1997; Long et al. 2007). These studies report the role of open water surfaces in moistening the atmosphere, especially in summer (e.g. Bonan 1995). However, Lofgren (1997) reports that the Laurentian Great Lakes, by cooling and stabilizing the lower atmosphere in summer, tend to reduce evaporation and precipitation in the region. In winter, when boreal lakes are frozen, their climatic role is generally reported to be weak, although the energy flux through lake ice is significantly higher than over normal continental surfaces.

This work presents the implementation of the lake model FLake (Mironov 2008) into the ECMWF LSM HTESSEL (Balsamo et al. 2009; Viterbo and Beljaars 1995). Offline (or stand-alone) simulations are often used to validate new parameterizations (Van den Hurk and Viterbo 2003) and in LSMs intercomparison initiatives (Dirmeyer et al. 1999; Rutter et al. 2009). The new reanalysis data from ECMWF ERA-Interim (Dee et al. 2011), hereafter ERAI, is suitable for such a modeling framework. The reanalysis is available since 1989 to present, and in this study is used for 17 years (1989 to 2005). Global stand-alone simulations allow the verification of the lake model and behavior of the proposed implementation in contrasting climate regions. Long-term simulations (17 years) also allow inter-annual verification and impacts analysis, since the model is exposed to different weather regimes.

Validation of global simulations requires independent global datasets. The lake surface water temperature (LSWT) derived from the Moderate-Resolution Imaging Spectroradiometer (*MODIS*) instrument on-board the TERRA platform is suitable for the validation exercise. Lake ice cover duration is an important feature of many high latitude lakes, but remote sensing LSWT only allow a clear validation in ice free conditions. The Global Lake and River Ice Phenology (Benson and Magnunson 2007) provides a comprehensive dataset of formation and breakup of lake ice on several hundreds of lakes in the northern hemisphere.

The snow insulation effect has been reported as an important mechanism controlling energy exchanges between soil and atmosphere (Cook et al. 2008). This energy exchange governs the lake ice growth (or reduction) and subsequently affects the lake surface temperature. Simulations with and without snow over lake ice are analyzed and the snow insulation effect is discussed. The lake depth is a crucially important model parameter, but there is not much relevant information regarding this parameter at the global scale. The sensitivity of the present validation to lake depth is also discussed. From the point of view of the atmosphere, the representation of lakes will change the surface fluxes. The impact of the representation of sub-grid scale lakes is evaluated on monthly time scales for different climatic regions.

2.2 Methods

2.2.1 Models

The LSM HTESSEL (Hydrology Tiled ECMWF Scheme for Surface Exchanges over Land) represents vertical transfers of water and energy using four vertical layers to represent soil temperature and moisture (Viterbo and Beljaars 1995). The model evaluates the soil response to the atmospheric forcing, and estimates the surface water and energy fluxes and the temporal evolution of soil temperature and moisture content. At the interface between the surface and the atmosphere, each grid-box is divided into fractions (tiles), with up to six fractions over land (bare ground, low and high vegetation, intercepted water, shaded and exposed snow) and two extra tiles for open water (ocean) and sea-ice. Each fraction has its own properties defining separate heat and water fluxes used in the energy balance equation solved for the tile skin temperature. The model is part of the integrated forecast system (IFS) at ECMWF in applications ranging from short range weather forecast to reanalysis such as ERA-40 (Uppala et al. 2005) and ERAI. Along with its operational use, the model has served as a research test bed for a variety of applications ranging from leaf area index assimilation (Jarlan et al. 2008) to drought characterization (Dutra et al. 2008).

Currently in HTESSEL only grid-scale lakes (lake fraction larger than 50%) are considered. In these grid points, the surface temperature is prescribed, constant during integration, from the assimilation system of sea surface temperature for points close to large ocean bodies, and the remaining points are set to a monthly climatology. This treatment of lakes in the model does not account for the diurnal changes of surface temperature and inter-annual variability. The model does not consider partial lake cover within a grid-box. All the grid-points with lake fraction less than 50% are treated as land only. The current lake representation in the model has two main drawbacks: (i) the continuous increase in horizontal resolution of the forecast system led to an increase in the number of resolved lakes with ill-defined properties, and (ii) sub-grid fraction occupied by lakes is not represented in coarser resolutions (used for seasonal or climate applications).

FLake is a numerical model, describing the thermodynamic processes in a lake, including the temperature of the water mass, underlying bottom sediments, ice and snow cover (Mironov 2008). Mironov et al. (1991) described a model that served as prototype to develop FLake and Mironov et al. (2010) presented a brief description of FLake, along with its implementation into a limited-area atmospheric model. FLake can be considered as a 0.5-dimensional model, since it has intermediate features between purely bulk models and multi-layer one-dimensional models. The vertical temperature profile specified in FLake consists of a top mixed layer, with uniform distribution of temperature, and a thermocline, with its upper boundary located at the mixed layer bottom, and the lower boundary at the lake bottom. The profile in the thermocline is parameterized according to the self-similarity concept (Kitaigorodski and Yu.Z 1970), which has been supported by many theoretical (Barenblatt 1978; Zilitinkevich and Mironov 1992) and observational studies (Tamsalu and Myrberg 1998). In FLake, this concept is also applied to calculate temperatures in the snow-pack, ice cover and the layer of bottom sediments. The above mentioned assumptions led to a significant model simplification in comparison with multi-layer one-dimensional models, while still containing much more realistic physics than bulk models. In particular, the unrealistic assumption of fully mixed temperature profile in a lake, which has been applied in many bulk models, is avoided here. Instead,

the mixed layer depth is calculated taking into account both wind and thermally driven mixing (Mironov 2008). The volumetric heating of the water column by solar radiation is also accounted for. Therefore, FLake meets the requirements for physical parameterizations in weather forecast systems, in terms of both physical realism and numerical efficiency. The FLake model package, available at http://lakemodel.net, contains the source code of the model itself and some auxiliary procedures, e.g. subroutines that calculate turbulent fluxes at the lake-atmosphere interface.

A new tile (ninth) was created in HTESSEL to represent the lakes interface with the atmosphere. Since turbulent fluxes are already calculated inside HTESSEL for each tile, FLake subroutines calculating these fluxes over a lake were omitted. Another simplification of the original FLake model deals with the snow cover and bottom sediments. HTESSEL has its own snowpack parameterization, which is used in this study for frozen lakes instead of the original FLake self-similarity model to be consistent with other parts of the code. HTESSEL snow scheme was coupled to the new lake tile, allowing the representation of snow cover over frozen lakes. The other simplification was to neglect bottom sediments. Considering the present global application for numerical weather prediction, the representation of bottom sediment would imply an extra set of external parameters which are not well known. In addition to the technical motivation, the heat storage and response time scales associated with bottom sediments in relatively large lakes (typically more than several meters deep) can be neglected when compared with the remaining energy forcings acting on a lake. As an extra physical motivation, one may notice that the parameterization of heat transfer in bottom sediments used in FLake is based on the self-similarity concept of the temperature profile (Mironov et al. 2003). This concept application has been extensively validated for the water column, but not for the bottom sediments.

2.2.2 Data

ERAI reanalysis provided the set of near-surface meteorological forcing to drive the LSM in stand-alone mode. ERAI covers the period of January 1989 to present. The atmospheric forcing data were gridded on the original Gaussian reduced grid N128 (resolution of 0.7° over the equator) globally on a domain of 25979 grid points (land and lake points only) at a three-hour interval. The state variables of the surface pressure, air temperature, specific humidity and wind were provided as instantaneous values from the lowest model level (approximately 10 m above the surface). State variables correspond to the 3–12-h forecast interval from initial conditions at 00:00 and 12:00 UTC. Surface fluxes represent three-hour averages and include precipitation, snowfall, and downwelling solar and thermal radiation. To avoid the initial spin-up in precipitation, the three-hourly surface fluxes are taken from the 9h to 21h forecasts initialized at 00 and 12 UTC.

The remotely-sensed lake surface water temperature (LSWT) derived from the observations taken by the Moderate-Resolution Imaging Spectroradiometer (*MODIS*) instrument aboard the NASA TERRA satellite platform in the original 4 km resolution (http://oceancolor.gsfc.nasa.gov/) were aggregated to the ERAI grid. The weekly composites from January 2001 to December 2005 of daytime and nighttime data were averaged, resulting in single weekly time series for each ERAI grid-box. This dataset has been mainly prepared for ocean sciences (Esaias et al. 1998), but it has also been applied to derive LSWT of the Great Salt Lake (Crosman and Horel 2009).

Observations of the lake ice duration were taken from the Global Lake and River Ice Phenology (Benson and Magnunson 2007). This dataset contains freezing and breakup dates and some other ice-cover characteristics for 750 lakes and rivers. Of the 429 water bodies that have records longer than 19 years, 287 are in North America and 141 are in Eurasia. Krinner (2003) used this dataset to validate lake simulations within a climate model, and Magnuson et al. (2000) analyzed trends in lakes and rivers ice cover. Using the raw data, the mean lake ice duration was calculated by aggregating all the data within each grid-box of ERAI and calculating the mean from all the lakes and available periods. The lake characteristics of each lake within a specific grid-box might vary significantly. However, in the present modeling framework each grid-box can only have one lake that responses to the grid-box mean surface energy and water fluxes

2.2.3 Simulations setup

Global offline simulations forced by ERAI were performed for the period January 1989 to December 2005. Since lake depth is an important parameter in the lake thermodynamics, three simulations were performed with globally constant lake depths of 10, 30 and 50 meters. A constant lake depth approach was chosen, since information on lake depths is not available globally. Other global studies of lakes within GCMs also used global uniform lake depths (e.g. Bonan 1995). One control experiment, with the lake model deactivated, was also performed. In this simulation, grid-points with a lake fraction less than 50% were treated as land and all the grid-points with a lake fraction larger than 50% (resolved lakes) were treated as water with time-constant temperature.

To examine the effect of the snow insulation effect on lake ice, one extra set of simulations was performed with the lake ice snow-free. In the following discussion, WL (with lake, and overlaying snow deck) and WLns (with lake, but no snow on top of lake ice) refer to simulations with the lake model activated with snow deck and no snow deck on the lake ice, respectively, and NL (no lake) refers to simulations with the lake model switched off. The evolution of lake ice with no overlaying snow (always the case in WLns simulations and when there is no snowfall in WL simulations), is mainly controlled by the albedo. In the present implementation, the lake ice albedo was equal to that of sea ice (already defined in HTESSEL) which is prescribed as a monthly climatology from Ebert and Curry (1993). Initial conditions were derived by performing one 11-year run (1989 through 1999) for each simulation, starting from arbitrary values. The first year of simulation was discarded and the following ten years were retained to create climatological initial conditions. This initialization methodology guarantees enough spin up time to stabilize the lake model results, in particular for simulations with lake depths of 50 meters.

The lake fraction was derived from the GLCC land-cover dataset (see Figure 2.1) (Loveland et al. 2000). It includes all inland open water surfaces, and does not distinguish between lakes and rivers. Besides the lake fraction, all the other input fields (e.g. land sea mask, vegetation type and cover, monthly albedos, soil types) were the same as in ERAI.

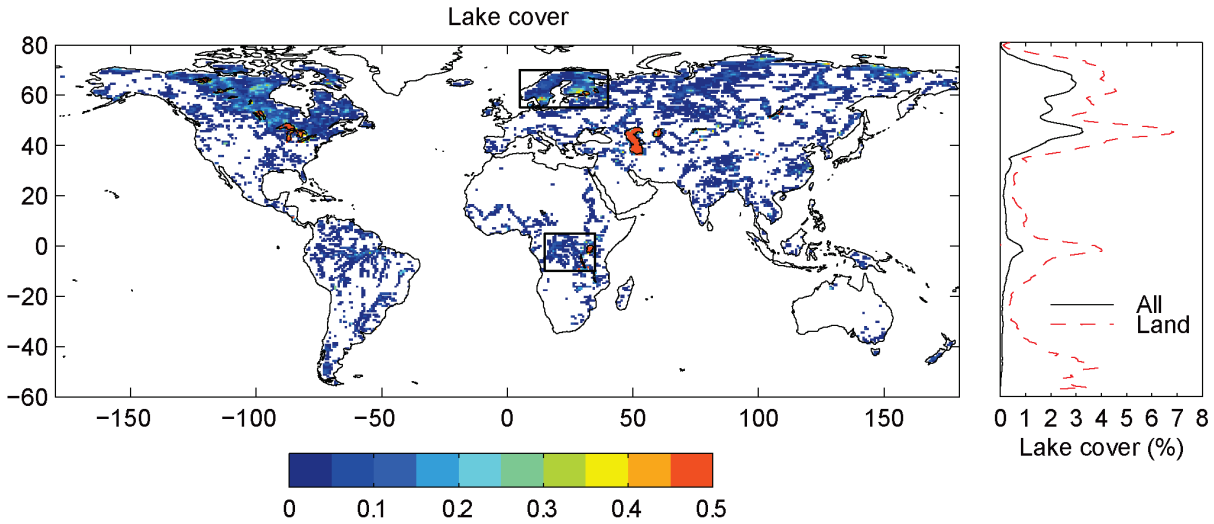

Figure 2.1. Lake fraction in the Gaussian reduced grid N128 and zonally averaged fractional lake cover with respect to land points only (dashed) and all points (solid).

2.3 Results

2.3.1 Validation

An eight-day running mean was applied to the modeled LSWTs (see Figure 2.2). This allowed for a coherent comparison with the weekly composites of remotely sensed LSWTs. For high-latitude lakes (Figure 2.2), the RMSEs varied significantly with the total lake depth. When exposed to the same meteorology, deeper lakes had higher heat content, leading to reduced ice cover durations than in shallower lakes. In general, deeper lakes also occupy larger areas (Lehner and Doll 2004), resulting in more intense lateral mixing/transport that is not represented by FLake. This affects the timing of freezing/melting.

For each grid point, the lowest LSWT RMSE was selected from one of the three simulations with different lake depths (BEST in Figure 2.2). This simple approach is able to improve the LSWT RMSE distribution for high latitude lakes, when compared with globally constant lake depth simulations. These results confirm that a lake-depth tuning procedure, based on LSWT RMSE, would be able to improve the model skill in representing surface temperatures. Balsamo et al. (2010) showed that it is feasible to derive an effective lake depth using satellite LSWT. In low-latitude lakes, the RMSEs did not vary significantly with the lake depth (Figure 2.2b. Low-latitude lakes have normally a strong vertical stratification during the entire year due to a large amount of available solar energy. With this thermodynamic behavior, the surface temperature is not as strongly constrained by the lake depth as it is for high-latitude lakes. The overall RMSEs were higher for high-latitude lakes. However, the ratio between RMSEs and the amplitude of the mean annual cycle of LSWT was higher in low-latitude lakes.

Further analysis was performed by removing the systematic differences between observed and modeled temperature before the RMSE calculation. After this procedure, only the BEST RMSE (lower RMSE in each grid point from different simulations) was chosen (BEST (bias removed) in Figure 2.1). In this way, we distinguished the systematic errors from variability errors of modelled LSWTs. In high-latitude lakes, the systematic bias removal had a small impact on the statistical distribution. On

the other hand, in low-latitude lakes most of the errors were associated with systematic biases. These differences between the partitioning of systematic and variability errors for high and low latitude lakes can be explained as follows: (i) the errors in high-latitude LSWTs arise mainly from the inaccurate representation of the formation/disappearance of lake ice, and (ii) the errors in low-latitude lakes are mainly systematic. The systematic errors found can, in part, be associated with the forcing (e.g. uncorrected temperature due to differences between model orography and real lake altitude).

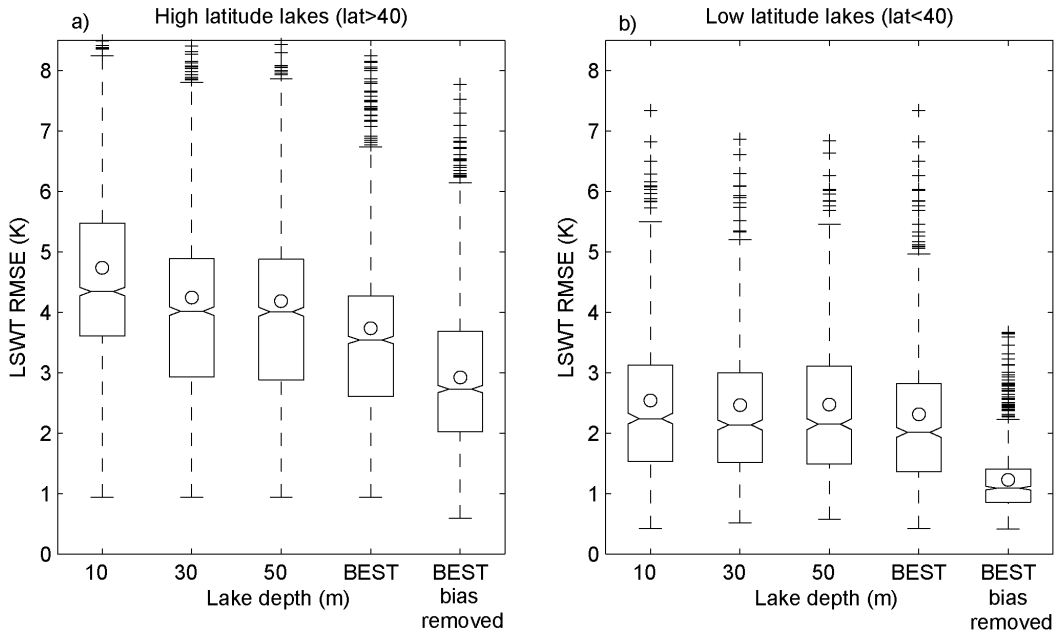

Figure 2.2. Root mean square error distributions of the model vs. MODIS observations of lake surface-water temperature (LSWT, WL) of (a) high latitude (latitude > 40°) lakes, and (b) low latitude (latitude < 40°) lakes for all ERAI grid-boxes with more than 10% of available remotely sensed LSWTs data in the period January 2001 to December 2005. Separate statistics are given, since the dependence of the lake thermodynamics on the latitude is very pronounced due to the impact of freezing in high-latitude lakes. Distributions of RMSE are presented as function of lake depths (10, 30 and 50 m) and BEST (lake depth that minimizes the RMSE for each grid point). The rightmost "BEST (bias removed)" give results with the model-observations bias removed before computing RMSE. The boxes have horizontal lines at the lower quartile, median, and upper quartile, and outliers are data with values beyond 1.5 times the inter-quartile range indicated with '+'. Open circles are the means.

Simulations of lake ice duration were compared against Global Lake and River Ice Phenology database (Benson and Magnunson 2007). Model data were averaged for the entire simulation period (1989–2005) (Figure 2.3). For each lake-depth simulation (including BEST), the distributions are displayed side by side for the WL and WLns (indicated with *). The WLns simulations were conducted in order to evaluate the importance of the snow insulation effect in the lake ice thermodynamics. The snow insulation effect reduces the coupling between the atmosphere and underlying surface (Cook et al. 2008). The simulations WLns produced higher positive errors in the lake-ice duration, as compared with the WL simulations. Snow insulates the lake ice, preventing its growth during the cold season, and thus reducing its duration. Despite the wide dispersion of errors in lake ice durations, 75% of the errors in the BEST lake depth selection were within ±30. These errors refer to the total lake ice duration. If the errors associated with the freezing and breakup were similar, 75% of the evaluated grid points would lie within an error margin of two weeks for the formation and

breakup of lake ice. It should be noted that the time periods covered by the lake ice observations are not necessarily the same as the simulations. Additionally, the spatial averages (for all the lakes lying in each grid-box) can mix lakes that can have completely different error characteristics, leading to possible biases in the comparisons.

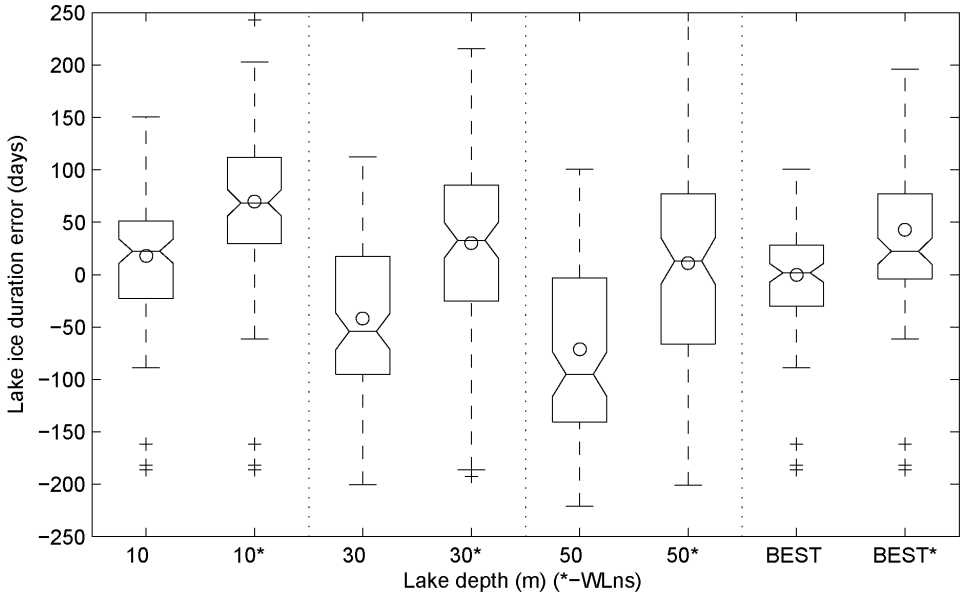

*Figure 2.3. Distributions of lake ice duration errors (observations minus model) from the simulations with lake (WL), and with lake and no snow (WLns). The latter is indicated with * in the horizontal axis. Data are from 123 grid points in the northern hemisphere. The boxes have horizontal lines at the lower quartile, median, and upper quartile, and outliers are dates with values beyond 1.5 times the inter-quartile range indicated with '+'. Open circles are the means.*

To further examine the impact of snow coupling over frozen lakes, lake ice durations, given by both coupled (WL) and uncoupled snow (WLns) simulations were performed (Figure 2.4a). The lake ice duration was calculated for each year as the number of days with ice cover from September of the previous year to August of the following year. Simulated ice cover durations were always longer in WLns than in WL. These results reinforce the importance of the snow insulation effect on the thermodynamics of the underlying surface. Snow deposition over the lake ice reduces its cooling and growth. The formation period of lake ice was very similar in both WL and WLns simulations, while the breakup was delayed in WLns due to excessive ice thickness. As discussed before, the WLns simulations had a positive bias in lake ice duration (Figure 2.3). These results show that coupling the snow deck with the lake ice improves the model skill to properly represent the lake ice melting. Lake ice albedo was prescribed as a climatology (Ebert and Curry 1993) in both WL and WLns simulations. In WL simulations this is not critical, since during most of the cold season the lake ice is covered by snow. On the other hand, the lake ice albedo controls the amount of solar radiation penetrating the ice in WLns. The Ebert and Curry (1993) albedo climatology might not be suitable for lake ice, which could explain the results of WLns simulations. A possible solution to mimic the snow insulating effect would be to change the lake ice albedo, which is further discussed in appendix.

The effect of snow on frozen soil is similar to that of snow on ice: a snow-free soil will be colder and the soil melting will be delayed as compared with a snow-covered soil. In order to highlight the similarity of the effects, a comparison between the duration of frozen soil and lake ice was made

(Figure 2.4b, including only the grid points where lakes are represented). The frozen soil duration was evaluated by calculating the number of days, in each period from September to August, when the uppermost soil layer (7-cm depth) was frozen. The frozen-soil period durations of 150 to 250 days were similar to those for lake ice for all lake depths. For frozen soil durations of less than 150 days, the relation with lake ice duration strongly depended on the lake depth. Shallow lakes stayed frozen for longer periods, while deeper lakes might not even freeze. In the scatter plot (Figure 2.4b), many symbols lying at or just above the horizontal axis, correspond to grid points where the soil froze but the lakes (in the same grid box) did not. This behavior can mainly be attributed to the higher thermal inertia of lakes when compared with soil. It is reasonable to assume that in many locations, the top soil layer can freeze but nearby lakes remain unfrozen.

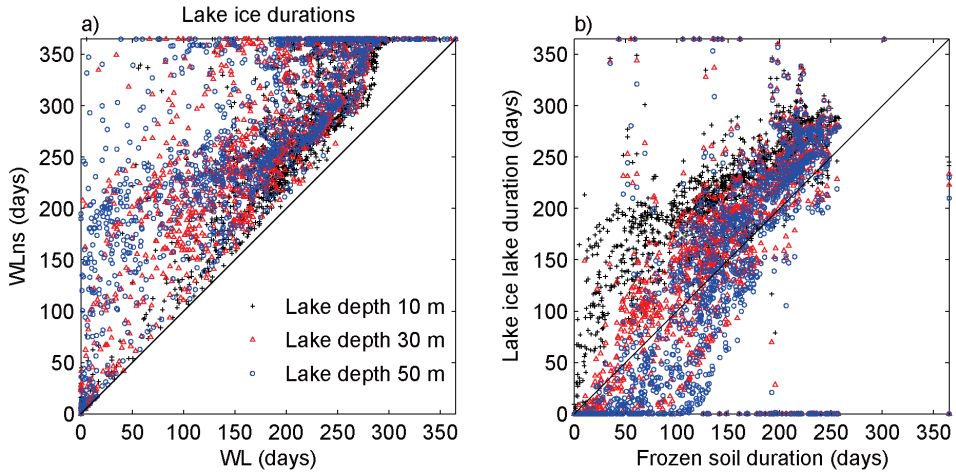

Figure 2.4. (a) Mean lake ice duration simulations from WLns (with lake, no snow) versus the same quantity for WL (with lake) simulations. (b) Mean lake ice duration (only sub-grid scale lakes), in WL simulations, as a function of the mean frozen soil duration for the same grid-box in the 17-year simulation

2.3.2 Impact on surface fluxes

In the following analysis we discuss only the simulations NL and WL with a globally constant lake depth of 30 m. Comparisons between the WL simulations with different lakes depths showed that on a monthly time scale the differences are not significant. The WLns simulations were also discarded from the following analysis due to the systematic biases on lake ice duration described before (see Figure 2.3).

The main purpose of the implementation of the lake model within the LSM is to better represent the sub-grid cover variability and its impacts on land surface fluxes. Figure 2.5 shows the impact of sub-grid scale lakes on surface fluxes over two climatic regions: northern Europe (55°N–70°N, 5°E–40°E) and Africa (10°S–5°N, 15°E–35°E). These areas are represented as squares in Figure 2.1 and comprise 385 and 585 grid-points for northern Europe and Africa, respectively. The analysis was performed for the mean annual cycle of the latent and sensible heat flux, solar and thermal net radiation, and surface net energy. The sign of the fluxes follow the model convention, with positive values for incoming and negative ones for outgoing energy from the surface. By using only grid points with a sub-grid lake cover > 5%, the mean annual cycles of area-averaged fluxes for the NL simulation (Figure 2.5a-b) and for the difference WL – NL (Figure 2.5c-d) were calculated. The differences were tested for

significance with a two-tailed t-test. Grid points where sub-grid scale lake cover > 5%, composed 44% and 12% of the total analysed areas of northern Europe and Africa, respectively. Over northern Europe, there was a significant increase of the energy storage on the surface during summer and release during autumn. This kind of behavior has been already documented in other works (e.g. Bonan 1995), with cooling and warming effects on the atmosphere during summer and autumn, respectively. Over Africa, the impacts of the representation of sub-grid scale lakes differed from those at high latitudes. The net surface energy remained similar throughout the year, but there was a significant change in the flux partitioning, indicating an increase of the latent heat flux and decrease of the sensible heat flux. This decrease in the Bowen ratio (ratio between sensible and latent heat fluxes) can impact the boundary layer development and convection triggering. Over northern Europe, there was a reduction of the net short-wave radiation during spring due to an increase of the surface albedo, but the differences were not significant. In both areas the changes in thermal net radiation were small and not significant in most of the months. This analysis was performed in other high and low latitude regions with similar results.

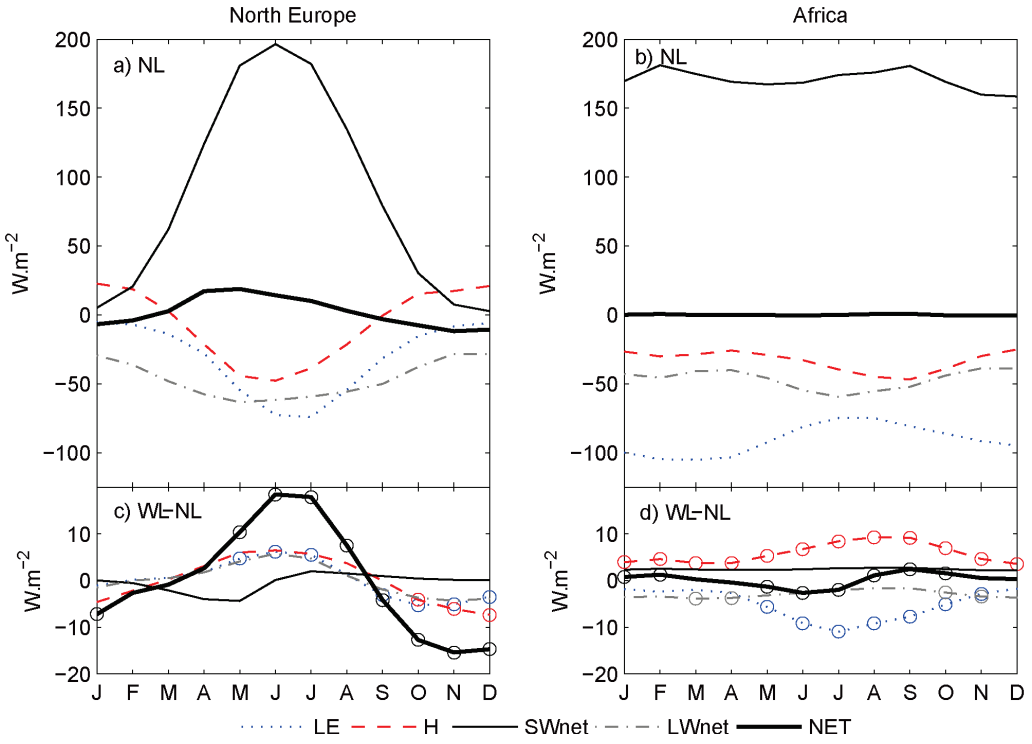

Figure 2.5. Mean annual cycle from simulation WL (lake depth of 30 m) of Latent heat (LE, dotted blue), sensible heat (H dashed red), surface solar radiation (SWnet solid blac), surface thermal radiation (LWnet dash-dot black) and surface net radiation (NET thick black) for all sub-grid scale lake grid points inside (a and c) northern Europe and (b and d) Africa (see Figure 2.1 for areas definition). c and d: differences between simulations with lake minus no lake (WL – NL); circles mark differences significant at $p < 0.01$(two-tailed t-test).

A global overview of the impact on evaporation is presented in Figure 2.6. The setup of the NL simulation included constant LSWT during the run, which is not realistic. To overcome this problem, evaporation for all resolved lakes of NL simulation was replaced by ERAI data. The mean annual evapotranspiration from the NL simulation (Figure 2.6a) was compared against ERAI (Figure 2.7). The main differences between NL and ERAI evapotranspiration can be primarily attributed to the soil

moisture assimilation scheme used in ERAI. The assimilation corrects soil moisture in the first three layers based on 6-hour increments of atmospheric analysis of specific humidity and temperature at the lowest model level (Douville et al. 2000). When ERAI soil moisture increments were added to the evaporation, a good match with NL was found (see Figure 2.7). A good agreement between offline and ERAI evapotranspiration shows that the stand-alone modeling methodology is able to reproduce, apart from the assimilation, the evapotranspiration fluxes of the reanalysis. The patterns of impact of the representation of lakes (both grid and sub-grid scale) on evaporation (Figure 2.6b) were very similar to those of the lake cover fraction (Figure 2.1), with an increase of evaporation throughout the globe. On a yearly scale, the differences were small when compared with the total evapotranspiration, and very localized. Nevertheless, the impact can be significant in some specific areas and seasons.

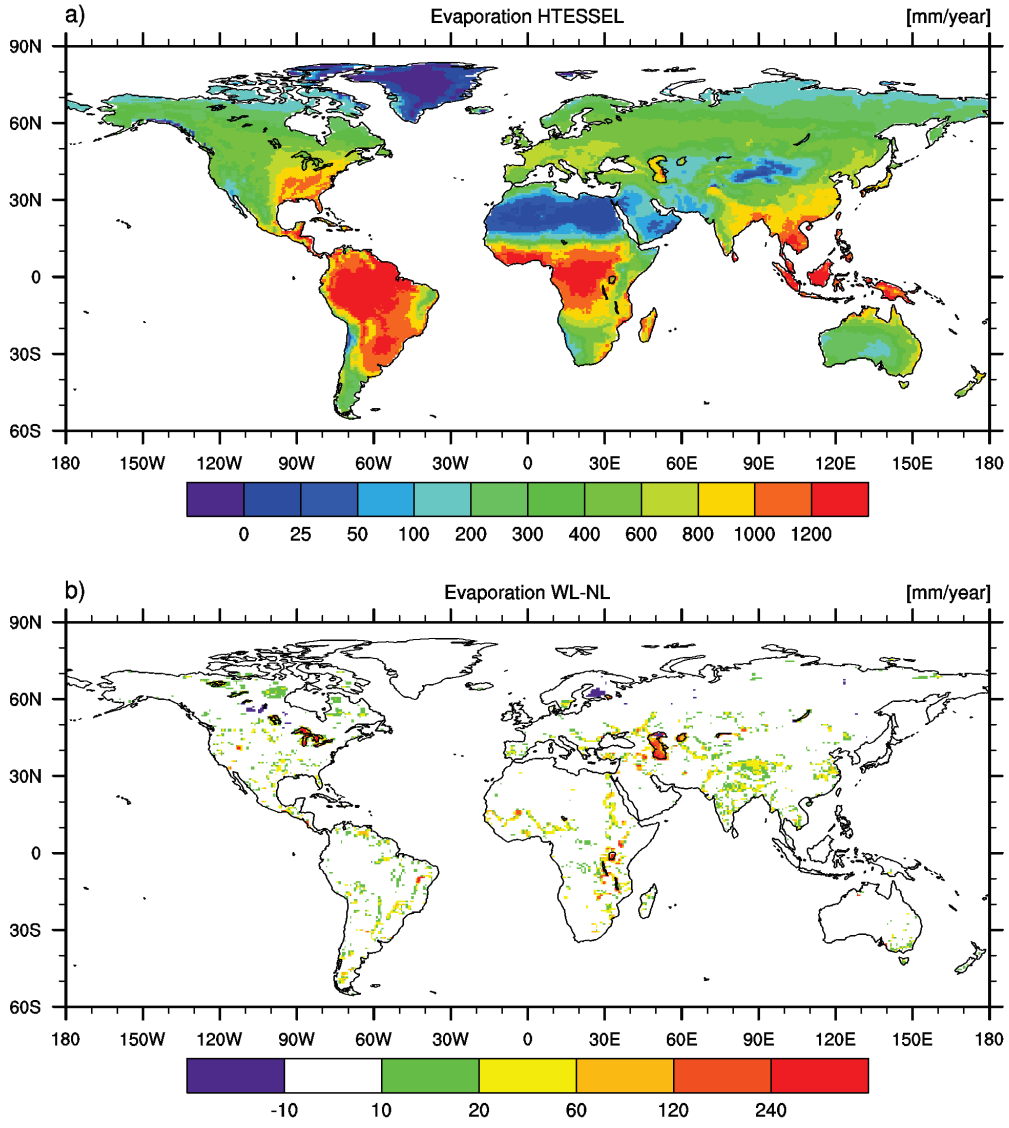

Figure 2.6. (a) Global yearly evapotranspiration from the simulation NL (no lakes). (b) Yearly evapotranspiration differences between the simulations WL (lake depth 30 m) and NL (no lakes). Evaporation for all resolved lakes of NL simulation was replaced by ERAI data. Note the different color scales.

2.4 Summary and discussion

Here we presented the implementation of the FLake lake model into the LSM HTESSEL. Stand-alone global simulations forced by the ERAI reanalysis were performed and LSWT was validated against remotely sensed LSWTs derived from the *MODIS* TERRA satellite. Total lake depth appears to be the most important model parameter, but global information on lake depths is not available. To overcome this lack of information and to examine the model sensitivity to lake depths, simulations were performed with three different lake depths of 10, 30 and 50 meters. A simple minimizing strategy of choosing the lake depth (for each grid point) with the lowest RMSE was able to reduce significantly the LSWT RMSEs distribution. This tuning exercise proves to be effective for obtaining a first guess for a global-wide lake depth dataset (for all lakes with available remotely sensed LSWT) and is supported by the results of Balsamo et al. (2010). Further validation was performed by comparing simulated and observed lake ice duration. Regarding the lake ice evolution, the coupling with the current snow scheme of HTESSEL showed significant improvements. The snow insulation effect was evaluated in terms of the lake ice duration and compared against frozen soil at nearby locations.

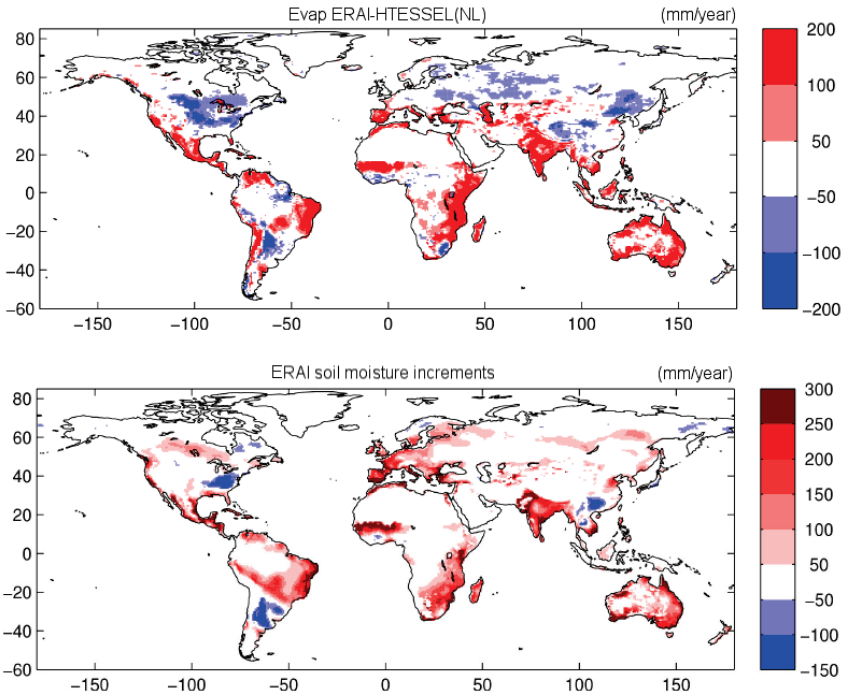

Figure 2.7. Top panel: yearly evapotranspiration difference between ERA-Interim and HTESSEL (NL) simulation. Bottom panel: annual mean soil moisture increments (top three layers) from the assimilation during ERA-Interim reanalysis.

The main drawback of the presented stand-alone simulation methodology is related to the fixed atmospheric forcing, with no representation of the atmospheric response to the presence of lakes. It is expected that adding a new lake component to the land surface will change the near-surface atmospheric fields. Since this new component will evaporate at the potential rate, one should assume that especially the near-surface relative humidity will change. A regional study based on measurements from high-latitude lakes (Rouse et al. 2005) found that lakes strongly enhanced evapotranspiration when added to a landscape, especially during autumn when vertical temperature and humidity gradients are larger. With more abundant water supply to the atmosphere, an increase of

the relative humidity is expected. However, a stronger free convective regime can also enhance a deepening of the boundary layer, thus reducing the relative humidity at the surface. An increase (or decrease) of the screen-level relative humidity will modify the water demand from the atmosphere, but such equilibrium can only be tested with coupled simulations.

In spite of the limitations of the stand-alone simulation methodology, the model performs as expected when compared with observed LSWTs and lake-ice duration. The impact of sub-grid scale lakes on surface fluxes was analyzed on a monthly scale and in different climates. In high-latitude regions, lakes change the terrestrial energy storage cycle, with increased storage during the summer and subsequent release during the autumn. In equatorial regions, lakes change the partition of energy fluxes to the atmosphere, with an increase of the latent heat flux and reduction of the sensible heat flux.

Further simulations are needed to properly investigate the impact of lakes on surface fluxes. Coupled atmosphere simulations are necessary but require significant computational resources. Nevertheless, the present work shows that lakes significantly impact on the surface energy and water balance. Global lake depths are required as the most important lake parameter. Besides the lake depth, the lack of global data on other lake related parameters, such as optical characteristics of lake water, is still an impediment to further progress.

Acknowledgments

This work was supported by the Portuguese Foundation for Science and Technology (FCT) under project AMIC PTDC/AAC-CLI/109030/2008 co-financed by the European Union under program FEDER. E. Dutra acknowledges the financial support of FCT under the grant SFRH/BD/35789/2007, and expresses his gratitude to ECMWF for travel support. Viktor Stepanenko's stay in Lisbon was supported by the European Commision FP6 Integrate Project WATCH, proj. no. 036946.

2.5 Appendix: Lake ice albedo

The lake ice albedo controls the amount of solar radiation penetrating the ice. The Ebert and Curry (1993) albedo climatology might not be suitable for lake ice, which could explain the results of WLns simulations (in section 2.3.1). A possible solution to mimic the snow insulating effect would be to change the lake ice albedo. The following empirical formulation for lake ice albedo (α_{LICE}), also used in the original FLake model, was implemented

$$\alpha_{Lice} = \alpha_w (1-\beta) + \alpha_b \beta$$
$$\beta = \exp\left[-95.6\left(\frac{T_f - T_{ice}}{T_f}\right)\right] \qquad (2.1)$$

where α_b and α_w are the blue and white ice albedo, respectively. The lake ice albedo varies between the maximum white ice albedo (for low lake ice temperatures T_{ice} , K) to the minimum blue ice albedo (melting temperature T_f , K) following the empirical exponential decay in Eq. (2.1) Several sets of values for the blue and white ice albedos were tested, and α_b=0.4 and α_w=0.7 were chosen. Ehn et al. (2006) reported observed values of ice albedo ranging between 0.52 and 0.95 for blue ice and 0.73 and 0.91 for white ice. Figure 2.8 compares the mean lake ice duration (in all grid points with lake ice formation) between the WL (with coupled snow) and WLns (but with lake ice albedo given by Eq.

(2.1)). In both simulations, lake ice duration is very similar for the three sets of lake depths tested. These results show that lake ice albedo given by Eq. (2.1) compensates for the snow insulation effect in terms of lake ice duration. The lake ice duration errors (not shown) are very similar to the WL simulation (in Figure 2.1). Nevertheless, the physical mechanisms are different. Snow insulates the ice (reducing its growth during the winter), while the changed albedo allows for much thicker lake ice, but with an acceleration of melting in spring.

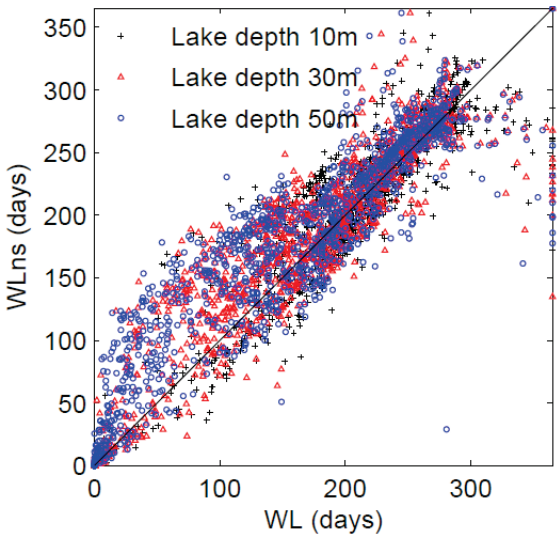

Figure 2.8. Mean lake ice duration simulations from WLns (with lake, no snow with lake ice albedo given by Eq. (2.1)*) versus the same quantity for WL (with lake) simulations.*

3

An Improved Snow Scheme for the ECMWF Land Surface Model: Description and Offline Validation*

Abstract

A new snow scheme for the European Centre for Medium-Range Weather Forecasts (ECMWF) land surface model has been tested and validated. The scheme includes a new parameterization of snow density, incorporating a liquid water reservoir, and revised formulations for the subgrid snow cover fraction and snow albedo. Offline validation (covering a wide range of spatial and temporal scales) includes simulations for several observation sites from the Snow Models Intercomparison Project-2 (SnowMIP2) and global simulations driven by the meteorological forcing from the Global Soil Wetness Project-2 (GSWP2) and by ECMWF Re-Analysis ERA-Interim. The new scheme reduces the end of season ablation biases from 10 to 2 days in open areas and from 21 to 13 days in forest areas. Global GSWP2 results are compared against basin-scale runoff and terrestrial water storage. The new snow density parameterization increases the snow thermal insulation, reducing soil freezing and leading to an improved hydrological cycle. Simulated snow cover fraction is compared against NOAA/National Environmental Satellite, Data, and Information Service (NESDIS) with a reduction of the negative bias of snow-covered area of the original snow scheme. The original snow scheme had a systematic negative bias in surface albedo when compared against Moderate Resolution Imaging Spectroradiometer (*MODIS*) remote sensing data. The new scheme reduces the albedo bias, consequently reducing the spatial- and time-averaged surface net shortwave radiation bias by 5.2 W m^{-2} in 14% of the Northern Hemisphere land. The new snow scheme described in this paper was introduced in the ECMWF operational forecast system in September 2009 (cycle 35R3).

---

* Dutra, E.[1,2], G. Balsamo[3], P. Viterbo[4], P. M. A. Miranda[1], A. Beljaars[3], C. Schar[2], and K. Elder[5], 2010: An Improved Snow Scheme for the ECMWF Land Surface Model: Description and Offline Validation, *J. Hydrometeor.*, **11**(4), 899-916.

Also available as ECMWF *technical memorandum N. 607.*

[1] Centro de Geofísica da Universidade de Lisboa, Instituto Dom Luiz, University of Lisbon, Lisbon, Portugal.

[2] Institute for Atmospheric and Climate Science, ETH, Zurich, Switzerland.

[3] European Centre for Medium-Range Weather Forecasts, Reading, United Kingdom.

[4] Institute of Meteorology, Lisbon, Portugal.

[5] Rocky Mountain Research Station, USDA Forest Service, Fort Collins, Colorado.

3.1 Introduction

The extent and variability of snow cover are important parameters in weather and climate prediction systems because of their effects on energy and water balances, justifying a strong dependency of surface temperature on the presence or absence of snow cover (Armstrong and Brun 2008). Eurasian snow cover has been linked with the variability of the Indian summer monsoon (Douville and Royer 1996; Liu and Yanai 2002; Robock et al. 2003) and with significant changes in the hemispheric circulation (Cohen et al. 2007; Fletcher et al. 2009b; Gong et al. 2007). Snow cover also acts as a water reservoir, which is released by snowmelt in spring, influencing runoff, soil moisture, evaporation, and thus precipitation and the entire hydrological cycle (e. g. Douville et al. 2002; Groisman et al. 2004). Therefore, an accurate simulation of snowprocesses is essential for many applications ranging from hydrological forecast to numerical weather prediction (NWP), seasonal forecast, and climate modeling. Observed climate change during the twentieth century, particularly visible in the Northern Hemisphere surface warming in spring, has been significantly enhanced by the associated depletion of snow cover (Groisman et al. 1994a).

The presence of snow modulates the exchanges between the atmosphere and the surface. When compared with other natural surfaces, snow is remarkable in three different ways: an anomalously high albedo, an anomalously low thermal conductivity, and the ability to change phase (sometimes leading to coexisting liquid and solid water reservoirs). High surface albedo in the presence of snow causes rapid shifts in surface reflectivity in autumn and spring at high latitudes. Viterbo and Betts (Viterbo and Betts 1999) showed that changing the albedo of boreal forest in the presence of snow in the European Centre for Medium-Range Weather Forecasts (ECMWF) model reduced the model systematic cold bias at the surface at high northern latitudes in spring. Changes in the snow cover fraction and in its subgrid-scale variability are largely responsible for the observed interannual variability of surface albedo (Roesch and Roeckner 2006). On the other hand, the large amount of energy required to melt ice means that snow retards warming during the melting period. When melting occurs but is incomplete, liquid water may remain in the snowpack, significantly changing its properties and allowing for later refreezing. Because of that, the representation of a heterogeneous snowpack is important (Rutter et al. 2008), as are the effects of incident rainfall on the energy and mass balances (Belair et al. 2003). The thermal insulation property of snow also has important climatic consequences. Cook et al. (2008) evaluated the impact of snow thermal conductivity in a climate model, reporting changes in soil temperature up to 20 K and in the air temperature up to 6 K during winter, just by prescribing snow thermal conductivity to its observed upper and lower limits. Grippa et al. (2005) showed that later snowmelt dates and thicker winter snowpacks are related to higher normalized difference vegetation index (NDVI) values over a large latitudinal band around 65°N. The authors suggested that this could be related to either an increased water availability for plants after snowmelt, or thermal insulation of the soil by snow.

The different treatment of snow processes in land surface models (LSMs) has been demonstrated in several offline LSM intercomparison experiments. The Tiled ECMWF Scheme of Surface Exchanges over Land (TESSEL) (a previous version of the model, but with the same snow scheme) participated in the Thorne–Kalix experiment (Nijssen et al. 2003; Van den Hurk and Viterbo 2003), the Rhône Aggregation experiment (Boone et al. 2004), and the Snow Models Intercomparison Project-2 (SnowMIP2) (Essery et al. 2009; Rutter et al. 2009). Initial results of TESSEL in SnowMIP2 revealed

some model weaknesses, such as early snowmelt in open sites and late melting in forest sites. These results motivated the development of the revised snow model described in the present paper.

Snow parameterizations in LSMs used in NWP, climate modeling, and in various applications such as hydrological forecasting or avalanche prediction vary greatly in complexity. Boone and Etchevers (2001) divided snow schemes in three general categories according to their complexity: 1) simple force-restore or single explicit snow layer schemes (Douville et al. 1995; Slater et al. 1998; Verseghy 1991; Yang et al. 1997); 2) detailed internal-snowprocess schemes (Anderson 1976; Brun et al. 1989; Jordan 1991); and 3) intermediate-complexity schemes based on class 2 but using simplified versions of the physical parameterizations (Boone and Etchevers 2001; Loth et al. 1993; Lynch-Stieglitz 1994; Sun et al. 1999). The Hydrology Tiled ECMWF Scheme of Surface Exchanges over Land (HTESSEL, Balsamo et al. 2009; Van den Hurk et al. 2000; Viterbo and Beljaars 1995) included in the ECMWF model has a simple snow scheme, lying within the first category, with an explicit snow layer similar to the schemes described in Verseghy (1991) and Douville et al. (1995).

The present work describes a revision of HTESSEL's snow scheme and its validation. The snow scheme revision includes four main processes: 1) representation of liquid water content as a diagnostic, following a similar approach applied to soil phase changes by Viterbo et al. (1999); 2) new snow density parameterization following Anderson (1976) and Boone and Etchevers (2001); 3) revised snow cover fraction; and 4) revision of exposed snow albedo and new forest albedo in the presence of snow adapted from Moody et al. (2007). When compared to the original snow scheme three main differences can be identified: (i) dry versus wet snow in new scheme, (ii) simple exponential increase of snow density against a more physically based formulation in the new scheme, and (iii) constant forest albedo in the present of snow against a vegetation cover type dependence based on observations in the new scheme. The changes to the model (section 3.2) were performed keeping the same level of complexity (single explicit snow layer). This constraint allowed a simple integration with the ECMWF Integrated Forecast System (IFS) in its several applications ranging from data assimilation for short-range weather forecast to seasonal prediction. Offline validation covering several spatial and temporal scales considered (i) site simulations for several observation locations from SnowMIP2 (section 3.3), and (ii) global simulations driven by the meteorological forcing from the Global Soil Wetness Project 2 (GSWP2) (Dirmeyer et al. 1999; Dirmeyer et al. 2002; Gao et al. 2004) and by ECMWF Re-Analysis ERA-Interim (Dee et al. 2011). GSWP2 Results are compared against basin-scale runoff and terrestrial water storage variation (TWSV) in section 3.4. In section 3.5 ERAI simulated snow cover fraction and surface albedo are compared with remote sensed products. Model results are presented and discussed throughout the text and the main conclusions of the work are summarized in section 3.6.

3.2 Models

3.2.1 HTESSEL

HTESSEL represents vertical transfers of water and energy using four vertical layers to represent soil temperature and moisture. The model evaluates the land surface response to the atmospheric forcing and estimates the surface water and energy fluxes along with the temporal evolution of the snowpack, soil temperature, and moisture. At the interface between the surface and the atmosphere, each grid box is divided into fractions (tiles), with up to six fractions over land (bare ground, low and high

vegetation, intercepted water, shaded and exposed snow). Each fraction has its own properties defining separate heat and water fluxes used in the energy balance equation solved for the tile skin temperature. The snow scheme in HTESSEL is an energy- and mass balance model that represents an additional layer on top of the upper soil layer, with independent prognostic thermal and mass contents. The formulation of the snow mass [or snow water equivalent (SWE)] and energy budgets in HTESSEL are described in the appendix (section 3.7) along with the snow density and albedo parameterizations.

3.2.2 Revised snow scheme

Snow liquid water content

The HTESSEL snow scheme does not account for snow liquid water (SLW) in the snowpack (see appendix). A proper consideration of the SLW requires several modifications: (i) the thermal effects related to the latent heat of fusion (Tribbeck et al. 2006), (ii) changes in the snow runoff [following Rutter et al. (2008), as opposed to the current scheme in which melted snow leaves the snowpack immediately], and (iii) interception of rainfall by the snowpack [as in Belair et al. (2003) correcting for the rainfall bypass of the snowpack in the current scheme].

The snow energy budget, in Eq. (3.17) in the presence of SLW changes can be written as

$$\begin{aligned} (\rho C)_{sn} D_{sn} \frac{\partial T_{sn}}{\partial t} &= R_{sn}^{N} - H_{sn} - L_s E_{sn} - G_{sn}^{B} - L_f M_{sn} - Q_{sn}^{INT} \\ Q_{sn}^{INT} &= L_f M_{sn}^{INT} = L_f \frac{\partial S_l}{\partial t} \end{aligned} \tag{3.1}$$

where $(\rho C)_{sn}$ is the snow volumetric heat capacity (J m^{-3} K^{-1}); D_{sn} is the snowpack depth (m); T_{sn} is the snow temperature (K); and the energy fluxes R_{sn}^{N}, H_{sn}, and G_{sn}^{B} are the net radiation (shortwave and longwave), sensible heat flux, and basal heat flux (W m^{-2}), respectively. The mass fluxes E_{sn} and M_{sn} are the snow sublimation and melting (kg m^{-2} s^{-1}), respectively, that are associated with the latent heat of sublimation L_s and fusion L_f (J kg^{-1}). The superscript INT denotes internal phase changes, where Q_{sn}^{INT} is the heat change associated with internal phase changes, and S_l is the snow liquid water content (SLW) (kg m^{-2}). Without loss of generality, it can be assumed that for the grid squares characteristic of NWP,

$$S_l = S_l\left(T_{sn}, S, \rho_{sn}\right) \approx f\left(T_{sn}\right) S_l^{c}\left(S, \rho_{sn}\right) \tag{3.2}$$

where S_l^{c} (kg m^{-2}) is the snow liquid water capacity, S (kg m^{-2}) is the sum of snow and water in the snowpack (also referred as SWE along the text), and ρ_{sn} is the snow density (kg m^{-3}). The snow temperature function is prescribed in an analytical form—following a similar approach described by Viterbo et al. (Viterbo et al. 1999) for soil phase changes:

$$f\left(T_{sn}\right) = \begin{cases} 0 & , T_{sn} < T_f - d/2 \\ 1 + \sin\left(\dfrac{\pi\left(T_{sn} - T_f\right)}{d}\right) & , T_{sn} \geq T_f - d/2 \end{cases} \tag{3.3}$$

where T_f is the melting temperature for water and d is a characteristic temperature difference, with respect to T_f, limiting the phase change regime. In the numerical implementation d = 4 K was chosen.

Snow liquid water capacity is approximated as a function of SWE and snow density, following Anderson (1976)

$$S_l^c = S\left[r_{l,\min} + \left(r_{l,\max} - r_{l,\min} \right) \max\left(0, \rho_{sn,l} - \rho_{sn}\right) \Big/ \rho_{sn,l} \right] \tag{3.4}$$

with the constants $r_{l,min}$ = 0.03, $r_{l,max}$ = 0.1, and $\rho_{sn,l}$ =200 kg m^{-3}. This equation is a simple parameterization of a very complex phenomenon and has been used recently in other snow schemes for NWP, for example, Boone and Etchevers (2001).

Combining Eqs. (3.1) and (3.2) results in a modified snow energy budget equation,

$$\left[\left(\rho C\right)_{sn} D_{sn} + L_f S_l^c \frac{\partial f\left(T_{sn}\right)}{\partial T_{sm}} \right] \frac{\partial T_{sn}}{\partial t} = R_{sn}^N - L_s E_{sn} - H_{sn} - G_{sn}^B - L_f M_{sn} \tag{3.5}$$

with one extra term in the lhs of the equation, that can be interpreted as an additional snow heat capacity - or heat capacity barrier. In compacted snowpacks, the representation of SLW as a diagnostic increases the snow heat capacity by a factor of 5 **(**Figure 3.1**).** This increase acts as a heat barrier near T_f, representing the increased snow temperature inertia due to freeze–melt events.

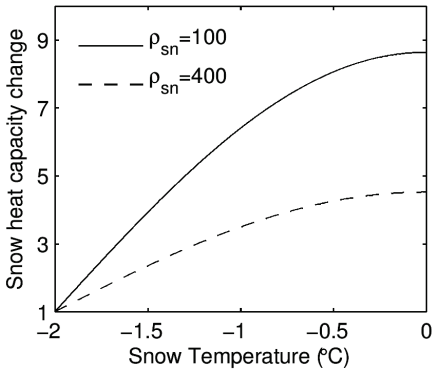

Figure 3.1. Ratio between the apparent snow heat capacity [multiplicative term in the lhs of Eq. (3.5) *] and snow heat capacity [multiplicative term in the lhs of Eq.* (3.17)*], as function of snow temperature for constant SWE of 100 kg m^{-2} and snow densities of 100 (solid line) and 400 (dashed line) kg m-^{3}.*

This diagnostic approach for SLW also allows the representation of rainfall interception. The new snow mass balance reads as

$$\frac{\partial S}{\partial t} = F + c_{sn} F_l - c_{sn} E_{sn} - R_{sn} \tag{3.6}$$

where F, F_l, and R_{sn} are the mass fluxes of snowfall, rainfall, and runoff (kg m^{-2} s^{-1}), and c_{sn} is the snow cover fraction. Rainfall is considered to reach the snowpack at T_f, and the latent heat released by the freezing of the intercepted rainfall, if $T_{sn} < T_f$, is also accounted in the energy-balance solution. Runoff is defined as the rate at which liquid water leaves the snowpack and parameterized as follows:

$$R_{sn} = c_{sn} M_{sn} + \max\left(c_{sn} F_l - \frac{S_l^c \left(1 - f\left(T_{sn}\right)\right)}{\Delta t}, 0 \right). \tag{3.7}$$

Liquid water is generated by melting (M_{sn}) and by rainfall interception (F_l). When snow liquid water content exceeds the snow liquid water capacity [defined in Eq.(3.4)] runoff is generated.

Snow density

The original snow density parameterization assumed an exponential evolution toward a maximum density [Eq. (3.19)]. In the new scheme, the rate of density change is parameterized as

$$\frac{1}{\rho_{sn}}\frac{\partial \rho_{sn}}{\partial t} = \frac{\sigma_{sn}}{\eta_{sn}\left(T_{sn,}\rho_{sn}\right)} + \xi_{sn}\left(T_{sn},\rho_{sn}\right) + \frac{\max\left(0,Q_{sn}^{INT}\right)}{L_f\left(S-S_l\right)} \tag{3.8}$$

where the first two terms represent overburden and thermal metamorphism (Anderson 1976; Boone and Etchevers 2001), respectively, and the last term represents the compaction related to meltwater retained in the snowpack, adapted from Lynch-Stieglitz (1994). In the overburden term [first term on the rhs of Eq. (3.8)], σ_{sn} and η_{sn} are the pressure of the overlaying snow (Pa) and snow viscosity (Pa s), respectively. Melted water retained in the snowpack led to a decrease of snow depth while keeping the SWE constant. Following the original scheme, in snowfall conditions a weighted average is taken between the current snow density and the density of snowfall [see Eq. (3.18)]; the updated snow density is used in the rhs of Eq. (3.8). Snowfall density is changed from a constant value, in the original scheme, to an expression from CROCUS (Brun et al. 1992; Brun et al. 1989) where fresh snow density (ρ_{new}) is a function of near-surface air temperature and wind speed [see also Boone and Etchevers (2001)]

$$\rho_{new} = a_{an} + b_{sn}\left(T_{air} - T_f\right) + d_{sn}\left(V_{air}\right)^{1/2} \tag{3.9}$$

where T_{air} and V_{air} are the near surface air temperature (K) and wind speed (m s^{-1}), respectively. The coefficients are a_{sn}=109 kg m^{-2}, b_{sn}=6 kg m^{-3}, and d_{sn}=26 kg m$^{-7/2}$. Snow density is constrained to be between 50 and 450 kg m^{-3}.

The snow viscosity is formulated following Anderson (1976) as

$$\eta_{sn} = \eta_0 \exp\left(a_\eta\left(T_f - T_{sn}\right) + b_\eta \rho_{sn}\right) \tag{3.10}$$

where η_0=3.7 × 10^7 Pa s, a_η=8.1 ×10^{-2} K^{-1} and b_η=1.8×10^{-2} m^3 kg^{-1}. The pressure of the overlying snow is given by $\sigma_{sn} = \frac{1}{2} S \times g$, where g is the standard gravity (m^2 s^{-2}).

The thermal metamorphism (second term on the rhs of Eq. (3.8)) is parameterized as

$$\xi_{sn} = a_\xi \exp\left[-b_\xi\left(T_f - T_{sn}\right) - c_\xi \max\left(0,\rho_{sn} - \rho_\xi\right)\right] \tag{3.11}$$

using the constant values of Anderson (1976): a_ξ = 2.8×10^{-6} s^{-1}, b_ξ = 4.2×10^{-2}, c_ξ = 460 m^3 kg^{-1}, and ρ_ξ = 150 kg m^{-3}.

Snow cover fraction

Snow cover fraction in the original scheme was only a function of SWE [see Eq. (3.15)], whereas the new formulation depends on both SWE and snow density:

$$c_{sn} = \min\left(1, \frac{S/\rho_{sn}}{0.1}\right) \tag{3.12}$$

This new formulation, although very simple, is expected to represent the hysteresis of snow cover between the beginning of the cold season (low snow densities) and the later stage of ablation (high snow densities). In the beginning of the cold season a reduced amount of SWE is needed to fully cover an entire grid box. During the ablation period, the emergence of snow-free patches reflects the need of much more SWE to have a fully covered grid box. Figure 3.2 shows the different paths of snow cover fraction as function of SWE for a low-and high-density snowpack. The original parameterization [Eq. (3.15)] lies between the two extremes of snow densities.

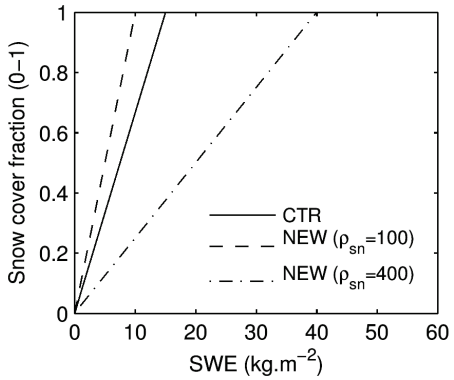

Figure 3.2. Snow cover fraction as function of SWE as in the original HTESSEL snow scheme [solid line, Eq. (3.15) *], and new [Eq.*(3.12) *] for snow densities of 100 (dashed line) and 400 (dashed dotted line) kg m^{-3}.*

Snow albedo

Snow albedo in exposed areas evolves according to the original scheme with an exponential or linear decay in melting and non-melting conditions, respectively [see Eq. (3.20)]. In the revised scheme the melting formulation for albedo decay is also activated when $T_{sn} \geq T_f$-2. The representation of SWL as a diagnostic [Eqs. (3.1)-(3.3)] is also activated, with internal phase changes, above this temperature threshold. The definition of this temperature threshold for both SLW and albedo decay also accounts for the subgrid-scale variability of the snowpack properties for typical climate and NWP resolutions.

The original snow albedo in exposed areas was reset to its maximum value when $F > 1$ kg m^{-2} h^{-1}. This threshold, and its definition, has been reported as a drawback in this type of snow albedo parameterization (Molders et al. 2008; Pedersen and Winther 2005), which is also used in other NWP models. To reduce the importance of the threshold a continuous reset was implemented:

$$\alpha_{sn}^{t+1} = \alpha_{sn}^{t} + \min\left(1, \frac{F\Delta t}{10}\right)\left(\alpha_{max} - \alpha_{sn}^{t}\right) \tag{3.13}$$

where α_{sn} is the snow albedo. Superscripts t and $t+1$ represent the current and next time step, respectively, and Δt is the model time step (s). This formulation assumes that 10 kg m^{-2} of fresh snowfall are needed to reset the snow albedo to its maximum value ($\alpha_{max} = 0.85$).

The albedo of shaded snow (snow under high vegetation) was changed from a constant value of 0.15 to a vegetation-type-dependent albedo (Table 3.1) adapted from Moody et al. (2007). Moody et al. (2007) provide 5-yr (2000–04) climatological statistics of Northern Hemisphere broadband (0.3–5.0 μm) white-sky albedo for the 16 International Geosphere-Biosphere Program (IGBP) ecosystem classes when accompanied by the presence of snow on the ground. The statistics were obtained using

validated, high quality Moderate Resolution Imaging Spectroradiometer (*MODIS*) land surface albedo data, flagged as snow in the associated quality assurance fields. The retuned forest albedo toward significantly higher values accounts implicitly for trees' intercepted snow effect, which is neglected in the current scheme.

Table 3.1. Mean values of Northern Hemisphere 5-yr (2000–04) broadband surface albedo (in presence of snow) aggregated by high vegetation type (adapted from Moody et al. 2007).

Vegetation type	Albedo
Evergreen needleleaf trees	0.27
Deciduous needleleaf trees	0.33
Deciduous broadleaf trees	0.31
Evergreen broadleaf trees	0.38
Mixed forest–woodland	0.29
Interrupted forest	0.29

3.3 Site validation

3.3.1 Simulation setup and observations

Different sets of experiments were performed (Table 3.2). These experiments include the original (CTR) and new (NEW) snow schemes and intermediate model configurations with progressive activation of the described changes to the model. All the activated parameterizations were described in the previous section except liquid water prognostic plus rainfall interception (LWPR) and new snow scheme with prognostic liquid water (NEW_PR; Table 3.2). In those two experiments SLW is represented using a prognostic approach. In this approach a new prognostic equation for SLW was implemented following very simple assumptions: i) SLW only coexists with ice when $T_{sn} = T_f$, ii) melted snow goes to the SLW reservoir with maximum capacity defined by Eq. (3.4), and iii) snow runoff is generated when the amount of SLW exceeds the liquid water holding capacity. This parameterization is not described in detail since its formulation is not essential to the discussion.

HTESSEL, with its original snow scheme, participated in the SnowMIP2 intercomparison project. Rutter et al. (2009) and Essery et al. (2009) report the main conclusions of the project along with information regarding the different observational sites, which included five locations with data in both open and forest sites for two winter seasons: Alptal (47°3'N, 8°43'E, 1200 m, Switzerland), Berms (53°55'N, 104°42'W, 579 m, Canada), Fraser (39°53'N, 105°53'W, 2820 m, United States), Hitsujigaoka (42°59'N, 141°23'E, 2820 m, Japan, only one winter), and Hyytiaälä (61°51'N, 24°17'E, 181 m, Finland) (see also Figure 3.8). Near-surface atmospheric forcing data were available for all locations and observations include snow depth, snow density, and SWE. Simulations were performed for all five SnowMIP2 locations summing a total of 18 different cold seasons 3 sites. Initial conditions and climatological data were made available by the data providers.

The results of TESSEL presented by Rutter et al. (2009) are not identical to the CTR results presented in this paper. The model has the same snow and soil hydrology, but the surface roughness lengths were changed from input fields to land cover type dependent. In the present paper, all the simulations

were performed with the revised roughness lengths. That modification improved the simulations over forested areas. Such changes are prior to the development of the new snow scheme and, because of its different physical and technical nature, they are not described or discussed here.

Table 3.2. Sensitivity experiments acronyms and respective activated parameterizations.

Exp. name	Parameterizations activated
CTR	- (see appendix 3.7 for description)
DENS	Snow density [Eq. (3.8)]
LWD	Snow density + liquid water diagnostic [Eq. (3.5) + Eq. (3.6), setting $F_l = 0$]
LWDR	LWD + rainfall interception [Eq. (3.6)]
LWDR_A	LWDR + exposed snow albedo [Eq. (3.13)]
LWDR_FA	LWDR + forest snow albedo (Table 3.1)
LWDR_AFA	LWDR+ exposed snow albedo [Eq. (3.13)]+ forest snow albedo (Table 3.1)
LWDR_SC	LWDR + snow cover fraction [Eq. (3.12)]
NEW	LWDR_AFA + snow cover fraction [Eq. (3.12)]
LWPR*	Snow density + liquid water prognostic + rainfall interception
NEW_PR*	LWPR + exposed snow albedo + forest snow albedo + snow cover fration

* *Prognostic representation of snow liquid water content*

3.3.2 Snow depth, density and SWE

Model results and observations of SWE, snow depth, and snow density for the 2004/05 winter season in the Fraser open and forest sites are shown in Figure 3.3. CTR and NEW underestimate SWE (Figure 3.3 a, d) from the beginning of the winter season throughout mid-spring in both forest and open sites, suggesting either too much melting or excessive sublimation. During the ablation period, CTR showed an early melting in the forest site and a late melting in the open site. These distinct errors between open and forest sites during the ablation period were also observed in other SnowMIP2 locations (not shown). Averaged for all 18 CTR simulations, the final ablation is delayed by 10 days and accelerated by 21 days in open and forest sites, respectively. The NEW snow scheme prediction of final ablation is closer to observations with an average delay of 2 days in open sites (6 out of 9 improved) and an acceleration of 13 days in forest sites (8 out of 9 improved).

Figure 3.3 c, f compare simulated versus observed snow density. Snow density is overestimated by CTR throughout the winter season until the final ablation period when it is underestimated. The simulations show a fast [exponential—Eq. (3.19)] density increase in the beginning of the winter, keeping snow density close to its maximum value of 300 kg m^{-3} during the remaining cold season. This behavior was observed in all available locations. The NEW snow density is closer to the observations representing the low densities during the accumulation stage and the fast increase in the final ablation. Snow depth in CTR and NEW was underestimated in both sites (Figure 3.3 b, e), resulting from the SWE underestimation. However, NEW snow depth has a reduced error, when compared with CTR, because of the significant improvement of snow density.

3.3.3 Snow and soil temperature

Simulated snow and soil temperatures at the Fraser open site during the 2004/05 winter are compared against observations in Figure 3.4.Observations of snow temperature were conducted using a thermocouple string at fixed depths, every 10 cm up to 180 cm. Mean snowpack temperature was derived by averaging the thermocouple observations covered by snow, where snow depth was measured using an acoustic sensor. The observed mean snowpack temperature (Figure 3.4 a) has a lower thermal amplitude than CTR and NEW, and both simulations underestimate snow temperature throughout the cold season. In a single layer snow scheme it is not possible to represent properly the thermal insulation within the snowpack. This explains the differences between simulated and observed mean snowpack temperature. However, at the end of the cold season, NEW reaches the freezing point faster than CTR and stays in an isothermal state, as the observations suggest, while CTR shows some cooling cycles.

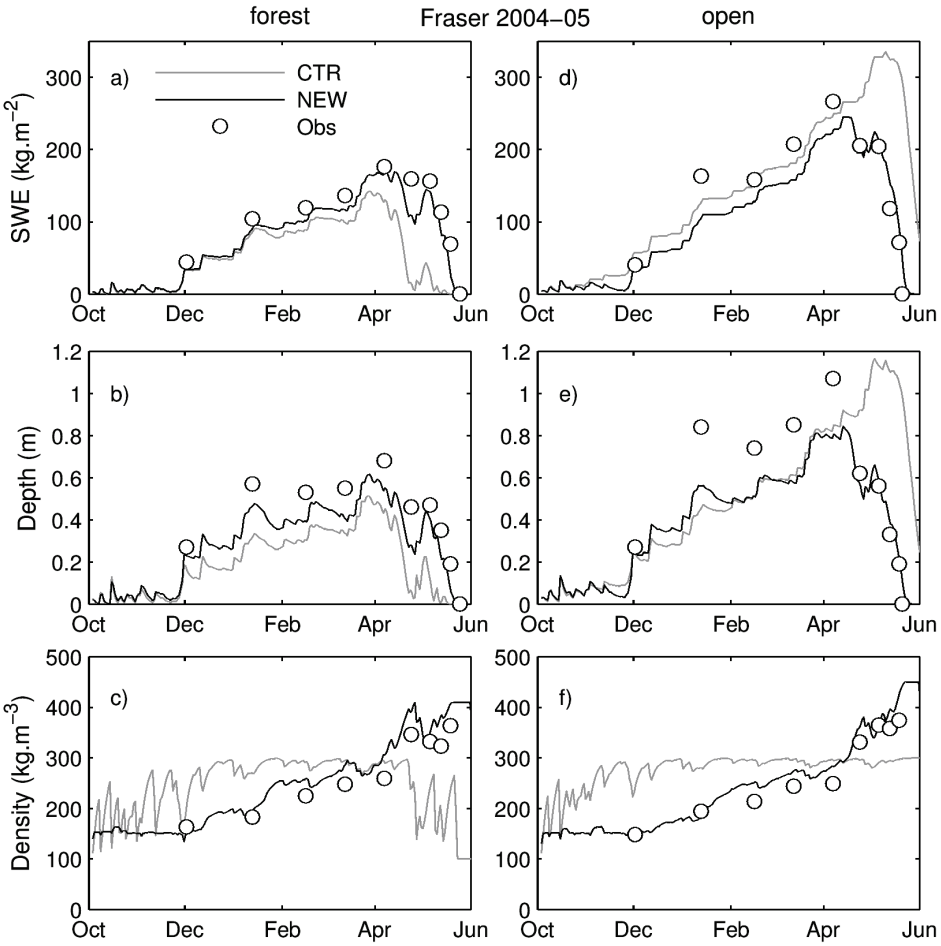

Figure 3.3. Simulations results for CTR (gray) and NEW (black) for the 2004/05 winter season at (left) Fraser forest and (right) open sites: (a),(d) SWE, (b),(e) snow depth, and (c),(f) snow density. Observations are represented by open circles.

Simulated soil temperatures respond to the different basal heat fluxes, due to the increased insulation in NEW, with a faster cooling in CTR when compared with NEW (Figure 3.4 b, c). This behavior is observed both near the surface and at 50-cm depth. Averaged from December to mid-May CTR has a negative bias of -5.2 and -3.9 K at 5- and 50-cm depth, respectively. NEW reduces significantly the soil temperature bias to -1.8 and -1.3 K at 5- and 50-cm depth, respectively. NEW improves the

prediction of final ablation (see Figure 3.3 d), which affects soil heating after snow disappearance. There is a reduction of the soil temperature bias near the surface by the end of May from -11.4 K in CTR to -2.8 K in NEW.

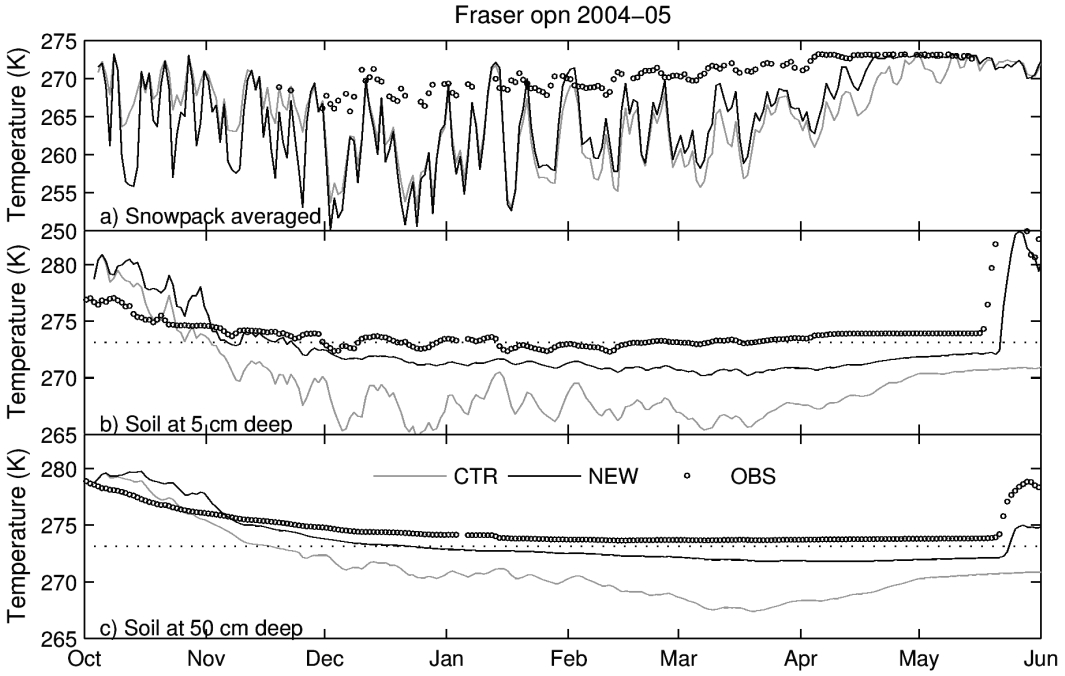

Figure 3.4. Model-simulated (a) snow temperature and soil layer temperature at (b) 5-cm depth and (c) 50-cm depth by CTR (gray) and NEW (black) for the 2004/05 winter season in Fraser open site. The simulations and observations (open circles) represent daily means.

3.3.4 Sensitivity to activated parameterizations

Sensitivity tests, where the components of NEW were gradually activated, are detailed in Table 3.2. The comparison was made to the root-mean-square errors (RMSE) in modeled SWE normalized by standard deviations of the observations (errors in snow depth, rather than SWE, were calculated for Hitsujigaoka and Hyytiaälä open sites). Figure 3.5 summarizes the RMSE for all locations classified as open or forest sites. The new snow density (DENS) has a limited impact on SWE simulation, whereas, when combined with SLW representation [liquid water diagnostic (LWD)], it improves SWE in forest sites. The interception of rainfall in the snowpack (LWDR) has also a positive impact on forest sites simulations, while keeping the open plots unchanged. The changed albedo formulation (LWDR_AFA) shows a significant improvement in open sites, with a small impact on forest sites. When all the new components are activated (NEW) the RMSE of SWE is lower than any of the other experiments in both open and forest sites. Open sites had a delayed ablation in CTR, which was mainly reduced with the new exposed albedo formulation. The early ablation in forest sites was corrected mainly by the incorporation of SLW. This shows that the underlying physical processes responsible for the observed biases in open and forest sites were of different nature: i) early melting in forest sites due to neglecting the refreezing of melted liquid water and ii) late melting in open sites due to an underestimation of absorbed solar radiation resulting from an overestimation of snow albedo.

SLW is often represented in snow schemes following a prognostic approach. The experiments LWPR and NEW_PR were conducted to analyze the impact of such approach when compared to the

diagnostic implementation described in this paper. This simple validation aims to examine whether the approaches are comparable, not to decide which one is better. The RMSE of SWE in LWPR is comparable with LWDR for forest sites, but LWPR has a better performance than LWDR in open plots. On the other hand, the inclusion of all physical mechanisms in NEW_PR dilutes the advantages of the prognostic water reservoir.

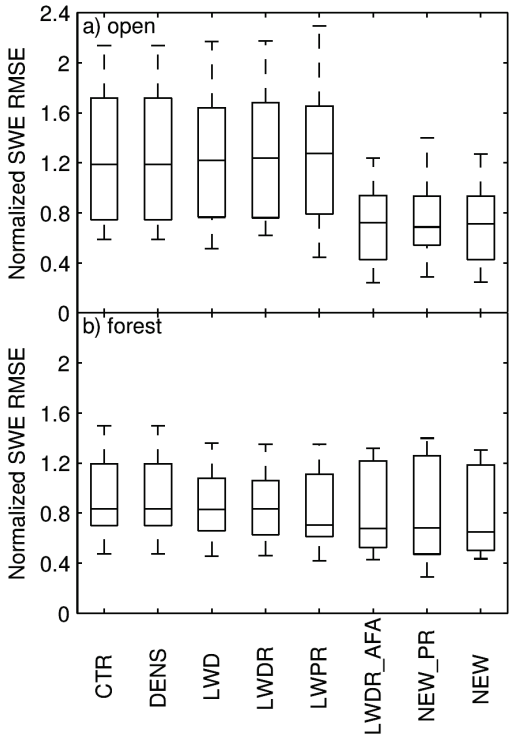

Figure 3.5. Box plot summaries describing the normalized RMSE of SWE for different model configurations, combined at all SnowMIP2 locations at (a) open sites and (b) forest sites. The boxes have horizontal lines at the lower quartile, median, and upper quartile and the whiskers (vertical lines) extend from the end of each box to 1.5 x the interquartile range; outliers beyond this range are represented by + symbols.

3.4 Basin-scale validation

3.4.1 Simulation setup

GSWP2 provides a set of near-surface forcing to drive land surface schemes in an offline mode. The atmospheric forcing data are provided at a resolution of 1° globally. In the current work, we have used the latest release ofGSWP2 atmospheric forcing based on the 40-yr ECMWF Re-Analysis (ERA-40, Uppala et al. 2005) where only precipitation is corrected using the Global Precipitation Climatology Project (GPCP) dataset. The dataset is available for the period January 1986 to December 1995. Surface pressure, air temperature, and specific humidity at 2-m, and wind at 10-m, are provided as instantaneous values. Downward surface radiation fluxes and precipitation fluxes represent 3-h averages. Climatological data, such as land-cover and vegetation types, were interpolated to a 1° x 1° grid from ERA-40.

3.4.2 Basins and observations

Terrestrial water storage is the sum of all forms of water storage on the land surface. Seasonal and interannual variations in storage are determined by the combined effect of soil moisture, groundwater, snow cover, and surface water. Diagnostics of monthly TWSV for 41 midlatitude basins all over the globe were used to validate the new snow scheme. The Basin Scale Water Balance (BSWB) dataset described in Hirschi et al. (2006) was derived with the combined atmospheric and terrestrial water-balance approach (Seneviratne et al. 2004) using conventional streamflow measurements and vertically integrated atmospheric moisture convergence data from ERA-40. The runoff data are partially composed of data from the Global Runoff Data Centre (GRDC) and other local sources. In the following discussion HTESSEL simulations were spatially aggregated for each basin.

Such large-scale basins are composed by many types of land cover, rivers, and lakes, each one with different hydrological characteristics. Simulated integrated values such as runoff and TWSV were spatially averaged. This simple procedure neglects river routing and effects of water and soil freezing. Such processes may delay basin streamflow when compared with instantaneous local runoff. However, the BSWB dataset consists of monthly data, which are compared against time-averaged monthly simulated fluxes. This approach has been also used by Balsamo et al. (Balsamo et al. 2009) during the validation of HTESSEL soil hydrology.

3.4.3 Impact in the Ob basin

The Ob River is a major river in western Siberia, Russia. The basin consists mostly of steppe, taiga, swamps, tundra, and semi-desert, with an average high vegetation fraction of 50%. Basin-averaged simulated SWE, snow density, percentage of frozen surface, and runoff are presented in Figure 3.6 for the 1989–90 period. SWE simulated by the new snow scheme is higher than in CTR (Figure 3.6a). The interception of rainfall in the snowpack was 53 mm, while snowfall was 218 mm. The additional accumulation of 53 mm to the snowpack in NEW explains the differences in SWE, resulting in a 14-day difference during final ablation between NEW and CTR. As in the SnowMIP2 Fraser site simulations (Figure 3.3), snow density is lower in NEW throughout the winter, reaching higher values than CTR only during the ablation period.

Lower snow density and higher SWE result in a thicker snowpack, with an increased insulation effect. The percentage of frozen soil in Figure 3.6c is the fractional basin area where the uppermost soil layer (0–7 cm) is frozen. The increased insulation in NEW reduces soil cooling, which reduces soil freezing. In CTR the basin surface is completely frozen from January to mid-February, while in NEW only 20%–30% of the basin is frozen. The runoff partitioning between surface and bottom drainage is shifted in NEW, with a reduction of surface runoff (Figure 3.6d) and an increase of bottom drainage (Figure 3.6e). In HTESSEL all rainfall and melted water are discharged as surface runoff when the first soil layer is frozen. The NEW snow scheme reduces soil freezing, thereby reducing surface runoff and increasing soil water storage. The overall impact in total runoff is represented in Figure 3.6f where NEW and CTR are compared against BSWB monthly data. The peak runoff date is accelerated and volume overestimated by CTR and NEW. However, the NEW snow scheme improves both the timing and magnitude of the total basin runoff.

3.4.4 Monthly TWSV and runoff

Figure 3.7 compares the mean annual cycles of simulated runoff and TWSV with BSWB data over the Ob and Mackenzie basins. The mean annual cycles of CTR runoff show an early peak in both basins with overestimation in the Ob but with a correct volume in Mackenzie. Both timing and volume are improved in NEW over the Ob basin (as discussed before), while the volume in the Mackenzie is poorer than in CTR. The simulated TWSV in CTR displays timing errors similar to the runoff in both basins. The increased water storage during spring in NEW resulted in a better agreement with BSWB TWSV during summer. The reduction of total runoff in both basins in NEW was compensated by an increase in evapotranspiration, especially during spring (not shown). Less soil freezing and early thaw increase evapotranspiration in NEW, since more water is available for the plant root uptake.

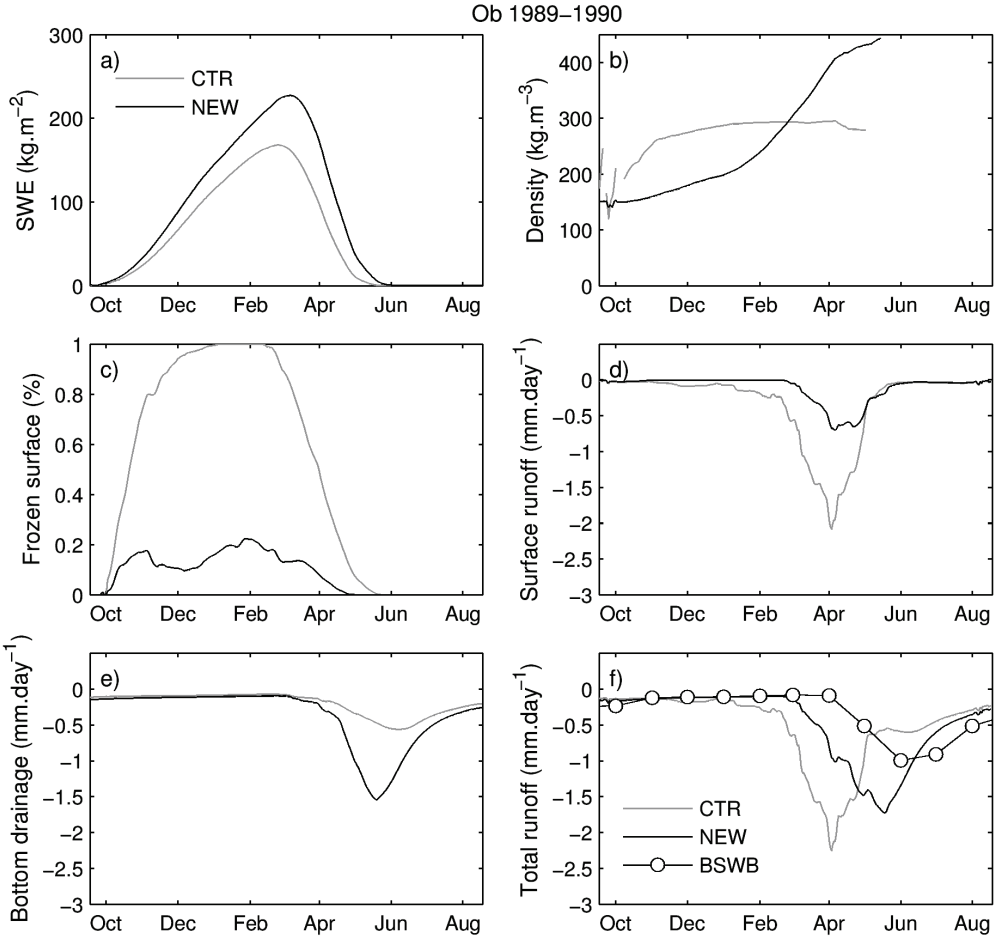

Figure 3.6. Simulation results for CTR and NEW during the period October 1989 to August 1990 spatially averaged for the Ob basin: (a) SWE, (b) snow density, (c) fraction of basin area frozen at the surface, (d) surface runoff, (e) bottom drainage, and (f) total runoff. Total runoff simulations are compared with monthly BSWB data. Simulated daily data were smoothed with a 30-day moving average.

Table 3.3 summarizes the RMSE of runoff in 10 high latitude basins, corresponding to the subset of the original 41 basins of the BSWB dataset where more than 30% of available data has mean snow cover duration exceeding 100 days. The mean snow cover duration was calculated for all grid points and then averaged for each basin using the CTR simulation. For all the basins with snow cover duration less than 100 days the differences between CTR and NEW are negligible. This result is due to the smaller impact of snow in the hydrological cycle.

Figure 3.8 represents the location and runoff RMSE improvement between NEW and CTR for the 10 basins listed in Table 3.3. The figure highlights central Siberia as the area with higher improvements in runoff. These results show that the inclusion of the new snow density, with higher insulation, was more effective in flat terrain areas dominated by low vegetation/bare ground, where the shading effects of high vegetation and subgrid orography variability (not addressed in this model revision, and with a very simplified treatment in the model) play a secondary role.

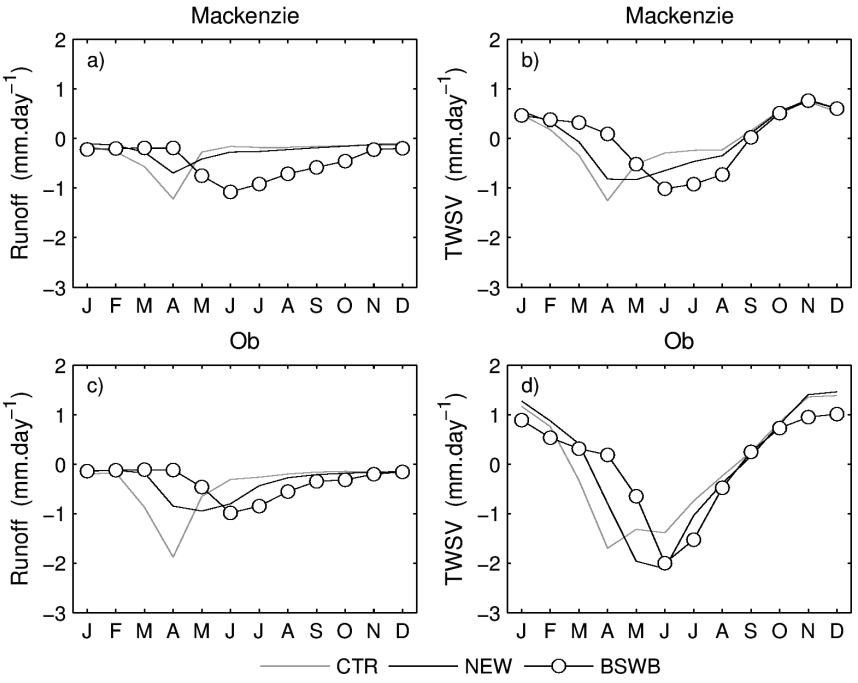

Figure 3.7. Mean annual cycles of (a),(c) runoff and (b),(d) TWSV in (top) Mackenzie and (bottom) Ob basins simulated by CTR and NEW during GSWP-2 period and compared with BSWB data.

Table 3.3. RMSE of simulated vs BSWB runoff in 10 high-latitude basins. Simulations forced by GSWP2 for the period 1986–95. For each basin are presented the catchment area (adapted from Hirschi et al. (2006), mean snow cover (SC) duration, and mean annual amplitude of runoff.

				Runoff RMSE (mm day^{-1})			
Basin	**Catchment area (km^2)**	**SC duration (days)**	**Runoff (mm day^{-1})**	**CTR**	**NEW**	**LWDR**	**LWPR**
1)Yukon	779 081	198	2.18	0.95	0.53	0.58	0.58
2)Podka[a]	205 591	190	3.47	0.90	0.45	0.50	0.57
3)Lena	2 351 052	182	3.07	0.96	0.84	0.86	0.87
4)Tom	62 830	158	6.92	1.88	1.59	1.68	1.64
5)Ob	2 859 889	154	1.06	0.69	0.32	0.34	0.38
6)Yenisei	2 513 361	151	2.79	0.77	0.46	0.51	0.54
7)Mackenzie	1 587 878	140	1.34	0.55	0.42	0.45	0.44
8)Volga	1 333 747	137	1.16	0.65	0.53	0.55	0.57
9)Irtish	403 309	129	0.41	0.42	0.22	0.21	0.25
10)Neva	233 423	116	0.80	0.60	0.63	0.64	0.63
Average[b]	12 334 161[c]	157	1.96	0.75	0.51	0.54	0.56

[a] Podkamennaya Tunguska ; [b] Average weighted by catchment area ; [c] Total catchments area

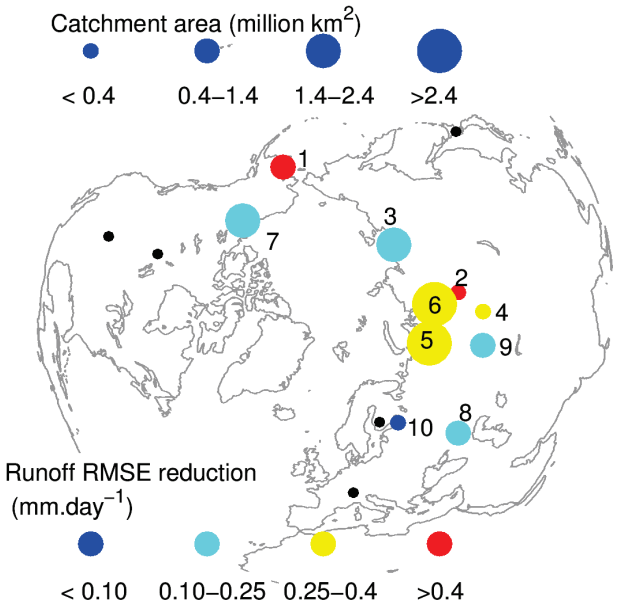

Figure 3.8. Basin locations represented by colored symbols. Each basin is numbered as in Table 3.3 and the location refers to the runoff station observations from Hirschi et al. (2006). The catchment area is associated to the size of the symbol, and the runoff RMSE difference between NEW – CTR is represented by the symbol face color. The black symbols represent the five SnowMIP2 sites.

3.5 Global validation

3.5.1 Simulations setup

ERAI reanalysis covers the period January 1989 to the present. The atmospheric forcing data were gridded on the original Gaussian reduced grid N128 (resolution of 0.7° over the equator) globally at 3-h intervals. The state variables are provided as instantaneous values from the lowest model level (approximately 10 m above the surface) and correspond to the 3–12-h forecast interval from initial conditions at 0000 and 1200 UTC. Surface precipitation and radiation fluxes represent 3-h averages. To avoid the initial spinup in precipitation, the 3-hourly surface fluxes are taken from the 9–21-h forecasts initialized at 0000 and 1200 UTC.

Unlike GSWP2, ERAI precipitation was not corrected with GPCP (or other) observational dataset. Errors in total precipitation and partitioning between liquid and solid rainfall may produce biases in the simulated snowpack. Such corrections are out of the scope of the present work. Nevertheless, the ERAI dataset has already been explored in offline LSM works (Balsamo et al. 2010; Dutra et al. 2010b).

3.5.2 Snow cover

IMS NOAA/NESDIS snow cover

The interactive Multisensor Snow and Ice Mapping System (*IMS*) is a workstation-based application, which allows the analyst to process various snow cover data in a manner timely enough to release a real-time daily product (Helfrich et al. 2007; Ramsay 1998). Northern Hemisphere (NH) snow-covered maps are primarily based on satellite imagery. In addition, the analyst can rely on station data and the previous day's analysis. Since February 1997, the *IMS* product has been produced daily at

approximately 24-km resolution (1024 x 1024 grid). This dataset has already been applied to the validation of model-simulated snow cover extent in other studies (e. g. Sheffield et al. 2003). *IMS* National Oceanic and Atmospheric

Administration/National Environmental Satellite, Data, and Information Service (NOAA/NESDIS) snow cover product (NOAA/NESDIS/OSDPD/SSD 2004, updated 2006) was spatially aggregated to the N128 Gaussian reduced grid. Fractional snow cover in the Gaussian grid was evaluated from the original ‘‘snow-free/100% snow-covered’’ binary information. Snow cover fraction was calculated by counting all the 100% snow-covered pixels of NOAA/NESDIS lying within each N128 grid box.

Snow cover simulations

NH simulated snow-covered area is compared against NOAA/NESDIS in Figure 3.9. Snow-covered area maximum extents exceed 40 million km^2, which is coherent with the results presented by Brown and Armstrong(2008). The differences between simulated and NOAA/NESDIS (Figure 3.9b) snow-covered area show a distinct annual cycle. The bias is reduced during low variability periods, namely summer and late winter. On the other hand, the bias increases during the high variability accumulation and ablation seasons. During the initial accumulation period both CTR and NEW show a growing underestimation of snow-covered area that reaches roughly 6 million km^2. After the initial accumulation, NEW reduces the bias significantly near the peak snow-covered area. During spring, both schemes tend to ablate snow cover too quickly, with increasing underestimation. This behavior was also documented by Frei et al. (2005) in the AGCMs participating in phase 2 of the Atmospheric Model Intercomparison Project (AMIP-2). Averaged over the entire period (January 1999 to December 2008) CTR and NEW have a negative bias in snow-covered area of 3.1 and 1.6 million km^2, respectively. During spring, CTR and NEW biases are higher: 5.3 and 2.6 million km^2. LWDR_SC (all new components of NEW except the exposed and forest albedo) simulation partially reduces the bias of CTR with a negative bias in snow-covered area of 2.5 and 4.4 million km^2, during the whole period and spring, respectively, showing that the new snow cover fraction [Eq.(3.12)] has an important effect in the model-simulated snow cover extent. The simulated snow-covered area RMSE normalized by the observations temporal standard deviation are 25%, 21%, and 15% for CTR, NEW, and LWDR_SC, respectively.

The NOAA/NESDIS data compose a daily product allowing for a more detailed comparison with simulations. Figure 3.10 presents the spatial distribution of the frequency of missing snow cover in the simulations during spring, defined as the frequency of occurrence of snow-covered NOAA/NESDIS (c_{sn}> 0.75) and simulated snow free (c_{sn} < 0.25). Drusch et al. (2004) applied a similar diagnostic to validate the snow depth analysis system in ECMWF. Scandinavia, western Russia, and central/eastern Canada are dominated by high-frequency snow cover missing in CTR (Figure 3.10a), reaching one month (30%) in some localized areas. These results agree with the pronounced underestimation of snow-covered area during spring in CTR, analyzed before. NEW reduces the missing snow cover during spring, when compared with CTR, up to a factor of 2 in areas where CTR has higher errors.

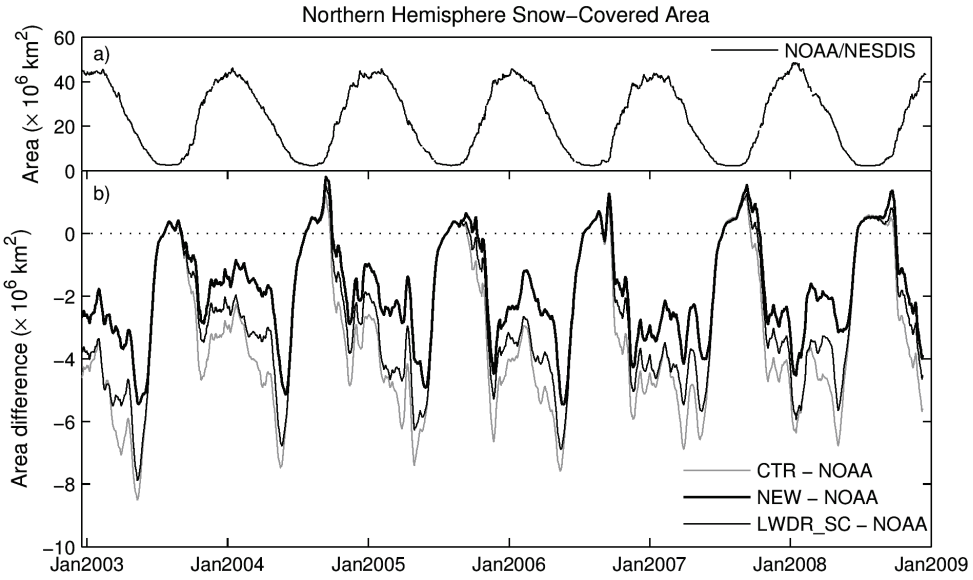

Figure 3.9. (a) Northern Hemisphere daily snow-covered area from NESDIS and (b) snow-covered area differences between simulations and NESDIS. Note the different order of magnitude in the vertical axis between the two panels.

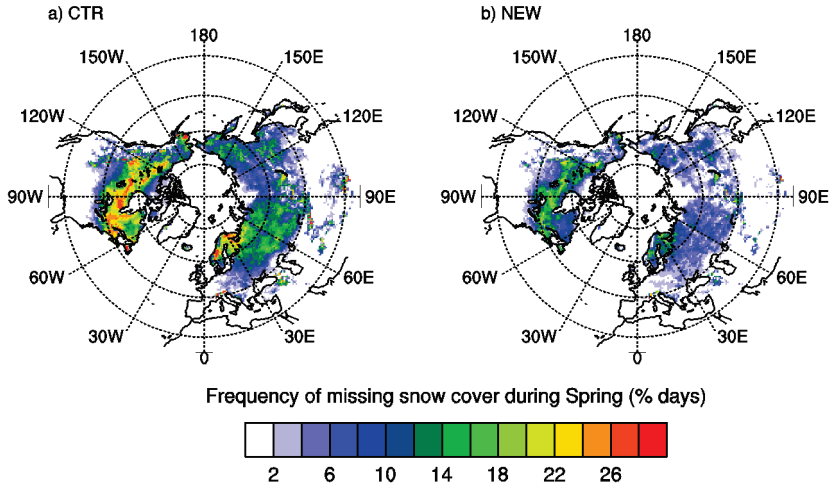

Figure 3.10. Frequency of occurrence of snow-covered NESDIS data (c_{sn} > 0.75) and simulated snow-free (c_{sn} < 0.25) during spring (March–May) for ERAI simulations in the period 2001–08 by (a) CTR and (b) NEW. The number of days in each grid box is normalized by the total number of days of the season.

3.5.3 Surface albedo

MODIS albedo

The *MODIS* albedo productMCD43C3 provides data describing both directional hemispheric reflectance (black-sky albedo) and bihemispherical reflectance (white-sky albedo). Both black-sky and white-sky albedos are available in seven different bands and aggregated visible, near infrared and broadband shortwave. Both *Terra* and *Aqua* platforms are used in the generation of this product. The product also includes snow-free and quality parameters, and is produced every 8 days with 16 days of acquisition projected to a 0.05° grid. These data are distributed by the Land Processes Distributed Active Archive Center (LP DAAC), located at the U.S. Geological Survey (USGS) Earth Resources Observation and Science (EROS) Center (https://lpdaac.usgs.gov/). The accuracy and quality of this

albedo product have been evaluated by Stroeve et al. (2005), Salomon et al. (2006), Shuai et al. (2008), and Roman et al. (2009). The white-sky broadband shortwave albedo was spatially aggregated from the original 0.05° grid to the N128 Gaussian reduced grid.

Albedo simulations

Figure 3.11a compares simulated albedo against *MODIS* derived albedo in the snow-covered area in the NH. In the following discussion, snow-covered area was derived from the *MODIS Percent_Snow* layer. Therefore, the mean fractional land area with available data (top of each panel in Figure 3.11) excludes snow-free *MODIS* grid boxes and also missing data (e.g., because of cloud cover or low quality of the albedo inversion algorithm).

CTR albedo shows a systematic negative bias that increases in magnitude throughout the cold season until May. The exposed albedo parameterization by itself (LWDR_A) improves the simulation in all months except October. The new lookup table for shaded snow (LWDR_FA) has a positive impact in all months. The NEW snow scheme significantly reduces the albedo bias in all months except October and November. During these two months the signal shift of the albedo bias (from negative in CTR to positive in NEW) and increased magnitude is due to the new exposed albedo parameterization (cf. LWDR_A with LWDR_FA in Figure 3.11a). Groisman et al. (1994b) showed that the impact of snow cover in the planetary albedo has the greatest magnitude in spring. Therefore, the degradation of simulated albedo in NEW during late autumn should have a smaller impact than the improvements during late winter and spring. The new snow cover fraction by itself (LWDR_SC) has results similar to CTR, showing that the improved simulated albedo is mainly due to the modified exposed and shaded snow parameterizations.

The impact of albedo biases on the snowpack is modulated by the amount of available solar radiation. Net shortwave radiation (SWnet) is not a direct *MODIS* product. It was diagnosed using *MODIS* albedo and ERAI downward shortwave radiation and is compared against simulations in Figure 3.11. The above-mentioned CTR albedo negative bias is reflected in a positive SWnet bias during the entire snow-covered season. On the other hand, NEW SWnet bias is close to zero during late winter and spring but shows a negative bias in November and December. The reasons for this bias were discussed before. Averaged results from October to May and weighted by the snow-covered area, CTR has a mean positive bias of 17.1 W m^{-2}, while NEW has a mean negative bias of 21.9 W m^{-2}. In absolute terms, NEW reduces the SWnet bias by 5.2 W m^{-2} when compared with CTR. The area where such flux differences are found covers 14% of the NH land.

Figure 3.12 represents the mean (2000–08) spring *MODIS* albedo and respective simulated differences. The differences between simulated and *MODIS* albedo are shown only for snow-covered grid boxes flagged by *MODIS* with at least 50% of feasible data (excluding areas with systematic missing values in *MODIS*). The negative bias of CTR albedo (Fig. 12b) during spring spreads widely over the entire Northern Hemisphere. There are three main regions with an accentuated bias: northeast Asia, central Asia (north of the Caspian and Aral Seas), and northern Canada. These areas are dominated by low vegetation (tundra and short grass). NEW partially reduces the albedo bias over low vegetation areas, while over high vegetation areas the bias is close to zero. There are some small positive biases in NEW on the southern borders of tundra regions (areas dominated by bogs and marshes) in both continents.

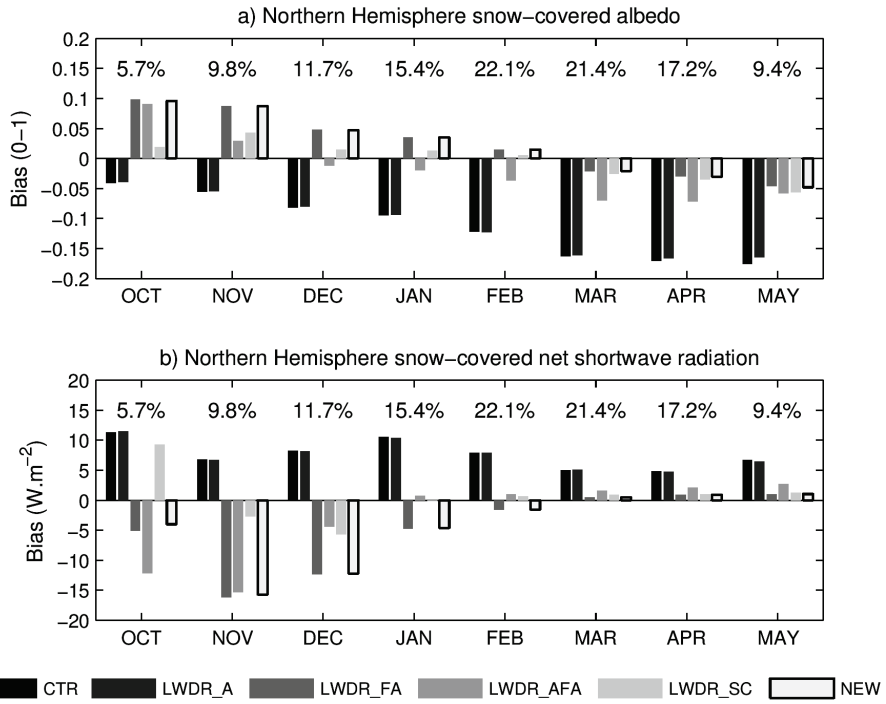

Figure 3.11. Monthly bias (simulation - observation) of (a) albedo and (b) net shortwave radiation calculated only over snow-covered grid boxes over the Northern Hemisphere. The fractional snow-covered land of Northern Hemisphere used in the calculations for each month is presented in the top of each graphic. ERAI simulations of albedo and net shortwave radiation are compared against MODIS albedo for the period Jan 2000 to Dec 2008.

3.6 Conclusions

An improved snow scheme for HTESSEL was presented and validated. The new scheme revises the formulations of snow cover fraction and snow albedo and includes a new snow density parameterization and representation of SLW using a diagnostic approach. An offline validation covering several spatial and temporal scales considered (i) site simulations for several observational locations from SnowMIP2 and (ii) global simulations driven by the meteorological forcings from GSWP2 and ERAI.

SnowMIP2 simulations revealed that the original snow scheme had a systematic early and late prediction of the final ablation in forest and open sites, respectively. The NEW scheme reduces the negative timing bias in forest plots from 21 to 13 days and the positive bias in open plots from 10 to 2 days. The new snow density parameterization in NEW has a good agreement with observations, resulting in an augmented insulation effect of the snowpack. The increased insulation and the new exposed and shaded albedo change the surface energy fluxes. There is a reduction of the basal heat flux that reduces the cooling of the underlying soil, which is warmer in NEW than in CTR during the cold season. Thus, reduced soil freezing decreased the surface runoff and increased soil water storage. The mean annual cycles of runoff and TSWV analyzed for the Ob and Mackenzie basins are closer to the observations in NEW. In 10 Northern Hemisphere basins, there is an average reduction of the monthly runoff RMSE from 0.75 to 0.51 mm day^{-1} when comparing CTR and NEW, respectively. These results illustrate the importance of snow insulation on the hydrological cycle, even at regional scales.

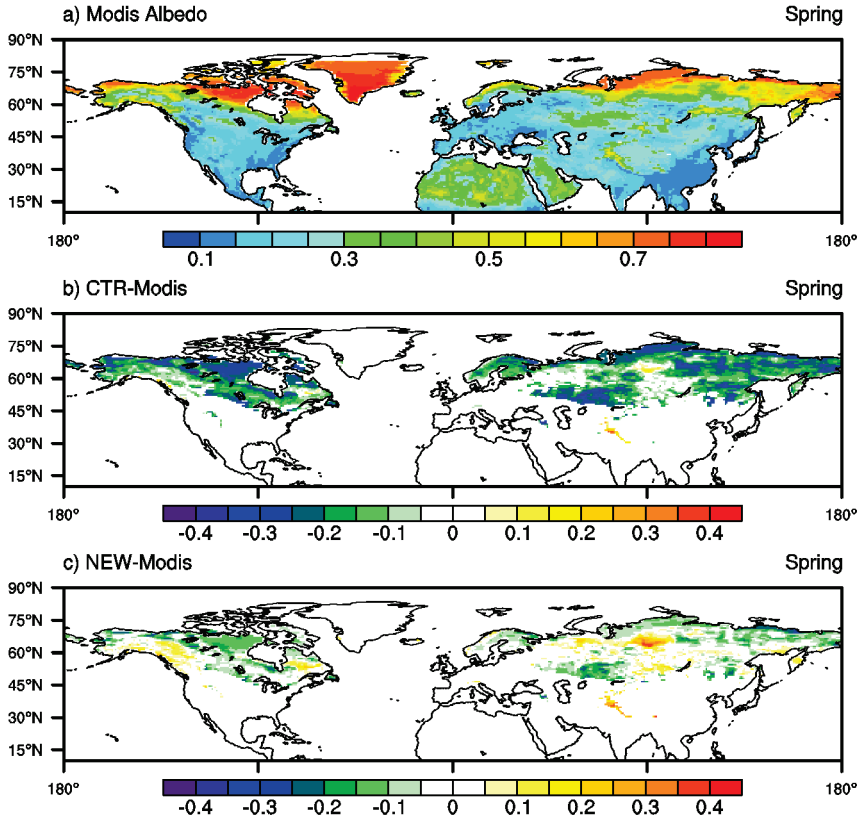

Figure 3.12. (a) Mean observed maps of spring albedo by MODIS for the period 2000–08 and differences between simulated albedo and MODIS for (b) CTR and (c) NEW. The differences (b) and (c) show only snow-covered grid boxes with, 50% MODIS missing data. Note the different color scales between panel (a) and panels (b) and (c).

On a hemispheric scale, the new snow scheme reduces the negative bias of snow-covered area, especially during spring. On a daily scale, using NOAA/NESDIS snow cover data, the early ablation in CTR is reduced by a factor of 2 in some identified regions over the Northern Hemisphere. The changes in snow-covered area are closely related with the changes in surface albedo. The original snow scheme had a systematic negative bias in surface albedo, when compared against *MODIS* remote sensing data. The new scheme reduced the albedo bias, consequently reducing the spatial- (only over snow-covered areas) and time- (October to November) averaged surface net shortwave radiation bias from +7.1 W m^{-2} in CTR to -1.8 W m^{-2} in NEW.

For each validation dataset, sensitivity experiments were performed to assess the impact of the new components of the presented snow scheme. Prognostic and diagnostic SLW representations display similar skill in SnowMIP2 (RMSE of SWE) and GSWP2 (RMSE of basin runoff) simulations. Simulated improvements of SWE in SnowMIP2 locations were mainly due to SLW representation on forest sites and due to the new exposed albedo on open sites. The increased snow insulation effect, due to the new snow density parameterization, had an important role on the basins'water balance. Impacts of the new snow cover fraction and exposed and shaded albedo parameterizations were evident when validating against remotely sensed data. Sensitivity tests highlight the role of the different components of the snow scheme with the behavior conditioned by the climate and vegetation conditions of each site. Thus, a robust verification of a LSM model should include a variety of different (and independent) validation datasets.

The present offline methodology is recurrent in validations of LSM (e. g. Boone and Etchevers 2001) and in intercomparison projects (e.g. Rutter et al. 2009). However, the associated nature of the one-way coupling has shortcomings due to the absence of atmospheric response. A complete validation can only be achieved with atmospherically coupled simulations. Tests have been performed and the new snow scheme showed improvements in the simulated near-surface temperature during winter over snow-covered areas; such results will be reported in future work. Future developments of HTESSEL snow scheme will focus on improvements of the representation of snowpack physics (e.g., via the development of a multilayer scheme), and on the coupling with the atmosphere, especially in forested regions. The NEW snow scheme described in this paper was introduced in the ECMWF operational forecast system in September 2009 (cycle 35R3).

Acknowledgments

The authors thank SnowMIP2 data providers: David Gustafsson and Manfred Stähliand (Alptal-Switzerland); Alan Barr and Paul Bartlett (Berms-Canada); Kazuyoshi Suzuki and Tomoyoshi Hirota (Hitsujigaoka-Japan); Nuria Altimir and Timo Vesala (Hyytiälä-Finland); and Richard Essery and Nick Rutter for the project organization and useful comments. The BSWB dataset was kindly provided byMartin Hirschi. We also thank the *MODIS* Land and Albedo teams and in particular Crystal Schaaf for the valuable support and comments regarding the use of *MODIS* albedo product. The comments of three anonymous reviewers are gratefully acknowledged. This work was supported by the Portuguese Foundation for Science and Technology (FCT) under project AMIC PTDC/AAC-CLI/109030/ 2008 cofinanced by the European Union under program FEDER. E. Dutra acknowledges the financial support of FCT under Grant SFRH/BD/35789/2007 and Fundação Calouste Gulbenkian.

3.7 Appendix: HTESSEL old snow scheme

The snow mass budget reads as

$$\frac{\partial S}{\partial t} = F - c_{sn} E_{sn} - M_{sn} \tag{3.14}$$

where the symbols are defined in section 3.2.2. The snow fraction is given by:

$$c_{sn} = \min\left(1, \frac{S}{15}\right) \tag{3.15}$$

Snow mass and snow depth are related by

$$D_{sn} = \frac{S}{\rho_{sn} c_{sn}} \tag{3.16}$$

where D_{sn} is the snow depth (m) in the snow-covered area (it is not a grid-averaged quatity).

The snow energy budget reads as

$$\left(\rho C\right)_{sn} D_{sn} \frac{\partial T_{sn}}{\partial t} = R_{sn}^{N} - L_s E_{sn} - H_{sn} - G_{sn}^{B} - L_f M_{sn} \,. \tag{3.17}$$

In this formulation the liquid water fraction is neglected. The snow thermal conductivity changes with changing snow density and is related to the ice thermal conductivity according to Douville et al. (1995).

Following Douville et al. (1995) snow density is assumed to be constant with depth and to evolve exponentially toward a maximum density (Verseghy 1991). First, a weighted average is taken between the current density and the minimum density for fresh snow, giving

$$\rho_{sn}^{*} = \frac{S\rho_{sn}^{t} + \Delta t F \rho_{\min}}{S + \Delta t F} \tag{3.18}$$

where ρ^{*} is a intermediate snow density, and after an exponential relaxation is applied,

$$\rho_{sn}^{t+1} = \left(\rho_{sn}^{*} - \rho_{\max}\right)\exp\left(-\tau_f \, \Delta t/\tau_1\right) + \rho_{\max} \tag{3.19}$$

where τ_1 = 86400 s, and τ_f = 0.24 are time scales, with minimum density ρ_{min} = 100 kg m^{-3} and maximum density ρ_{max} = 300 kg m^{-3}.

Snow albedo in exposed areas evolves according to the formulation of Baker et al. (1991), Verseghy (1991), and Douville et al. (1995) differing for melting and non-melting conditions:

$$\alpha_{sn}^{t+1} = \begin{cases} \alpha_{sn}^{t} - \tau_a \, \Delta t/\tau_1 & , \; M_{sn} = 0 \\ \left(\alpha_{sn}^{t} - \alpha_{min}\right)\exp\left(-\tau_f \, \Delta t/\tau_1\right) + \alpha_{min} & , \; M_{sn} > 0 \end{cases} \tag{3.20}$$

where σ_{min} = 0.5 and σ_{min} = 0.85. If snowfall F > 1 kg m^{-2} h^{-1}, the snow albedo is rest to the maximum value $\alpha_{sn}^{t+1} = \alpha_{\max}$. The albedo is reset for shaded snow is fixed at 0.15. ECMWF (2004) provides a detailed description of the scheme, along with the other components of the land surface model.

4

Snow cover sensitivity to horizontal resolution, parameterizations and atmospheric forcing in a land surface model*

Abstract

This study assesses the relative impacts of horizontal resolution, snow physics and atmospheric forcing in snow cover simulations by the ECWMF land surface model HTESSEL. Offline simulations are carried out forced by the ECMWF deterministic short-range weather forecasts (WFC) with a resolution of 25 km from March 2006 to June 2010. The horizontal resolution impact on snow cover is addressed by performing simulations at 25, 80 and 200 km forced by WFC. The impact of atmospheric forcing on snow cover is assessed by forcing the model additionally with the ECMWF Era-Interim (ERAI) reanalysis, at 80 km resolution. Snow physics effects are analyzed by performing an extra simulation forced by WFC using a different snow scheme. The simulations are validated against four independent observational datasets: (i) snow water equivalent (SWE) over Switzerland; (ii) snow cover duration in Europe (*SNOWCLIM*); (iii) interactive multisensor snow and ice mapping system (*IMS*) snow cover; and (iv) Moderate Resolution Imaging Spectroradiometer (*MODIS*) surface albedo. ERAI forced simulations show a systematic underestimation of SWE and snow cover fraction, due to an underprediction of snowfall by ERAI. The snow physics experiment highlights the sensitivity of the model to the partitioning between rainfall and snowfall when rainfall interception in the snowpack is neglected. The horizontal resolution has an important impact on snow cover over complex terrain regions, with improvements for increased resolution, while its impact on flat terrain regions is reduced. Here, the atmospheric forcing accuracy and model physics play a more important role.

---

* Dutra, E.[1,2], S. Kotlarski[2], P. Viterbo[3], G. Balsamo[4], P. M. A. Miranda[1], C. Schar[2], P. Bissolli[5], and T. Jonas[6], 2011: Snow cover sensitivity to horizontal resolution, parameterizations and atmospheric forcing in a land surface model. *Submitted to Journal of Geophysical Research*.

[1] Centro de Geofísica da Universidade de Lisboa, Instituto Dom Luiz, University of Lisbon, Lisbon, Portugal.

[2] Institute for Atmospheric and Climate Science, ETH, Zurich, Switzerland.

[3] Institute of Meteorology, Lisbon, Portugal.

[4] European Centre for Medium-Range Weather Forecasts, Reading, United Kingdom.

[5] Deutscher Wetterdienst (German Meteorological Service), Offenbach am Main, Germany.

[6] WSL Institute for Snow and Avalanche Research SLF, Davos, Switzerland.

4.1 Introduction

The extent and variability of snow cover are important parameters in weather and climate prediction systems, due to their effects on the surface energy and water balance, leading to a strong dependence of, for instance, surface temperature on the presence or absence of snow cover (Armstrong and Brun 2008; Dutra et al. 2010a; Hazeleger et al. 2010). There is evidence of links between large scale snow cover and hemispheric circulation anomalies in the Northern Hemisphere (e. g. Fletcher et al. 2009b). On smaller spatial scales, snow cover is an important component of local and regional scale energy and water budgets, especially in mountainous areas (Beniston et al. 2011; Schär et al. 2004). The latter, however are often poorly represented in climate models. Last, but not least, snow may affect daily life considerably e.g. in terms of transport networks and tourism, and therefore reliable estimates for future climate are needed.

Snow temporal evolution in land surface models (LSM) is mainly determined by the atmospheric forcing and model physics. When LSM are used within numerical weather prediction (NWP) or climate models, the forcing is directly provided by the atmospheric component, and the land-atmosphere coupling, including feedback mechanisms is fully represented. However, offline or stand-alone simulations are very common in inter-comparison studies (e. g. Boone et al. 2004; Bowling et al. 2003; Rutter et al. 2009), model evaluation and development (e. g. Dutra et al. 2010a; Livneh et al. 2010; Wang et al. 2010). Once snow settles on the ground, its temporal evolution is mostly controlled by the atmosphere that provides the upper boundary conditions for the physics and parameterizations of the snowpack. There is a wide variety of physical representations of the snowpack water and energy balance, ranging from single layer (e. g. Dutra et al. 2010a) to detailed multi-layer representations of snow stratigraphy (e. g. Brun et al. 1992). Other processes such as snow albedo and snow density evolution are based on parameterizations. On a grid box scale, the effects of vegetation (Wang et al. 2010) and subgrid-scale variability (Liston 2004) on snow cover are still topics of ongoing research. Due to the high spatial variability of snow processes and the importance of topography, resolution issues generally play an important role (e.g. *Giorgi et al.*, (2003)).

The goal of this study is to assess the relative impacts of atmospheric forcing, snow parameterization and horizontal resolution on simulating snow in a state-of-the-art LSM, using independent datasets to validate the simulations. The assessment is performed by conducting global offline simulations with the European Centre for Medium-Range Weather Forecasts (ECMWF) LSM HTESSEL (Hydrology Tiled ECMWF Scheme for surface Exchanges over Land) (Balsamo et al. 2009). The offline simulations methodology, although recurrent in LSM validations, has shortcomings due to the associated nature of the one-way coupling and the absence of an atmospheric response to land surface processes. Nevertheless, offline simulation can be an advantage since they isolate the land surface model response to the various factors in the analysis.

The effects of horizontal resolution are analyzed by performing offline simulations of HTESSEL at 25 km, 80 km and 200 km horizontal resolution forced by the ECMWF deterministic weather forecasts (hereafter WFC). Jung et al. (2010) and references therein report the major changes since 2005 in the physical parameterizations of the ECMWF model. WFC is available at 25 km resolution globally since February 2006 and is based on a state of the art NWP model and data assimilation system. WFC provides a high spatial and temporal resolution dataset covering the entire globe during four recent winter seasons. These characteristics in combination with the continuous development and validation

performed at ECWMF guarantees a realistic atmospheric forcing required for this study. The HTESSEL simulations with different resolution are forced with the same atmospheric fields. This can be interpreted as proxy for comparison resolved versus unresolved spatial variability from the 25 km to the 200 km resolution simulations. The subject of subgrid-scale variability on land surface processes has been addressed by many studies. For example, Liston (2004) proposed a representation of subgrid snow distribution within a grid box showing significant impacts on snow cover evolution in a regional climate model. Giorgi et al. (2003) developed a mosaic-type parameterization of subgrid-scale topography and land use in a regional climate model to bridge the scale gap between climate models and surface hydrological processes. This approach improved the simulation of snow and runoff at high-elevation sites in the Alpine Region (Im et al. 2010). However, the increase of horizontal resolution, or enhanced representation of subgrid-scale variability, in regional climate models is hampered by the lack of adequate station observations that can capture the complex climatology and provide means to validate model simulations (Rauscher et al. 2010).

The near surface atmospheric fields of the ECMWF reanalysis ERA-Interim (Dee et al. 2011) (hereafter ERAI), for the same period as WFC, are also used to force HTESSEL. This allows for a comparison between the two forcing datasets and their effects on the simulated snow cover. Among the differences due to different atmospheric model versions and assimilation systems, WFC and ERAI mainly differ in the horizontal resolution of the atmospheric model (25 km and 80 km, respectively). The foremost difference between the two forcing datasets is expected to be on precipitation. The largest effect can be expected for complex terrain regions, where WFC should, in principle, have a better representation of orographic-driven events. This is an important factor to evaluate, since model simulations of snow cover and snow water equivalent (SWE, also referred as snow mass) are sensitive to precipitation as shown by *Carrera et al.* (2010) in the Canadian Rockies. The impact of the model physics is assessed by performing an extra simulation forced with WFC but using an older version of the HTESSEL snow scheme. The old and the new snow scheme, as well as their comparison, are described by Dutra et al. (2010a). Both additional simulations, forced with ERAI and with the old snow physics, were performed on an intermediate resolution (80 km). In summary, we show the impact of running the model at different resolutions, forced by the same atmospheric conditions, and the impact of using different snow physics and different atmospheric forcings at the same resolution.

For model evaluation, results are compared against four different and independent datasets: (i) time series of daily mean SWE over Switzerland; (ii) mean monthly snow cover duration in Europe; (iii) daily snow cover maps of the Northern Hemisphere and; (iv) monthly maps of surface albedo. The first two datasets are based on local observations while the remaining two are remote sensed products. The model description, simulations setup and observational datasets are presented in the next section. The results of the different simulations to assess the relative impacts of atmospheric forcing, model physics and horizontal resolution are presented and discussed in section 3. The main conclusions of the study are summarized in section 4.

4.2 Methods

4.2.1 Model description

HTESSEL computes the land surface response to atmospheric forcing, and estimates the surface water and energy fluxes and the temporal evolution of soil temperature, moisture content and snowpack

conditions. At the interface to the atmosphere each grid box is divided into fractions (tiles), with up to six fractions over land (bare ground, low and high vegetation, intercepted water, shaded and exposed snow). Vegetation types and cover fractions are derived from an external climate database, based on the Global Land Cover Characteristic (Loveland et al. 2000). The grid box surface fluxes are calculated separately for each tile, leading to a separate solution of the surface energy balance equation and the skin temperature. The latter represents the interface between the soil and the atmosphere. The surface albedo is similar for all land tiles within a grid box except for those covered with snow. The climate database provides the snow-free background albedo on a monthly basis, produced for the combined 1982-1990 years and computed using the method of Sellers et al. (1996) and parameters by Los et al. (2000).

Below the surface, the vertical transfer of water and energy is performed using four vertical layers to represent soil temperature and moisture. Soil heat transfer follows a Fourier law of diffusion, modified to take into account soil water freezing/melting (Viterbo et al. 1999). Water movement in the soil is determined by Darcy's Law, and surface runoff accounts for the subgrid variability of orography (Balsamo et al. 2009). In the case of a partially (or fully) frozen soil, water transport is limited, leading to a redirection of most of the rainfall and snow melt to surface runoff when the uppermost soil layer is frozen. The snow scheme (Dutra et al. 2010a) represents an additional layer on top of the soil, with an independent prognostic thermal and mass content. The snowpack is represented by a single snow temperature, SWE, snow density, snow albedo, and a treatment for snow liquid water in the snowpack. HTESSEL is part of the integrated forecast system at ECMWF with operational applications ranging from short to seasonal weather forecasts, and research including lake modeling (Dutra et al. 2010b) and runoff routing (Pappenberger et al. 2010).

4.2.2 Simulations setup

Near surface meteorology and surface fluxes from the ECMWF deterministic weather forecast (WFC) were used to force HTESSEL in offline mode. Near surface meteorology includes instantaneous values at a 3-h interval of air temperature, wind speed and specific humidity from the lowest model level (level 91, approximately 10 m above the surface), and surface pressure. These correspond to the 3-12h forecast interval from initial conditions at 00 and 12 UTC. Surface fluxes include downward solar and thermal radiation and liquid and solid precipitation representing 3-h averages taken from the 9-21-h forecasts initialized at 00 and 12 UTC to avoid the initial spin-up in precipitation.

All simulations were performed from March 2006 to June 2010 for the Northern Hemisphere (NH). This period was chosen to exploit the high resolution of the forecasts. In February 2006 ECMWF increased the horizontal resolution of the deterministic forecast from TL511 (~ 40 km) to TL799 (Gaussian reduced grid N400 ~ 25 km resolution) and the number of vertical levels from 60 to 91. From 2006 to 2010, there was only one change in resolution of the deterministic forecast to T1279 (~ 16 km) in January 2010. Within the same period, many other changes occurred in the model physics and data assimilation system.

The effects of the horizontal resolution of the snow scheme are assessed by performing three offline simulations forced by WFC: i) high resolution (HIG - same resolution as the forcing - 25 km), ii) medium resolution (MED –Gaussian reduced grid N128 – 80 km), and iii) low resolution (LOW – Gaussian reduced grid N48 – 200 km) (see Figure 4.1). The forcing for the two lower resolution

experiments was upscaled from WFC using a conservative interpolation and accounting for altitude differences: air temperature with a constant lapse rate of 6.5 K $(1000\ m)^{-1}$, surface pressure with a barometric correction, and longwave downward radiation with a constant adjustment of 2.8 W m^{-2} $(100\ m)^{-1}$ (Wild et al. 1995). These corrections were applied prior to the interpolation to adjust the variables to a common level (target model orography). For specific humidity, first relative humidity was calculated and interpolated, and then transformed again to specific humidity but using the corrected surface pressure and air temperature. No corrections were performed to the remaining forcing fields (wind speed, shortwave radiation and liquid and solid precipitation). The applied corrections only account for the thermodynamic differences due to different altitudes. They do not account for the spatial and temporal variability of the lapse rate (e.g. Kotlarski et al. 2010) and for the partitioning of precipitation between the solid and liquid phases that was kept as in WFC.

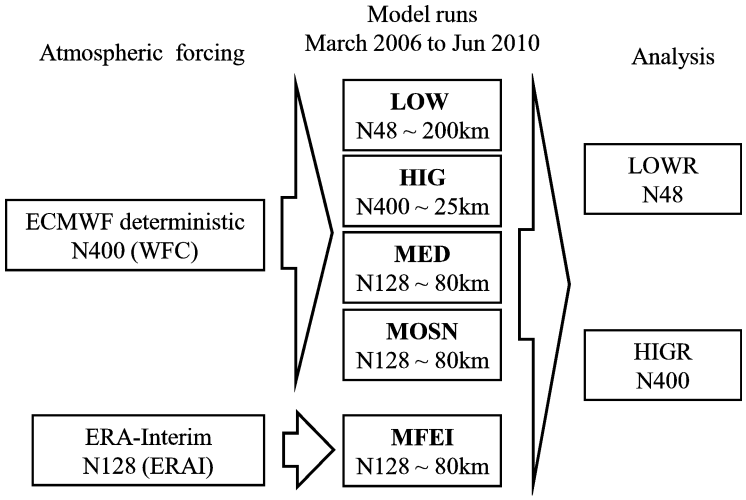

Figure 4.1. Experimental design: atmospheric forcing interpolation from simulations grid from left to center and model output interpolation to analysis grid from center to right.

The impact of the forcing on snow cover is assessed by forcing HTESSEL with the ECMWF reanalysis ERA-Interim (ERAI) near surface atmospheric fields and fluxes (MFEI) and comparing with the simulation forced by WFC at the same resolution (MED). ERAI provides a homogeneous atmospheric forcing that has been used in other offline studies (e.g. Dutra et al. 2010b); it differs from WFC in the horizontal resolution (~ 80 km), the atmospheric model physics, and the assimilation system.

The land surface snow physics impact on snow cover is assessed by performing an extra simulation at MED resolution driven by WFC and using an old snow scheme (MOSN). The old snow scheme was part of HTESSEL and used by the ECMWF forecasting system until December 2009 (including in ERAI). When compared with the NEW snow scheme three main differences can be identified: (i) dry versus wet snow in NEW including rainfall interception in the snowpack; (ii) simple exponential increase of snow density versus a more physically based formulation in NEW, and (iii) constant forest albedo in the presence of snow versus a vegetation cover type dependence based on observations in NEW. Dutra et al. (2010a) describe the differences between the two snow schemes in detail. The major changes in NEW are associated with an increased thermal snow insulation, with impacts on the surface water balance, and a better representation of snow cover, especially during the melting season. The purpose of this work is not to compare or validate in detail these two snow schemes. The impacts

of the different snow physics on snow cover are assessed and inter-compared with the impacts of changing the horizontal resolution and using different forcings in HTESSEL.

The simulations setup is summarized in Figure 4.1. The impact of horizontal resolution on snow cover is analyzed by comparing LOW, MED and HIG; the impact of atmospheric forcing by comparing MED and MFEI; and the impact of the snow physics by comparing MED and MOSN. All simulations were post-processed and interpolated to two common resolutions: (i) low resolution (LOWR – 200 km) to assess large scale temporal variability and; (ii) high resolution (HIGR – 25 km) to study spatial patterns. A spatial conservative interpolation, as for the atmospheric forcing, was applied to guarantee a fair comparison between the different resolution simulations. The conservative interpolation of any variable to the grid point y_j of the target Y grid from the original X grid is given by

$$y_j = \frac{1}{\sum_{i=1}^{n} w_i} \sum_{i=1}^{n} w_{i,j} x_i \tag{4.1}$$

where x_i is the value of the variable to be interpolated on grid point i of grid X, $w_{i,j}$ is the intersection area of the grid points $y_j \cap x_i$ and n is the number of grid points of grid X.

4.2.3 Observations

Four independent observational datasets are used for model validation: (1) *SLF* with snow water equivalent over Switzerland, (2) *SNOWCLIM* with snow cover duration over Europe, (3) *IMS* with snow cover and (4) *MODIS* with surface albedo.

The first reference dataset (*SLF*) was derived from ground observations of three snow monitoring networks in Switzerland by the WSL Institute for Snow and Avalanche Research. For this study we used daily snow depth data from a subset of 203 stations to allow a gap-free dataset that represented all Swiss snow meteorological regions (Laternser and Schneebeli 2003) and elevations bands as homogeneously as possible. The snow data were interpolated to a 25 km grid using methods particularly developed for snow depth mapping (c.f. Foppa et al. 2007). The resulting snow depth maps were converted into snow water equivalent (SWE) maps using a parametric snow density model based on Jonas et al. (2009). This model is particularly suited as it was calibrated using 11'000 snow profiles from the same snow monitoring networks that provided the snow depth data for this study.

The second reference dataset is *SNOWCLIM*, a snow climate monitoring project of Deutscher Wetterdienst (DWD, German Meteorological Service). Data basis are daily snow depths measured at 06 UTC at synoptic stations received via the Global Telecommunication System (GTS) of the WMO and quality controlled at DWD. Various snow quantities, aggregated to monthly data, are derived from the daily snow depth for each station, among them the number of snow-days (defined as the number of days for each month with a depth of at least 1 cm) which is used in this study. These monthly station data are interpolated onto a grid of 0.1°x0.1° resolution in latitude and longitude for the area of Europe and the Middle East, using a linear regression with latitude, longitude and altitude and afterwards the interpolation method "Radial Basis Functions, Multiquadratic". Radial Basis Functions show similar results as Ordinary Kriging as shown by Hogewind and Bissolli (2010).

The interactive multisensor snow and ice mapping (*IMS*) (Helfrich et al. 2007; Ramsay 1998) snow cover product represents the third observational reference dataset which has been compared with

model simulations. The *IMS* daily snow cover maps of the Northern Hemisphere are available at a nominal resolution of 24 km since February 1997 and of 4 km since February 2004, the latter being used in this study. The snow cover maps are produced every day in a workstation-based application where various remote sensing products and surface observations are processed by analysts. *IMS* has been evaluated against other satellite-based snow products (Brown et al. 2007) and in situ observations (Brubaker et al. 2005) showing a good performance during the core winter season and some deficiencies in the accumulation and melting periods that are common to other satellite-based products. There is a wide range of applications to this product including data assimilation (Drusch et al. 2004) and validation of land surface models (e.g., Carrera et al. 2010; Dutra et al. 2010a; Livneh et al. 2010; Sheffield et al. 2003).

The fourth reference dataset is based on the Moderate Resolution Imaging Spectroradiometer (*MODIS*) albedo product MCD43C3, which provides data describing both directional hemispheric reflectance (black-sky albedo) and bi-hemispherical reflectance (white-sky albedo) in seven different bands and aggregated bands. Data from the *Terra* and *Aqua* platforms are merged in the generation of the product that is produced every 8 days with 16 days of acquisition and available on a 0.05° global grid. The accuracy and quality of the product has been studied by several authors in different locations (e.g., Roman et al. 2009; Salomon et al. 2006; Stroeve et al. 2005).The *MODIS* albedo product has already served as reference for model validation (e.g., Dutra et al. 2010a; Wang and Zeng 2010; Zhou et al. 2003). In this study *MODIS* white-sky broadband shortwave albedo is compared against the offline simulations.

The *IMS* snow cover maps and *MODIS* surface albedo were aggregated to LOWR and HIGR resolutions. The spatial aggregation was performed using the relation in Eq. (4.1) setting $w_{i,j}$ to one (or zero) if the pixel (from *IMS* or *MODIS*) is inside (or outside) the grid point y_j. This is a reasonable approximation since the resolutions of *IMS* (4 km) and *MODIS* (about 5.6 km) are much smaller than LOWR (200 km) or HIGR (25 km). This procedure also allows the transformation of the *IMS* binary product (snow-covered / snow-free) to a grid point snow cover fraction.

4.3 Results

In the following section the HTESSEL offline simulations are compared to observational datasets in eight regions of the Northern Hemisphere poleward of 20° N. Table 4.1 presents the regions and their main characteristics: surface area, mean altitude above sea level and orographic variability (standard deviation of orography) and fraction of the region occupied by forests (high vegetation tile in HTESSEL), derived from the 80 km climate fields. There are four regions in Europe (following the definition of Christensen and Christensen (2007)) that include the Alps (AL) characterized by complex terrain orography, Scandinavia (SC) dominated by forests and Mid-Europe (ME) and Eastern Europe (EE). The remaining four areas include two mountainous regions, the Himalayas (HY) and Rockies (RK), and two rather flat regions with a reduced fraction of forests, Central Eurasia (CE) and Central Canada (CC). The regions were defined in order to sample different combinations of vegetation and orography in the Northern Hemisphere, where seasonal snow cover plays an important role. Along the discussion, three different measures of snow cover are used: (i) snow cover fraction (SCF - 0-1, fraction of a grid box or region covered by snow), (ii) snow cover duration (SCD – days, number of days covered by snow in a grid box or averaged in a region); and (iii) snow-covered area (SCA – km^2,

also referred as snow cover extent, denoting the area of a certain region that is covered by snow). The next section is focused over Switzerland, which was not previously defined as a study region, since the *SLF* SWE observational estimates are only available on the country area. This is a unique dataset for land surface models validation of daily SWE over a complex terrain region.

Table 4.1. Region definitions, including latitude and longitude limits, area, mean altitude above sea level, mean standard deviation of orography and fraction of the region occupied by forests, derived from the 80 km climate fields.

Region	Limits	Area (10^6 km^2)	Orography (m)	Std. Oro (m)	Forest (%)
Alps (AL)	5° 15° E 44° 48° N	0.28	912	383	64
Mid-Europe (ME)	2° 16° E 48° 55° N	0.66	243	74	57
Eastern-Europe (EE)	16° 30° E 44° 55° N	1.21	254	83	41
Scandinavia (SC)	5° 30° E 55° 70° N	1.37	275	84	72
Himalaya (HY)	65° 110° E 22° 47° N	11.35	1906	272	12
Rockies (RK)	-125° -100° E 44° 48° N	3.64	1352	217	22
Central Eurasia (CE)	53° 110° E 48° 75° N	8.65	421	83	43
Central Canada (CC)	-115° -90° E 48° 75° N	3.53	385	45	42
N. Hemisphere (NH)	-180° 180° E 20° 80° N	67.57	753	148	38

4.3.1 Snow mass in Switzerland

Figure 4.2 compares the times series of simulated mean SWE over Switzerland against the *SLF* observations. The observations show a marked inter-annual variability with a maximum SWE of 159, 236, 337 and 190 mm for 2006/07, 2007/08, 2008/09 and 2009/10 respectively. The LOW simulations show a systematic underestimation of SWE and an early melting. Part of the underestimation of SWE is due to lower values of snowfall, when compared with MED or HIG. Although the forcing was upscaled from WFC using a mass conservative approach, over Switzerland there are 66, 8 and 1 grid points at the HIG, MED and LOW resolution, respectively. All simulations, except HIG, were post-processed to HIGR resolution. Table 4.2 presents the accumulated water fluxes from 1 November to 1 March in 2006/07 and 2007/08 averaged over Switzerland. While both MED and HIG were forced with very similar rainfall and snowfall amounts LOW only received about 60%-70% of the snowfall. In addition, LOW is subject to a stronger snow melt, +34% (+164%) compared to HIG and -4% (+116%) compared to MED in 2006/07 (2007/08). Hence, the lower SWE in LOW compared to HIG/MED is caused by two factors: (i) lower snowfall rates due to resolution and (ii) higher melting rates. While the first aspect is associated with the modeling framework of this study, the second shows the importance of resolution in land surface modeling. Higher altitudes in complex terrain regions will mostly have colder and thicker snowpacks and later melting than lower altitudes, even with similar snowfall rates.

During 2006/07 all simulations underestimate SWE, but HIG is closest to *SLF*. In the other three years both HIG and MED show a similar SWE evolution until the beginning of April. MED has a faster melting rate then HIG that closely follows the observations until the end of May. For the four years analyzed, the simulated SWE mean absolute error is 91, 25, 20, 36 and 37 for LOW, MED, HIG,

MOSN and MFEI, respectively. MOSN has the same atmospheric forcing as MED, but neglects the liquid precipitation interception in the snowpack (with consequent refreezing and an increase of SWE). This results in an augmented sensitivity of the SWE evolution to the partitioning between liquid and solid precipitation. From 1 November to 1 March of 2006/07 MED accumulated 186 mm while MOSN only accumulated 116 mm of water in the snowpack. The ERAI forcing has lower values of total precipitation and in particular snowfall when compared with WFC (MED versus MFEI in Table 4.2). This can be primarily attributed to orographic effects that are enhanced in WFC due to the higher resolution of the atmospheric model. The differences between MED and MOSN and MFEI have different causes, but led to a similar temporal evolution of SWE in 2008/09 and 2009/10. Both simulations exhibit an underestimation of SWE throughout the cold season when compared with MED. Still, the total snow ablation occurs at the same time as in MED. These results highlight the importance of both the snow scheme parameterization and the atmospheric forcing accuracy, which contribute similarly to the evolution of SWE over Switzerland.

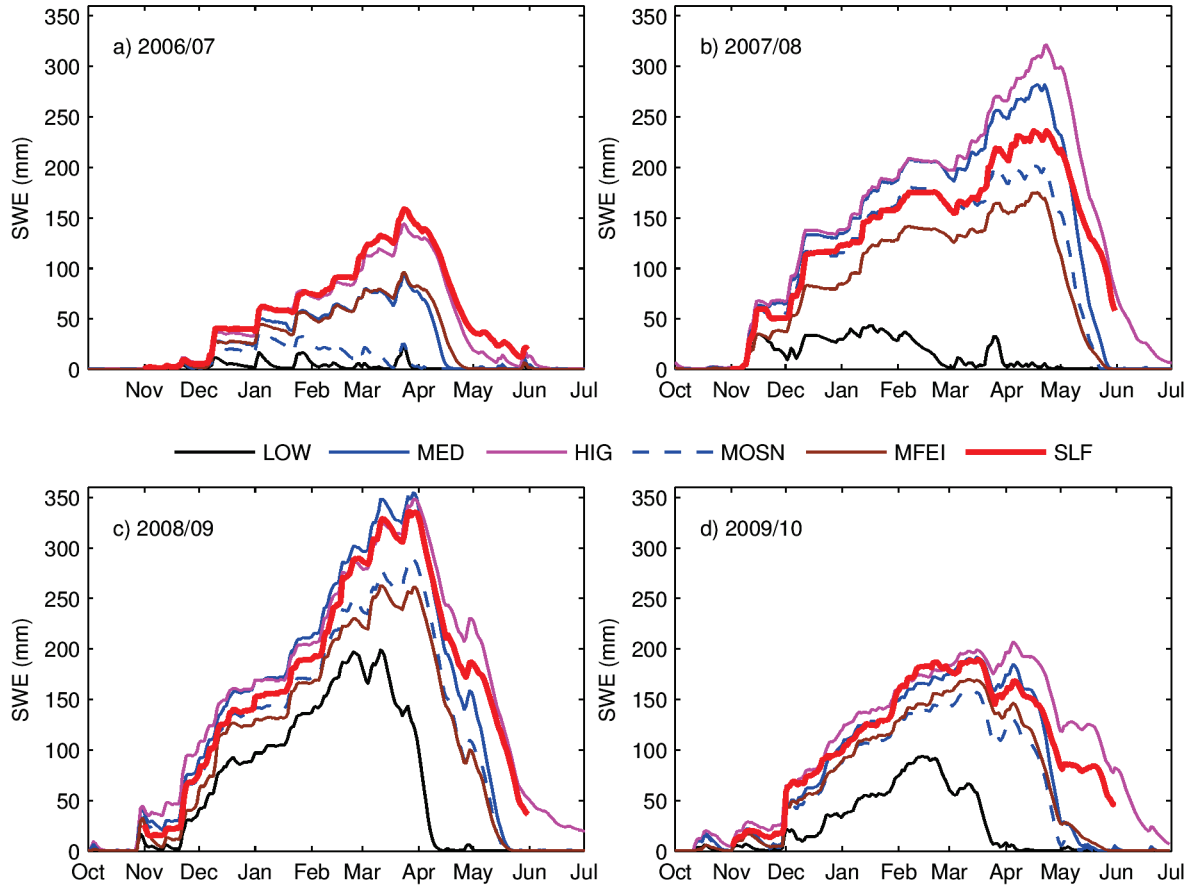

Figure 4.2. Mean SWE over Switzerland. Each panel presents the time series for October to June of 2006/07 (a), 2007/08 (b), 2008/09 (c) and 2009/10 (d). Simulations results include LOW (black), MED (blue), HIG (magenta), MOSN (dashed blue) and MFEI (brown) and observations from SLF (thick red).

Table 4.2. Accumulated water fluxes (mm) over Switzerland from 1 November to 1 March in 2006/07 and 2007/08: rainfall (rainf), intercepted precipitation by the snowpack (intercept), snowfall (snowf), and snow melting (melt). The values in brackets in the snowfall column represent the sum of snowfall and interception.

	2006/07				2007/08			
	Rainf	**Intercept**	**Snowf**	**Melt**	**Rainf**	**Intercept**	**Snowf**	**Melt**
LOW	256	36	74 (110)	107	175	83	180(263)	257
MED	224	70	116 (186)	112	122	59	252(311)	119
HIG	210	59	122 (181)	80	110	36	260(296)	97
MOSN	224	0	116 (116)	98	122	0	252(252)	94
MFEI	219	57	98 (155)	83	190	85	134(219)	87

4.3.2 Snow cover duration in Europe

Snow cover duration is analyzed in four European regions, where model simulations are compared against two independent datasets: *IMS* and *SNOWCLIM* (Figure 4.3). While SWE, SCA or SCF are precisely defined, the calculation of SCD implies the assumption of a certain threshold that defines if snow is present or not. Moreover, the threshold can be defined for a variety of variables, such as SWE, snow depth or SCF. In this study SCD is derived from SCF, to allow its calculation using the *IMS* snow cover maps. Three thresholds were tested, 0.25, 0.5 and 0.75. In Figure 4.3 the *IMS* estimates of SCD are presented for the threshold of 0.5 (red line) and the uncertainty between 0.25 and 0.75 as a light red shaded area. In the Alps region the uncertainty of SCD due to the threshold is large while almost inexistent for the other three regions. Similar behavior was found for the model simulations (not shown).

In general there is a good agreement between the *IMS* estimates and *SNOWCLIM* in the four regions, except in the 2008 winter over the Alps and Scandinavia where *SNOWCLIM* indicates a lower SCD than *IMS*. Part of the differences between *SNOWCLIM* and *IMS* are related to the definition of SCD in *SNOWCLIM* (a snow depth of at least 1 cm), or to missing station values. The different resolution simulations produce a similar SCD for all regions except in the Alps, with a strong underestimation by LOW during the 2006/07 winter that is consistent with the SWE results discussed before over Switzerland (although the Alps region covers a larger area than Switzerland). In Mid Europe SCD in 2009/10 shows anomalous high values both in the observations and the model simulations. This finding is also documented by Seager et al. (2010) who identified snow anomalies during this winter in the Northern Hemisphere. Also in Mid and Eastern Europe the MFEI shows an underestimation of SCD, especially during the 2007/08 and 2008/09 winters, that is associated with an underestimation of snowfall in ERAI when compared with WFC. In Eastern Europe from 1 November 2007 to 1 March 2008 WFC predicted 72 mm of accumulated snowfall, while ERAI only predicted 36 mm.

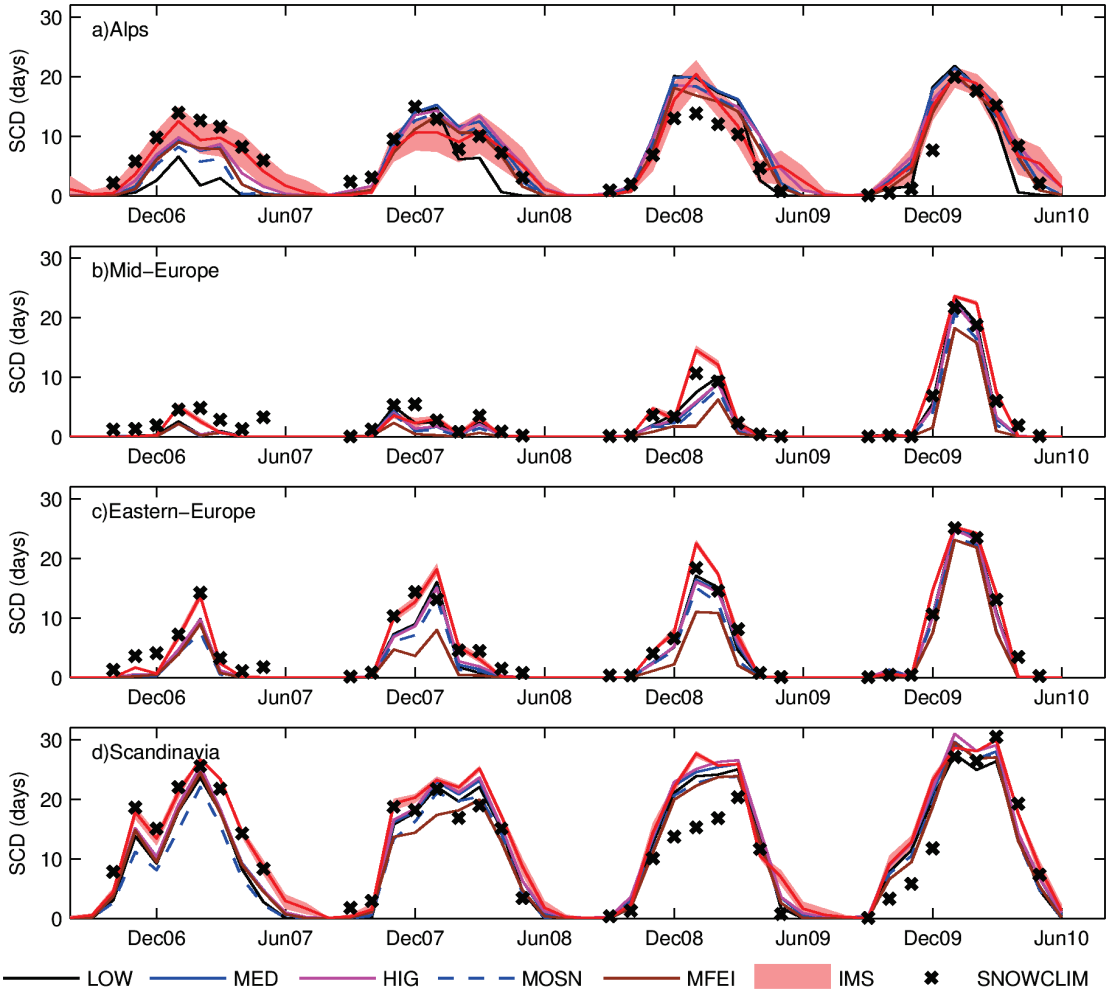

Figure 4.3. Time series of mean monthly snow cover duration (in days) in the Alps (a), Mid-Europe (b), Eastern-Europe (c) and Scandinavia (d). HTESSEL simulations LOW (black), MED (blue), HIG (magenta), MOSN (dashed blue) and MFEI (brown) are compared with SNOWCLIM (black symbols) and IMS estimates. The IMS estimates represent the uncertainty of the SCD calculation using 0.25 and 0.75 SCF for the threshold (fill solid light red), and SCD evaluated for a 0.5 threshold (red line).

4.3.3 Snow-covered area and fraction

The simulated snow-covered area is compared against *IMS* in Figure 4.4 for four regions. LOW simulations systematically overestimate SCA in the Alps during the accumulation period compared to an underestimation during the ablation period. When compared with LOW, both MED and HIG show a damping of the strong positive (negative) biases during the accumulation (ablation) period. The mean absolute errors (MAE) of SCA during spring normalized by the mean observed SCA in Table 4.3 illustrate the resolution impact with a reduction of 42% of the error from LOW to HIG in the Alps.

In the Rocky Mountains SCA is generally underestimated (Figure 4.4 c), with a reduction of the bias with increased resolution, whereas for other flat terrain regions such as ME, EE, SC, CE and CC the different resolutions show a limited impact (see Table 4.3). The SCA biases in the Northern Hemisphere depict the reduced impact of horizontal resolution on a global scale showing almost overlapping curves in Figure 4.4 d.

While the impact of the resolution of the land surface model is mainly restricted to complex terrain regions, the old snow physics (MOSN) and ERAI atmospheric forcing (MFEI) have a noticeable

impact on SCA. The spring biases in Table 4.3 show that MFEI has larger errors than MED, which is mainly due to a systematic underestimation of SCA (as shown for the NH in Figure 4.4 d) in all regions, except the Alps and the Himalayas. This is mainly due to the atmospheric forcing, with an underestimation of snowfall by ERAI when compared with WFC. For example, the accumulated snowfall amounts to 86 and 63 mm in WFC and ERAI, respectively, averaged over NH from 1 November 2007 to 1 March 2008. One of the reasons for these differences is the higher spatial resolution of WFC, with an improved representation of orographic features and the partitioning between liquid and solid precipitation. Interestingly, the effects of the old snow physics, forced with WFC, tend to be similar to those of the simulations forced with ERAI. Generally, MOSN is closer to MED than MFEI, but is subject to a similar SCA underestimation. This is primarily due to the lack of rainfall interception in the snowpack and early melting associated with an underestimation of surface albedo (see Dutra et al. (2010a) for a detailed evaluation of the NEW and old snow scheme). These results show that the underestimation of snowfall in ERAI, when compared with WFC, has a similar impact as neglecting the interception of rainfall in the snowpack in MOSN - which was already discussed in the previous section. The magnitude of SCA biases in Scandinavia is comparable with other areas with a lower forest fraction suggesting that the treatment of exposed versus shaded snow in HTESSEL does not contribute considerably to the errors.

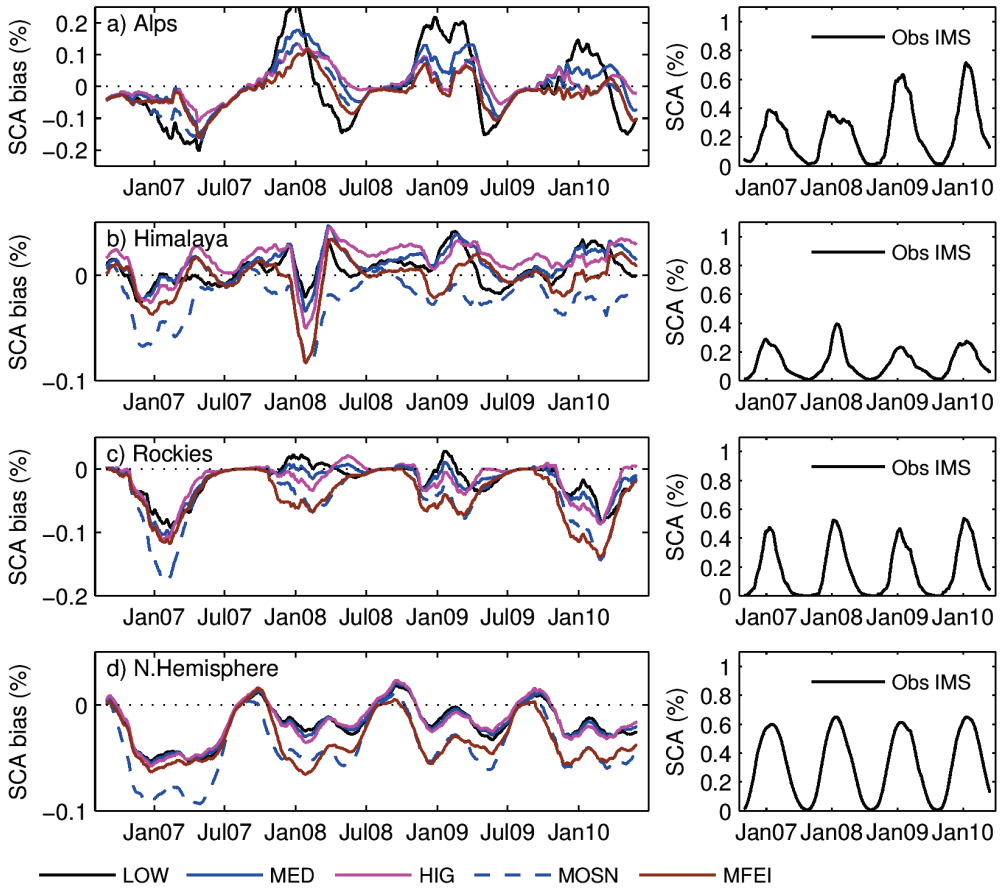

Figure 4.4. Bias of simulated snow-covered area (SCA) (simulations - IMS) in the Alps (a), Himalaya (b), Rockies (c) and Northern Hemisphere (d) and associated IMS observations on the right panels. Both simulated biases and observed SCA are normalized by the total area of each region. The vertical axes represent the bias (left), or observed (right), SCA in terms of the fraction of total area of each region.

Table 4.3. Mean absolute error (MAE) of snow-covered area in spring (March-May 2007-2010) for each simulation and each analysis region. MAE was normalized by the mean observed snow-covered area during spring in each region.

	AL	ME	EE	SC	HY	RK	CE	CC	NH
LOW	61	46	32	17	16	27	5	14	8
MED	38	48	34	13	24	21	6	15	7
HIG	26	46	33	14	28	18	6	15	7
MOSN	28	57	47	23	22	35	12	22	17
MFEI	35	65	48	20	19	31	8	19	12

The relation between resolution, snow physics and atmospheric forcing in simulating SCA is consistently observed in all regions except the Alps and the Himalayas. In the Alps, MOSN has a better performance than MED. In the Himalayas the increased horizontal resolution increases the SCA MAE in spring with an overestimation of SCA in HIG compared to LOW (see Figure 4.4 b). SCA is one of the most common measures used to validate simulations of snow by land surface models or climate models (e.g. Roesch 2006; Sheffield et al. 2003). It is an integral quantity with the shortcomings of hiding compensating errors in the spatial distribution of snow cover, i.e. SCA can be close to the observations in a certain region but geographically misplaced within that region. The spatial correlation (or pattern correlation coefficient) provides a measure of the degree of spatial coherence between simulated and observed snow cover fraction. The Pearson correlation is calculated for each month between HTESSEL simulations and observations of SFC at HIGR for all grid points in each region.

Figure 4.5 displays the temporal evolution of the spatial correlation between monthly simulated and observed snow cover fraction for the same regions as in Figure 4.4, and Table 4.4 summarizes the mean correlation values averaged for all spring months. The time series show a pronounced seasonal cycle in all regions with higher values in the cold season peak and a reduction as we move to summer. This measure is sensitive to the snow cover extent in the region. In the Himalayas, the correlations increase with increasing resolution while SCA MAE did not. This was due to compensating negative and positive SCF biases in LOW (compare the panels a. and c. of Figure 4.6) resulting in lower SCA errors than in HIG. These findings illustrate the shortcomings of using SCA as validation measure by itself and the benefits of complementing the analysis with the spatial correlation. In the Alps, MOSN and MED have similar spatial correlations, whereas SCA showed an improved performance of MOSN when compared to MED. As for SCA, the spatial correlations show a reduced impact of resolution in flat areas (SC, CE and CC) and in the Northern Hemisphere as a whole, whereas in mountain regions (AL, HY and RK) there is a consistent improvement with increased resolution. The smaller regions of Mid-Europe and Eastern Europe exhibit an increase of the spatial correlation with increased resolution, which was not the case for SCA. However, the spatial correlations are lower than for the remaining regions. A plausible reason for this is the low snow cover extent in areas where a relatively small error in simulating SCF can led to a very poor spatial correlation. Snow physics and atmospheric forcing do not show the large impacts found for SCA, nonetheless the deficiencies in MFEI and MOSN when compared with MED are still evident.

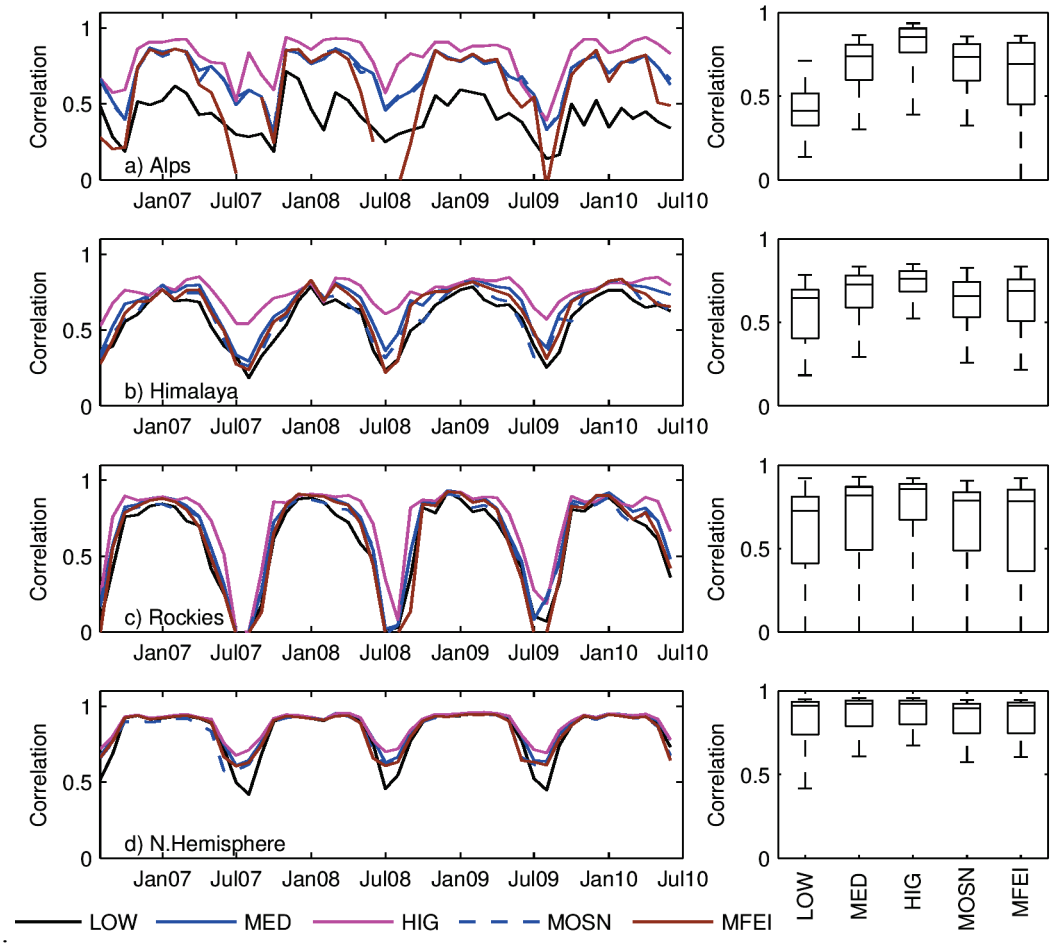

Figure 4.5. Temporal evolution of the spatial correlation (pattern correlation coefficient) between monthly simulated and observed snow cover fraction in the Alps (a), Himalayas (b), Rockies (c) and Northern Hemisphere (d). The right panels show, for each region, the box plot summaries of the pattern correlation coefficients. The boxes have horizontal lines at the lower quartile, median and upper quartile and the whiskers (vertical lines) extent from the end of each box to the maximum and minimum.

Table 4.4. Spatial correlation (pattern correlation coefficient) between monthly simulated and observed snow cover fraction in each analysis region averaged for all spring months (March-May 2007-2010).

	AL	ME	EE	SC	HY	RK	CE	CC	NH
LOW	0.46	0.20	0.35	0.83	0.66	0.67	0.85	0.85	0.92
MED	0.77	0.28	0.43	0.88	0.77	0.77	0.88	0.87	0.93
HIG	0.89	0.43	0.76	0.89	0.82	0.85	0.88	0.87	0.94
MOSN	0.76	0.28	0.42	0.79	0.69	0.74	0.84	0.81	0.91
MFEI	0.71	0.26	0.30	0.84	0.73	0.73	0.86	0.84	0.92

A spatial overview of the results discussed in this section is presented in Figure 4.6 with the representation of the mean spring biases of simulated snow cover fraction in Eurasia and the associated snow cover map from *IMS*. The snow line (snow fraction = 0.5) in spring (Figure 4.6 f) is located around 55° N in Eurasia with a southward displacement as we move from west to east. Several orographic features with increased snow cover can be observed such as the Alpine region, the Caucasus Mountains, the Ural Mountains, the Himalaya range and the Altai Mountains, among others.

In general, all simulations (panels a-e. of Figure 4.6) have limitations in representing snow cover in mountain regions, especially in the Himalayas. In the Alpine region there is an overestimation along the northern and southern rim of the mountain range and an underestimation along the Alpine ridge in LOW that is partially reduced in MED and almost inexistent in HIG. The different resolutions show similar patterns of early melting throughout the snow line with a remarkable performance over the Ural Mountains. The early melting is more pronounced in MFEI than MED both in intensity and spatial spread whereas MOSN shows even larger biases, especially in Eastern Scandinavia.

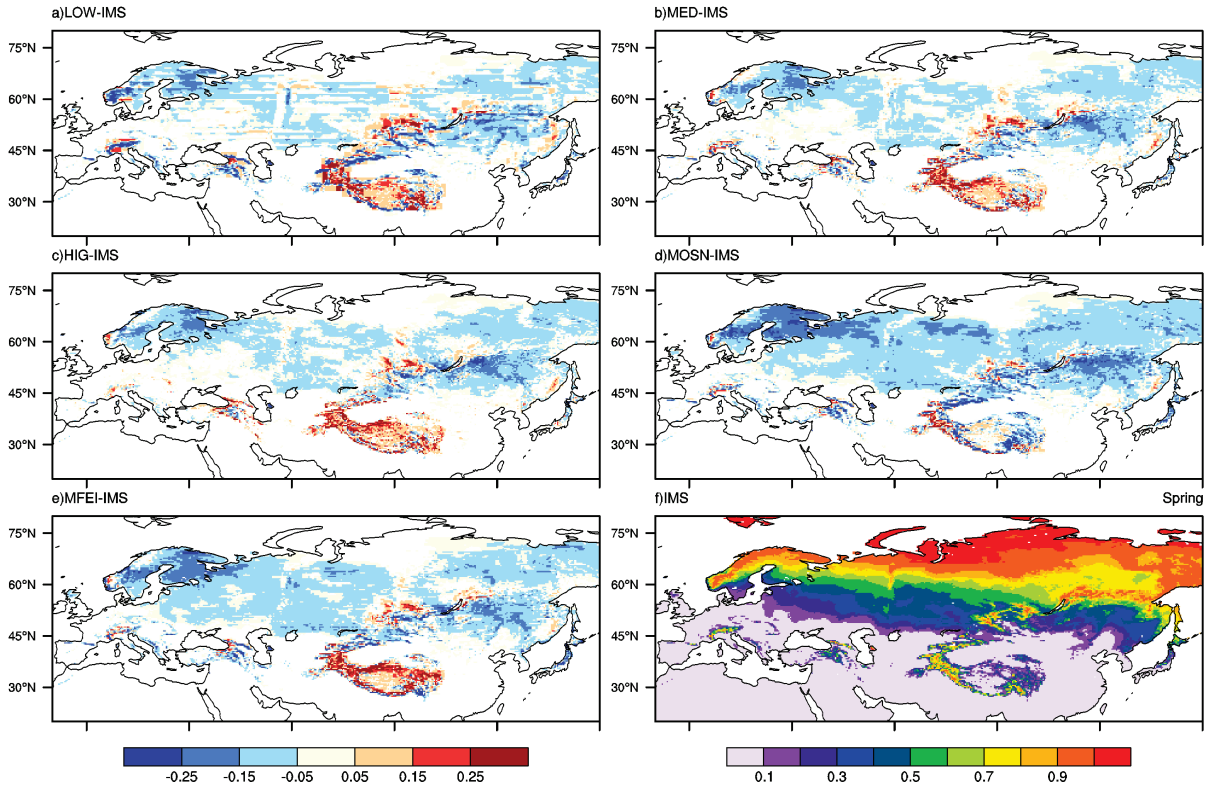

Figure 4.6. Mean spring (March-May 2007-2010) simulated snow cover fraction differences with respect to IMS: LOW (a), MED (b), HIG (c), MOSN (d), MFEI (e); and IMS mean spring snow cover (f). Note the different color scales between panels a) to e) and panel f).

4.3.4 Surface Albedo

The evaluation of surface albedo complements the above results since surface albedo gives a radiative balance perspective of snow cover presence over land. Time series of simulated and *MODIS* surface albedo in several regions are presented in Figure 4.7. As reported for the *IMS* SCA, *MODIS* albedo shows a distinct increase of surface albedo over the Alps in the 2009 and 2010 winter seasons. Mid and Eastern Europe also had high snow cover extent and duration during the 2010 winter (see Figure 4.3), which is also confirmed by the *MODIS* albedo (not shown). The 2008 winter in the Himalayas is also characterized by a higher surface albedo as well as by a high *IMS* SCA. Although these three examples are solely based on a visual inspection of the time series, they illustrate the coherency between the two independent datasets. However, the relation between SWE (the prognostic quantity in the model), SCF and surface albedo is still a research subject in the land surface modeling community. The model surface albedo background (snow-free) climatology, identical in all simulations, is also represented in Figure 4.7. Comparing the background climatology to the simulations, or *MODIS*, it is

possible to infer that the annual cycle of surface albedo, on the hemispheric scale, is mainly driven by snow cover presence. This shows the importance of a correct representation of snow cover and its relation to surface albedo in land surface models.

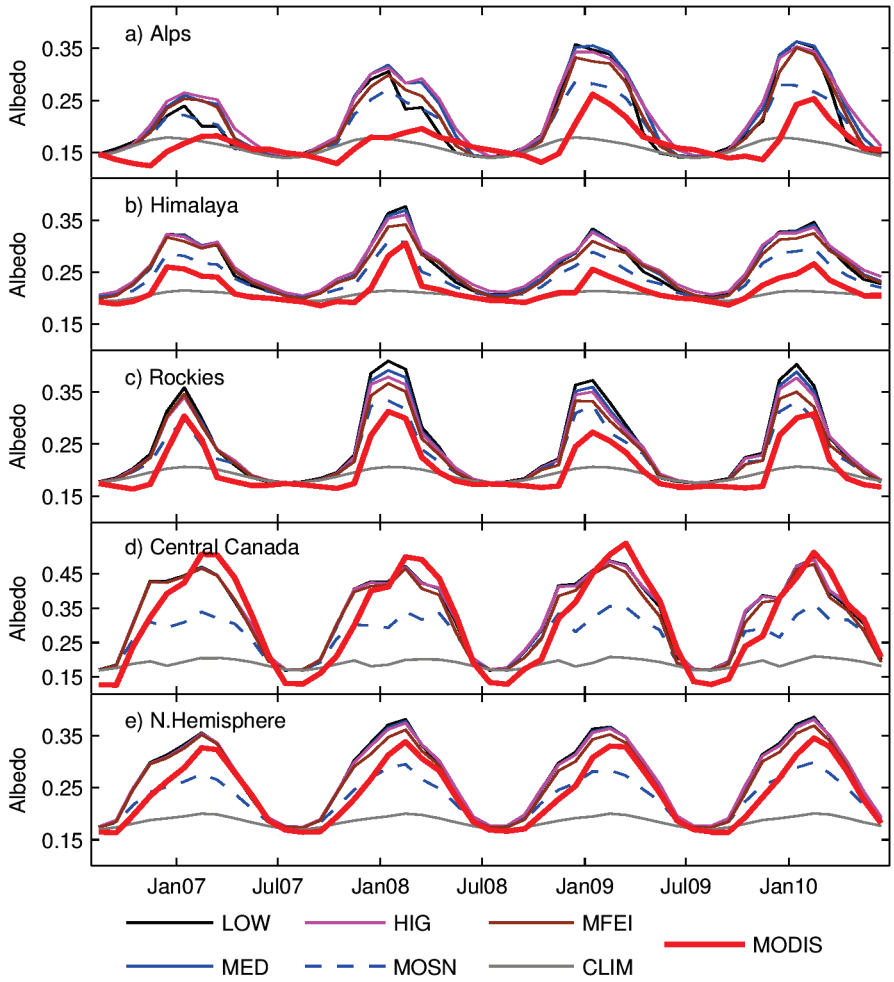

Figure 4.7 . Mean monthly simulated surface albedo in the Alps (a), Himalayas (b), Rockies (c), Central Canada (d), and Northern Hemisphere (e). Simulation results include LOW (black), MED (blue), HIG (magenta), MOSN (dashed blue) and MFEI (brown). Observations from MODIS (thick red) represent monthly means over each region. The simulations were spatially averaged using only grid points were MODIS was available to ensure a fair comparison. The model's background climatology (snow free) for each region is also represented as CLIM (gray).

In the three mountainous regions represented in Figure 4.7 (Alps, Rockies and Himalayas), there is a pronounced overestimation of surface albedo throughout the snow-covered period. Such a signal is not found in SCA for the mentioned regions. In Central Canada, and the Northern Hemisphere, all simulations applying the NEW snow scheme show an overestimation of surface albedo during the accumulation period that is reduced (almost inexistent) during the ablation period. The different resolutions and ERAI forcing have a small impact on surface albedo. In contrast, using the old snow physics leads to large differences to the remaining simulations in terms of a reduction of the surface albedo throughout the cold season.

The mean surface albedo maps in spring from *MODIS* and the respective simulation differences are shown in Figure 4.8. The presence of snow in spring has a distinct signal on the *MODIS* surface

albedo (panel f). All simulations show an overestimation in two distinct areas: Himalayan mountain range and Central Siberian Plateau. This signal is only present in snow cover extent in the Himalaya. The bias over the Siberian Plateau is not associated with snow cover extent but rather with snow albedo. Furthermore, the overestimation is larger in all simulations performed with the NEW snow scheme (e.g. MED) when compared with MOSN. On the other hand, MOSN presents a spatially spread pattern of surface albedo underestimation poleward of 60° N. This bias was addressed in the revision of the old snow scheme and is partially reduced with the NEW snow scheme. As for snow cover fraction, the horizontal resolution does not have a significant impact on surface albedo. ERAI forcing shows a significant impact on snow cover, but the impact on surface albedo is negligible (MED vs MFEI in panels b. and e. of Figure 4.8). The comparison of the model simulations against *MODIS* also highlights some differences in North Africa that are associated with the background climatology used in HTESSEL. In 2007, the background albedo of the ECMWF integrated forecast system changed to a climatology derived from *MODIS* discriminating between direct/diffuse, near infrared and visible surface albedo (in snow free conditions). The offline simulations with HTESSEL still use the old background climatology (described in section 4.2.1) since the usual atmospheric forcings (including ERAI and WFC) only provide the full (broad band) solar radiation downward flux. In summary, the differences found in the simulated surface albedo when compared to *MODIS* are due to three main factors: (i) deficiencies of the simulated snow cover fraction, (ii) deficiencies of the simulated snow albedo and (iii) deficiencies of the snow-free background climatology prescribed in HTESSEL.

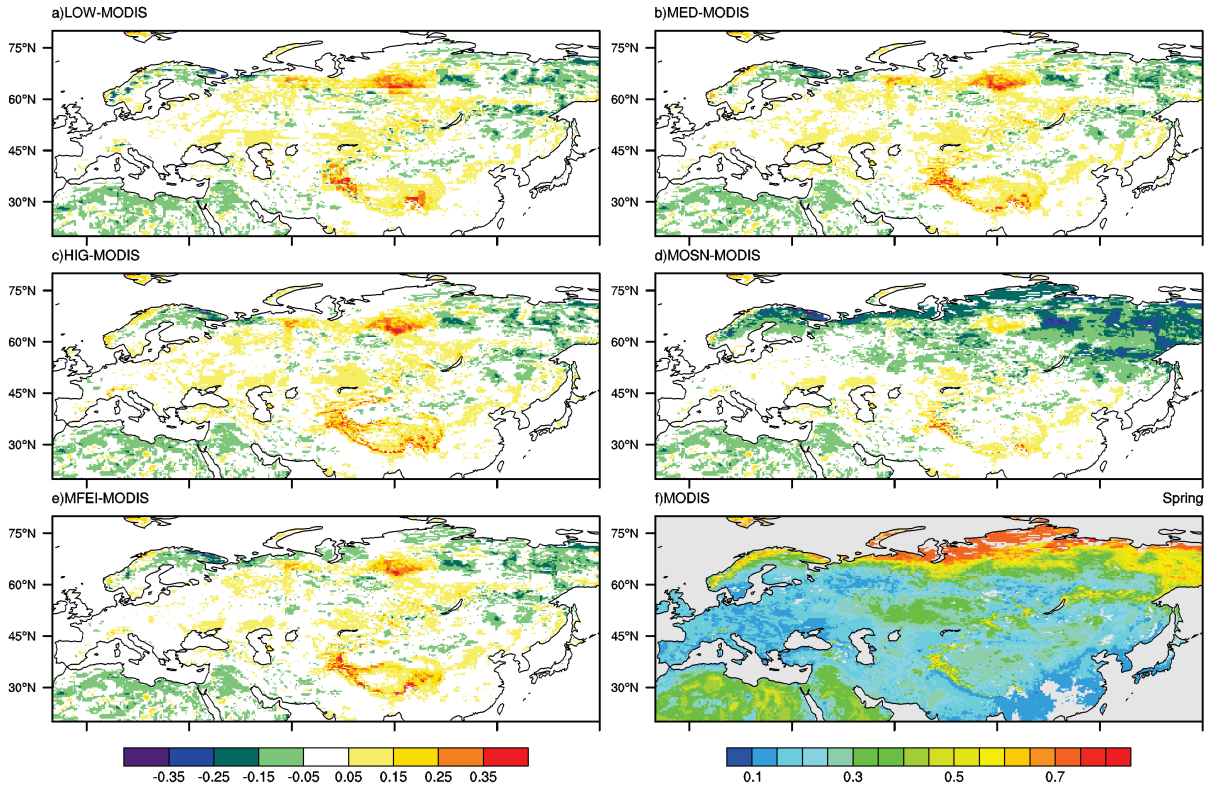

Figure 4.8. Mean spring (March-May 2007-2010) simulated surface albedo differences with respect to MODIS: LOW (a), MED (b), HIG (c), MOSN (d), MFEI (e); and MODIS mean spring snow cover (f). Note the different color scales between panels a) to e) and panel f).

4.4 Conclusions

This study presents an assessment of three different factors controlling offline simulations of snow cover in the LSM HTESSEL. The assessment was carried out by comparing the simulations against different observational datasets. Over topographically structured area of Switzerland, the simulations of snow water equivalent (SWE) were sensitive to the horizontal resolution. Pronounced differences were found between the low and intermediate resolutions, whereas the latter showed a similar behavior to the high resolution simulation, except during the final ablation period. The underestimation of SWE by the low resolution simulation was due to the underprediction of snowfall, resulting from forcing interpolation, and due to higher melting rates when compared with the higher resolution runs. The simulations forced with ERAI and forced with WFC running with the old snow physics underestimate SWE but showed a similar SWE temporal evolution. ERAI underpredicts snowfall (when compared with WFC) while the old snow physics neglects the interception of rainfall in the snowpack. While the resolution impact was significant for the runs at 200 km and 80 km, at 80 km the atmospheric forcing accuracy and snow scheme parameterization contribute almost equally to the evolution of SWE over Switzerland - more than increasing the resolution to 25 km.

Snow cover duration (SCD) analyzed in four European Regions showed a reasonable agreement between the *IMS* estimates and *SNOWCLIM*, which represent two independent datasets (remote sensing-based and station-based). The evaluation of SCD is constrained by the definition of the threshold for presence of snow. However, for snow cover fraction (SCF) the associated uncertainty of using values between 0.25 and 0.75 is mainly restricted to the Alps region where all the simulations, except at low resolution, are similar to *IMS* and *SNOWCLIM*. The simulation forced by ERAI tends to underestimate SCD, especially in Mid and Eastern Europe. The analysis suggests that a possible cause is the underprediction of snowfall in ERAI when compared with WFC.

Although snow-covered area (SCA) is commonly used as a validation metric, it was shown that it should be used in conjunction with the SCF spatial correlation. While SCA can hide compensating errors, the spatial correlation reflects the spatial coherency of the snow-covered versus snow-free areas in a certain region in different datasets. This was the case in the Himalayas, where SCA error during spring increased in the higher resolution run. However, the spatial correlation analysis showed that the high resolution simulation had a better spatial coherency with *IMS* than the lower resolution simulations. In general, increased resolution improves SCA and spatial correlations in complex terrain areas, such as Alps, Himalayas and Rockies while on the remaining regions including the Northern Hemisphere as a whole, the impact of resolution was reduced. Finally, the surface albedo evaluation against *MODIS* did not show a strong dependence on horizontal resolution or atmospheric forcing, but rather on the model physics, which includes the snow albedo parameterization. The evaluation of surface albedo highlights the importance of a correct representation of snow cover in the model, since on a hemispheric scale the annual cycle of surface albedo is mainly driven by snow presence.

This work identified some deficiencies of the NEW snow scheme of HTESSEL concerning the representation of snow processes in mountainous regions associated with both the snowpack physics and the surface albedo. These deficiencies were not clearly identified by Dutra et al. (2010a). They can be primarily attributed to missing processes associated with subgrid scale variability that are not accounted for in HTESSEL. This shows the need of a continuous validation of the model using different observational datasets. The positive snow cover anomaly in northwestern Europe during the

2010 winter as reported by Seager et al. (2010) is correctly simulated by HTESSEL and consistent with observations both in terms of SCF and surface albedo.

The horizontal resolution proved to play an important role on simulating snow cover in complex terrain regions, while its impact on flat terrain regions is reduced. In the latter regions, the atmospheric forcing accuracy and model physics play a more important role. These results are model dependent and their generalization is not certain, especially concerning the model physics. However, they show that developments in land surface models are strongly dependent on the available forcing and validation dataset quality. In this study, horizontal resolution was assessed by forcing the model with a high quality atmospheric dataset originally available at high resolution. The simulation setup framework presented in this study can also be applied to investigate other land-atmosphere processes, especially alternative approaches to describe land surface subgrid-scale variability, which is a critical point in climate models.

Acknowledgments

The National Snow and Ice Data Center is acknowledged for providing the *IMS* snow cover data. We also thank the *MODIS* albedo science team and the Land Processes Distributed Active Archive Center (LP DAAC) for providing the MCD43C albedo data. Part of the ground observations on snow depth were kindly provided by the Swiss Federal Office of Meteorology and Climatology MeteoSwiss. Deutscher Wetterdienst (DWD) has provided the SNOWCLIM gridded data. This work was supported by the Portuguese Foundation for Science and Technology (FCT) under project AMIC PTDC/AAC-CLI/109030/ 2008 cofinanced by the European Union under program FEDER. E. Dutra acknowledges the financial support of FCT under Grant FRH/BD/35789/2007.

5

Evaluation of three snow schemes of varying complexity in a climate model: impacts on surface energy and hydrology*

Abstract

Three different complexity snow schemes implemented in the ECMWF land surface scheme HTESSEL are evaluated within the EC-EARTH climate model. The snow schemes are: i) CTR, the original HTESSEL single bulk layer snow scheme (same as in the ECMWF interim reanalysis); ii) OPER, a new snow scheme in operations at ECMWF since September 2009; and 3) ML3, a multi-layer version of OPER. ML3 outperforms CTR and OPER in deep snowpack conditions through its ability to simulate sporadic melting events thanks to the lower thermal inertial of the uppermost layer. Coupled atmosphere-land/snow simulations performed by the EC-EARTH climate model, based on the current seasonal forecast system of ECMWF, are validated against remote sensed snow cover and surface albedo. CTR has a systematic early melting linked to an overestimation of surface albedo during spring. The snow albedo parameterization and interception of rainfall in OPER and ML3 reduced the early melting bias. The increased snow thermal insulation from CTR to OPER and ML3 led to warmer soil temperatures during winter and spring. This led to reduced soil freezing and increased soil moisture content, increased evapotranspiration and intensification of summer precipitation as a result of the increased moisture in the lower troposphere. The increased complexity of ML3 shows its potential in modeling thick snowpacks in open areas such as prairies or tundra in Northern Latitudes. This led to an improved match with observed near surface air temperature.

---

* Dutra, E.[1,2], P. Viterbo[3], P. M. A. Miranda[1], and G. Balsamo[4], 2011: Evaluation of three snow schemes of varying complexity in a climate model: impacts on surface energy and hydrology. *Submitted to Journal of Hydrometeorology*.

[1] Centro de Geofísica da Universidade de Lisboa, Instituto Dom Luiz, University of Lisbon, Lisbon, Portugal.

[2] Institute for Atmospheric and Climate Science, ETH, Zurich, Switzerland.

[3] Institute of Meteorology, Lisbon, Portugal.

[4] European Centre for Medium-Range Weather Forecasts, Reading, United Kingdom.

5.1 Introduction

Accurate simulations of the snow cover strongly impact on the quality of weather and climate prediction as the absorption of solar radiation at the land-atmosphere interface is modified by a factor up to four in response to the presence of snow (albedo effect) (Viterbo and Betts 1999). Changes in snow cover modify the surface albedo, which then feedbacks to surface temperature (Groisman et al. 1994b). In Northern latitudes and mountainous regions, snow also acts as an important energy and water reservoir (Immerzeel et al. 2010). Therefore, a correct representation of snow water equivalent (SWE) and density is crucial for predicting the snow thermal insulation, especially in climate change conditions, with direct consequences for soil hydrology and ground temperature (Bartlett et al. 2004, 2005; Lynch-Stieglitz 1994; Rangwala et al. 2010; Stieglitz and Smerdon 2007). This thermal process also plays an important role on controlling soil moisture freezing, with impact on the stable boundary layer (Viterbo et al. 1999).

The role of snow cover in the climate system has been a topic of research for a long time, including early field observations reported by Sverdrup (1935). On a modeling framework, Williams (1975) was one of the first to explore the influence of snow cover on atmospheric circulation and climate change. Snow models have been developed for many applications, such as snow process studies, runoff and avalanche forecasting and to be used in atmospheric models. Brun et al. (2008) compiled a detailed review of existing models and their applications. The snow schemes designed for atmospheric models (both global and regional) for applications in numerical weather prediction and climate modeling share a similar basic function, to provide lower boundary conditions to the atmosphere over snow covered regions.

This study evaluates the performance of three snow schemes, of different complexity, coupled to the EC-EARTH (Hazeleger et al. 2010) climate model. EC-EARTH was recently developed starting from the European Centre for Medium-Range Weather Forecasts (ECMWF) seasonal forecast system motivated by the seamless prediction concept of bringing weather forecast and climate change studies into a single framework. The land surface component of EC-EARTH is the Hydrology Tiled ECMWF Scheme of Surface Exchanges over Land [HTESSEL (Balsamo et al. 2009)]. The snow schemes evaluated include an old snow scheme used at ECMWF until 2009 (CTR), a new snow scheme in operations at ECMWF and default on EC-EARTH (OPER) and a multi-layer version of OPER (ML3). Dutra et al. (2010a, hereafter DU10), describes OPER and its validation against CTR in offline mode. This study is a natural extension of DU10, evaluating OPER in coupled atmosphere simulations. Additionally, a more complex snow scheme (ML3) is also evaluated.

The ML3 snow scheme is validated in offline simulations over several site locations. This is an important step to verify the behavior of the newly developed snow scheme. A three member ensemble of 30-years-long was carried out with each one of the snow schemes activated in EC-EARTH. The simulations were performed with prescribed sea surface temperature and sea ice cover from the ECMWF reanalysis. This framework to evaluate the different snow schemes guarantees that the coupling of the snow schemes with the overlying (underlying) atmosphere (soil) follows the same procedure. The evaluation of the performance of the three snow schemes in EC-EARTH is performed

by comparing the simulations with observed snow cover, surface albedo and 2-meter temperature, as in other studies that validate climate models (e.g. Roesch 2006). The simulated surface water and energy fluxes are also evaluated for the three snow schemes. Special attention is given to the role of snow thermal conductivity in controlling the land-atmosphere coupling (Cook et al. 2008; Ge and Gong 2010).

A brief overview of the snow schemes is presented in the following section. The validation of the ML3 snow scheme and comparison with CTR and OPER, in offline site simulations is presented in section 5.3. The EC-EARTH simulations in section 5.4 are validated against remote sensed data of snow cover extent and surface albedo. Additionally, the 2-metre temperature is compared against the Climate Research Unit (CRU) dataset and the snow albedo feedback (SAF) with observational estimates from Hall and Qu (2006, hereafter HQ06). Changes in upper air temperature and specific humidity are also discussed. Section 5.5 summarizes the main conclusions of this study.

5.2 Snow schemes

The three snow schemes coupled to HTESSEL are compared in Table 5.1 with respect to the number of snow layers, liquid water representation, snow density and snow albedo parameterizations. Control (CTR) (ECMWF 2004) was the snow scheme used at ECWMF since late 90's until 2009, including the ERA-40 (Uppala et al. 2005) and ERA-Interim (Dee et al. 2011) reanalysis. In 2009, a new snow scheme, operational (OPER), was introduced in the integrated forecast system at ECMWF and its description, validation and comparison against CTR in offline mode is presented by DU10. A multi-layer version of OPER (ML3) was developed for this study and its main characteristics are presented in appendix (5.6). The three snow schemes are identically coupled with the overlying atmosphere and underlying soil within HTESSEL.

Table 5.1. Summary of the main differences between the three snow schemes coupled to HTESSEL

Snow scheme	Number of Layers	Liquid water	Snow density	Snow albedo
CTR (ECMWF 2004)	One	Not represented (dry snow)	Exponential increase with age.	Exponential decay with age; 0.15 for shaded snow
OPER (Dutra et al. 2010a)	One	Diagnosed from temperature, mass and density of the snowpack	Overburden and thermal metamorphisms, melt water retention.	Exponential decay with age; vegetation type dependent for shaded snow
ML3 (Appendix 5.6)	Up to three	Bucket type prognostic in each layer	As OPER but solved for each layer	As OPER

The snow scheme represents one (CTR, OPER) or up to three (ML3) additional layers on top of the upper soil layer, with independent prognostics thermal and mass contents. The net energy flux at the top of the snowpack is the residual of the skin energy balance from the snow covered tiles in HTESSEL. The basal heat flux is given by a diffusion formulation between snow temperature (CTR and OPER and lower snow layer in ML3) and soil (uppermost layer) temperature. The absorbed energy is used to change the snow temperature or melt the snow when snow temperature exceeds the melting point. CTR assumes dry snow, in OPER liquid water is diagnosed from snow temperature,

mass and density while ML3 represents liquid water as a prognostic for each layer following a bucket type approach. In both OPER and ML3 the liquid water coexists in the snowpack leading to internal phase changes (freezing/melting), and rainfall can be intercepted. The heat capacity of the snow layer is a function of its depth, density and presence of liquid water. Snow thermal conduction changes with changing density (different for each layer in ML3). Snow density changes due to overburden and thermal metamorphisms (Anderson 1976), independently for each layer in ML3 and for the entire snowpack in OPER. Both snow cover fraction and snow albedo are parameterized similarly in OPER and ML3 and different to CTR (see DU10 for details).

5.3 Site simulations

Data from the micrometeorological site in Col de Porte (CdP) was used to force, validate and intercompare the three snow schemes. CdP is operated by the Center of Snow Studies in Grenoble, France, and is located at 45°N, 6°E at an altitude of 1320 m. Data from this site has been widely exploited in model validation (e.g. Boone and Etchevers 2001) and was one of the sites that participated in the first snow model intercomparison project [SnowMIP (Etchevers et al. 2004)]. Offline simulations of snow water equivalent (SWE), density and runoff for the winter seasons of 1996/97 and 1997/98 were validated against CdP observations (Figure 5.1). From November to mid January, in both years, all the simulations properly represent the snow accumulation. From February to May both CTR and OPER tend to overestimate SWE, whereas ML3 is closer to the observations. The final ablation is delayed in all simulations with a stronger overestimation by CTR. The mean absolute error (MAE) of SWE was 98, 82 and 42 kg m^{-2} during the 1996/97 winter in CTR, OPER and ML3, respectively; and 128, 84 and 40 kg m^{-2} during the 1997/98 winter. On average for the two winter seasons the MAE of SWE reduced 25% from CTR to OPER, and 64% from CTR to ML3. Snow density evolution is correctly captured by OPER and ML3. CTR shows a fast increase and saturation at 300 kg m^{-3}, similar to what was found by DU10 in other site locations. Pronounced density changes due to snowfall events are evident in the observations. In mid April 1998 the sharp increase of SWE is accompanied by a significant decrease of snow density that is poorly simulated by OPER but correctly captured by ML3.

The accumulated runoff (Figure 5.1 c, f) is defined as the liquid precipitation and snowmelt that is in excess of the snow-cover holding capacity. Its temporal evolution gives an integrated view the snowpack water balance. The difficulties of the three snow schemes in simulating short duration melting events during late winter and spring are evident. These melting episodes are mainly driven by synoptic conditions, and are poorly represented by CTR and OPER. On the other hand, ML3 partially reproduces those episodes with melting in the first layer. These results clearly show one of the main drawbacks of a single snow layer associated with the large thermal inertia of deep snowpacks (Marks et al. 2008). The multi-layer scheme has an enhanced accuracy in simulating mid-season sporadic melting events, since the top snow layer has a reduced thermal inertia. Other site locations were tested [from SnowMIP2 (Rutter et al. 2009)] and showed similar results with significant improvements from CTR to OPER (as presented by DU10). However, from OPER to ML3 the improvements are mainly restricted to deep snowpack locations, while for shallow snowpacks and highly forested locations ML3 returns very similar results to OPER (not shown).

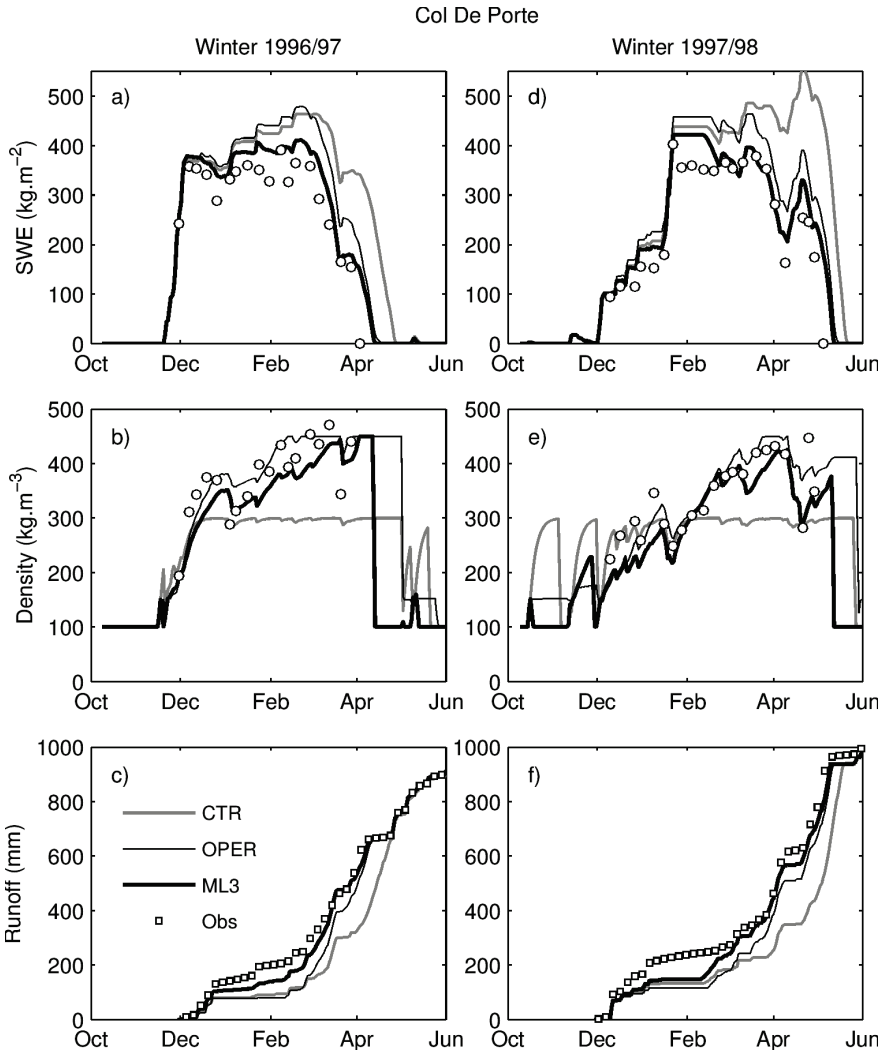

Figure 5.1. Simulation results for CTR (gray), OPER (thin black) and ML3 (thick black) for the 1996-97 (a-c) and 1997-98 (d-f) winter seasons at Col de Porte site: SWE (a, d), snow density (b, e) and runoff (c, f). Observations are represented by open circles. Runoff was accumulated since 1 December of each year and is defined as liquid precipitation and snowmelt that is in excess of the snow-cover holding capacity

5.4 Atmospheric simulations

The atmospheric model of EC-EARTH version 2 (Hazeleger et al. 2010) is based on ECMWF's Integrated Forecasting System (IFS), cycle 31R1, corresponding to the current seasonal forecast system of ECMWF. The model runs at TL159 horizontal spectral resolution (about 125 km on the grid point space) with 62 vertical levels that extend up to 5 hPa. Some aspects of newer IFS cycles have been implemented additionally, including a new convection scheme and the new land surface scheme HTESSEL. EC-EARTH also has ocean and sea ice model components, but in this study atmosphere only runs were carried out. The boundary conditions of sea surface temperature and sea ice cover are prescribed as time varying monthly fields derived from the ECMWF reanalysis ERA-40 up to December 1988 and ERA-Interim onwards. This setup was adopted over coupled atmosphere-ocean simulations, to avoid the long term spin-up necessary for the ocean, and to confine the impacts of the different snow schemes to the atmospheric evolution and variability.

Both CTR and OPER snow schemes are available in EC-EARTH, the latter being the default, and ML3 was implemented. A three member ensemble of 30-years-long (January 1979 to December 2008)

was performed for each one of the snow schemes. Each ensemble member differs in their initial conditions: 1 November 1977; 1 December 1977 and 1 January 1978; taken from ERA-40. The first months of simulation (until December 1978) were discarded from the analysis. The results will be presented as the ensemble mean unless otherwise stated. Throughout the discussion the statistical significance of the differences between the mean of the simulations (monthly or seasonal means) is assessed using a two-sample two-tailed Student's t-test assuming equal variances (Wilks 2006). In the following sections results are analyzed over the Northern Hemisphere land masses poleward of 40°N, excluding Greenland (hereafter NH40). This region was selected as representative of the area where seasonal snow cover plays an important role in controlling the surface water and energy fluxes.

5.4.1 Snow cover and surface albedo

Simulated snow cover is compared with the weekly snow cover data from the National Snow and Ice Data Center (NSIDC) (Armstrong and Brodzik 2005). The weekly files consist of gridded binary counts of snow or no snow at 25 km resolution available since 1979 to 2006. This dataset has been used to validate climate models simulations (e.g. Roesch 2006) and to analyze the spatial and temporal patterns of the snow season length during the last three decades of the 20th century (Choi et al. 2010). The weekly data was averaged into monthly means and aggregated to the model grid.

The simulated northern hemisphere snow-covered area (SCA) is compared against NSIDC in Figure 5.2. The bias was calculated for each month (synchronous in time) and normalized by the mean NSIDC SCA. CTR underestimates SCA throughout the cold season, with particular problems during spring, with an early melting. OPER significantly reduces the biases, especially during spring. ML3 shows similar results during early spring, but in May and June is outperformed by OPER. The mean NSIDC snow cover and the model biases during spring are represented in Figure 5.3. The early melting in CTR is marked in Central Canada, Eastern Europe, Scandinavia and North of the Himalayan range. On those regions both OPER and ML3 significantly reduce the early melting bias of CTR. In the Alpine and Caucasus regions the early melting in CTR is still evident in OPER and ML3. Over complex terrain regions, early melting is mainly due to unresolved orographic processes in the 125 km model grid, affecting both the snow accumulation and snow melting.

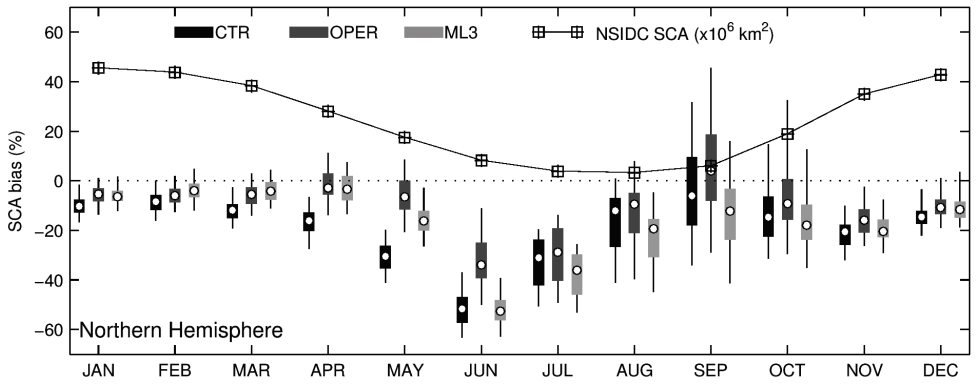

Figure 5.2. Northern hemisphere snow-covered area (SCA) biases normalized by the NSIDC snow-covered area. For each month (Jan 1979 to Dec 2006 three member ensemble) the simulated SCA biases were evaluated and are represented as box plots. The vertical boxes represent lower and upper quartiles, the circle the median and vertical lines extend from percentiles 5 to 95. The mean annual cycle of snow-covered area from NSIDC is represented by square symbols. The vertical axis represents area relative differences for the boxplots and SCA (x10^6 km^2) for NSIDC.

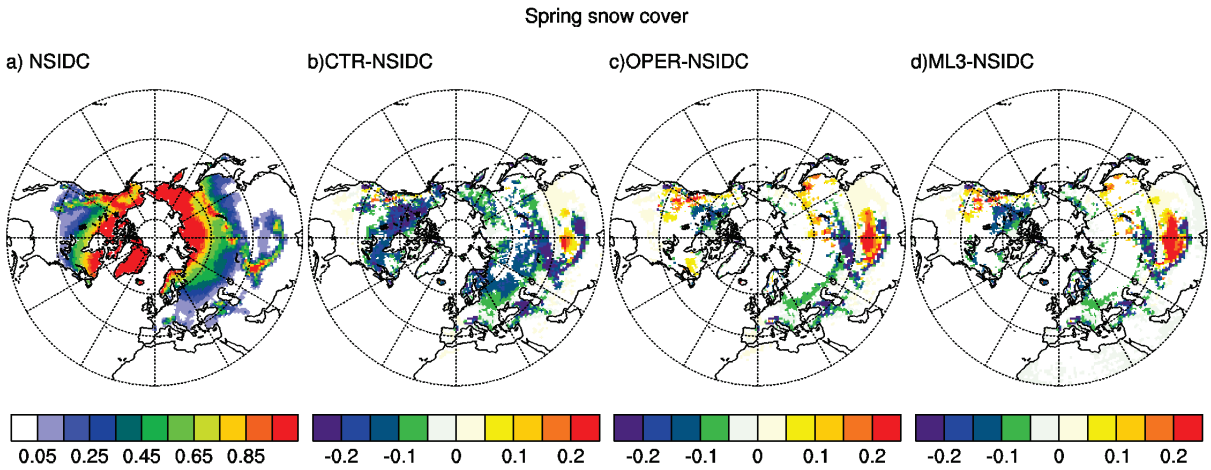

Figure 5.3. Mean observed snow cover during spring derived from NSIDC weekly snow cover extent (a) and simulated differences of CTR (b), OPER (c), and ML3 (c) with respect to NSIDC. Only differences significant at $p<0.05$ are represented. Note the different color scale of panel (a).

The Moderate Resolution Imaging Spectroradiometer (*MODIS*) albedo product MCD43C3 provides data describing both directional hemispheric reflectance (black-sky albedo) and bi-hemispherical reflectance (white-sky albedo) in seven different bands and aggregated bands. Data from the *Terra* and *Aqua* platforms are merged in the generation of the product that is produced every 8 days with 16 days of acquisition and available on a 0.05° global grid. The accuracy and quality of the product has been studied by several authors in different locations (e.g., Roman et al. 2009; Salomon et al. 2006; Stroeve et al. 2005).The *MODIS* product has already served as reference for model validation (e.g., Dutra et al. 2010a; Wang and Zeng 2010; Zhou et al. 2003). As for the NSIDC snow cover, the *MODIS* albedo was averaged to monthly fields and aggregated to the simulations grid.

In this study the mean annual cycle of *MODIS* white-sky broadband shortwave albedo (2001 to 2009) is compared against the model simulations (1979 to 2008) and is represented in Figure 5.4 for the NH40 region. OPER and ML3 have an almost coincident mean annual cycle on the hemispheric scale. This is expected since OPER and ML3 share the same snow albedo parameterization, and their evolution of snow cover is also similar (see Figure 5.2). From July to November all simulations overestimate surface albedo, whereas CTR is closest to *MODIS* from October to December. This overestimation of OPER and ML3 was also identified by DU10 in OPER and is mainly related with the snow albedo parameterization (in both exposed and forest regions), since such signal is not visible on snow cover. From March to June, OPER and ML3 are very close to *MODIS* while CTR shows a significant underestimation that is associated with the early melting discussed before. The mean spring surface albedo maps from *MODIS* and simulations differences are represented Figure 5.5. The strongest underestimation of spring surface albedo in CTR is mainly localized over snow covered regions poleward of 60°N. Both OPER and ML3 reduce those biases. However, over the Himalayan range and Rockies OPER and ML3 reinforce the overestimation of surface albedo that was already visible in CTR. This overestimation of surface albedo in complex terrain regions is associated with an overestimation of snow cover (see Figure 5.3). These results highlight a current deficiency of the model in representing snow cover over complex terrain regions. This is not surprising, since none of the snow schemes includes parameterizations for sub-grid scale processes. For such processes, the multi-layer representation of the snowpack does not improve the simulations, indicating that further

improving the model might need to address the representation of other important processes such as sub-grid scale variability.

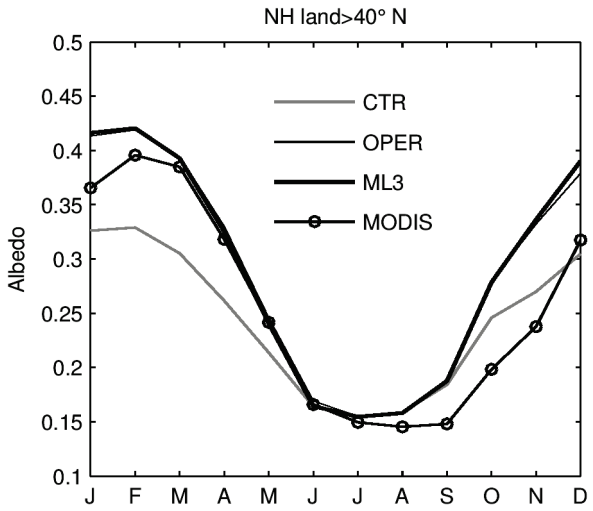

Figure 5.4. Mean annual cycle of surface albedo simulated by CTR (gray), OPER (thin black), ML3 (thick black) and observed from MODIS (open circles) averaged over Northern Hemisphere land masses poleward of 40° N, excluding Greenland. The spatial averages of simulations included only the grid-points were MODIS data was available.

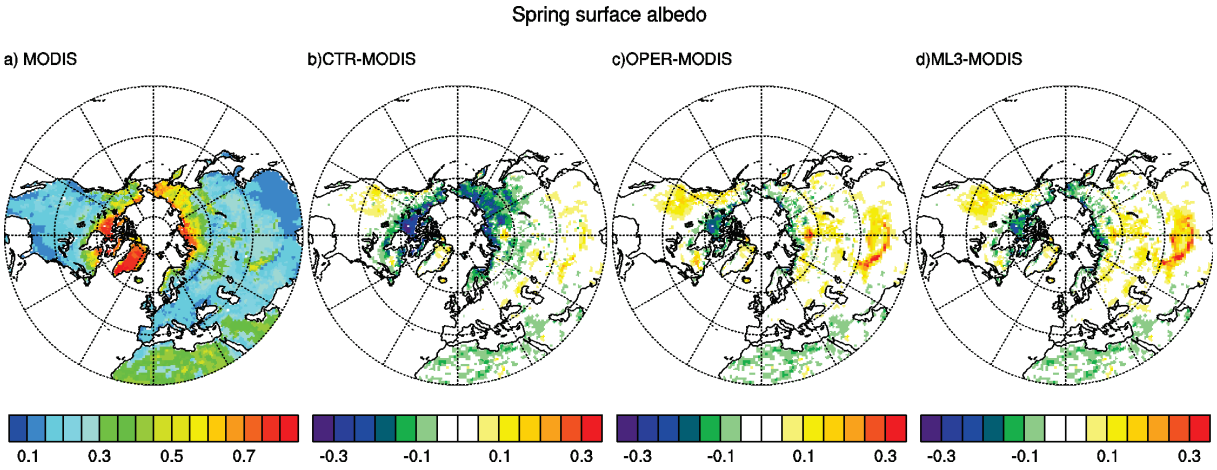

Figure 5.5. Mean observed surface albedo during spring derived from MODIS (a) and simulated differences of CTR (b), OPER (c), and ML3 (d) with respect to MODIS. Note the different color scales.

The early spring snow melt and underestimation of snow albedo in CTR are closely related, but it is not possible to clearly identify a cause-effect: low snow albedo leading to excessive energy absorbed on the snowpack resulting in an early snow ablation; or the early snow ablation exposing the land surface (with an albedo lower than a snow surface) leading to the underestimation of surface albedo. It is most likely to result from the conjunction of the two factors associated with the SAF.

5.4.2 Surface water balance

The mean annual cycle of the surface water fluxes averaged over NH40 are presented in Figure 5.6 a for the CTR simulation. Panels b) to e) of Figure 5.6 illustrate the differences of OPER and ML3 with respect to CTR for each component of the surface water balance. The sign of the fluxes follow the

model convention with positive for incoming water (or energy) to the surface and negative for outgoing water (or energy) from the surface. The runoff and terrestrial water storage variation (TWSV) exhibit a distinct behavior in spring and summer in both OPER and ML3 when compared with CTR. There is a significant reduction of runoff during spring (peak in April) matching an increase of soil water storage that is also evident in the mean soil moisture (see Figure 5.7 b). During summer there is the opposite signal with higher soil moisture depletion in OPER and ML3 then in CTR due to higher runoff rates.

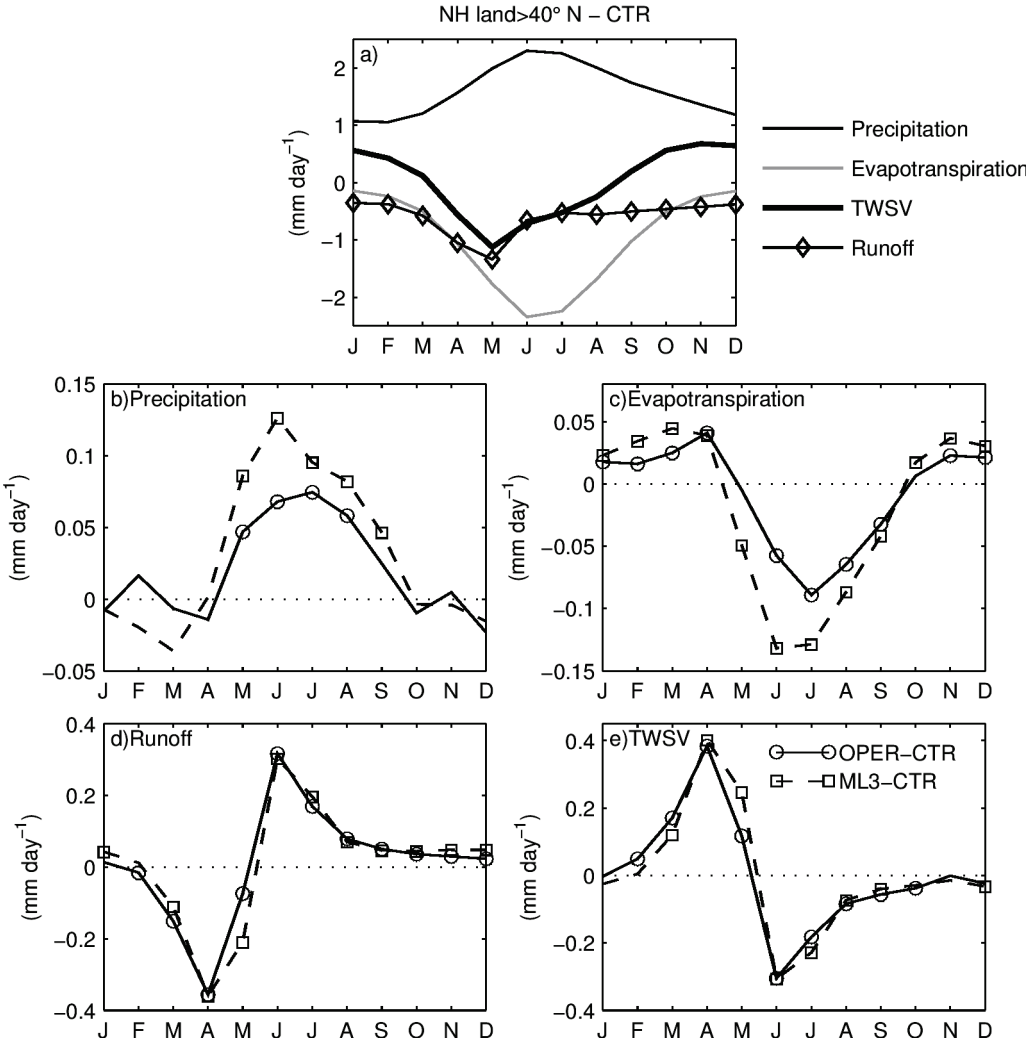

Figure 5.6. a) Mean annual cycles of surface water fluxes simulated by CTR averaged over the Northern Hemisphere land masses poleward of 40° N, excluding Greenland: total precipitation (thin black); evapotranspiration (gray); terrestrial water storage variation (TWSV thick black); and runoff (diamond symbol). The fluxes sign follow the model's convention: Positive – Incoming water to the surface; Negative – outgoing water from the surface. Panels b) to e) represent the mean annual cycle of simulated differences between ML3-CTR (dashed) and OPER-CTR (solid) of precipitation (b), evapotranspiration (c), runoff (d), and TWSV (e). The symbols mark if the monthly differences are significant at p<0.01 (two-tailed t-test) between ML3-CTR (squares) and OPER-CTR (circles).

OPER and ML3 also show a higher SWE peak in winter and delayed snow melt (Figure 5.7a) that contribute to the reduction of runoff. The delayed snow melt was discussed on the previous section in terms of snow cover. The delayed depletion of SWE in OPER and ML3 is also associated with the

interception of rainfall by the snow schemes (Table 5.1). The increase soil moisture availability during summer led to higher evapotranspiration rates in OPER and ML3. Following the increased moisture supply to the atmosphere, there is also an increase of the precipitation rates due to local/regional recycling and the soil-precipitation feedback (Schar et al. 1999). Compared with OPER, ML3 has a slightly higher spring and summer soil moisture content that explains the higher evapotranspiration rates and consequently precipitation changes in respect to CTR.

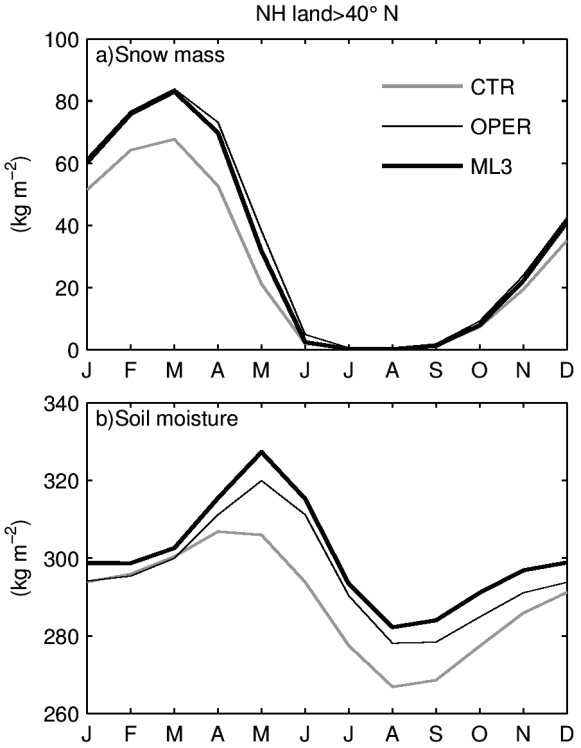

Figure 5.7. Mean annual cycle of simulated SWE (a) and top 1-meter soil moisture content (b) averaged over the Northern Hemisphere and masses poleward of 40° N, excluding Greenland by CTR (gray), OPER(thin black) and ML3 (thick black).

5.4.3 Surface energy balance

Following the analysis of the water balance components in the previous section, the mean annual cycle of the surface energy fluxes, averaged over NH40, are represented in Figure 5.8. There is a significant reduction of surface solar radiation (SSR - downward minus upward) from March to May in both OPER and ML3. This reduction is mainly associated with the increased surface albedo and delayed snow melt (see Figure 5.4 and Figure 5.7a). There is a reduction of both downward and upward thermal radiation resulting from the cooling of the atmosphere and surface from CTR to OPER and ML3 (Figure 5.9). This results in an increase of surface thermal radiation (STR downward minus upward), more pronounced during winter. The decrease (positive differences) of the surface sensible heat flux (SSHF) in OPER and ML3 is also associated with the cooling of the atmosphere and with the reduction of SSR. The surface latent heat flux (SLHF) shows a significant increase (negative differences) in summer due to increased evapotranspiration rates (Figure 5.6 c). The surface net radiation reflects the combination of above mentioned changes, with a warming of the soil and cooling of the atmosphere during winter in OPER and ML3 when compared with CTR.

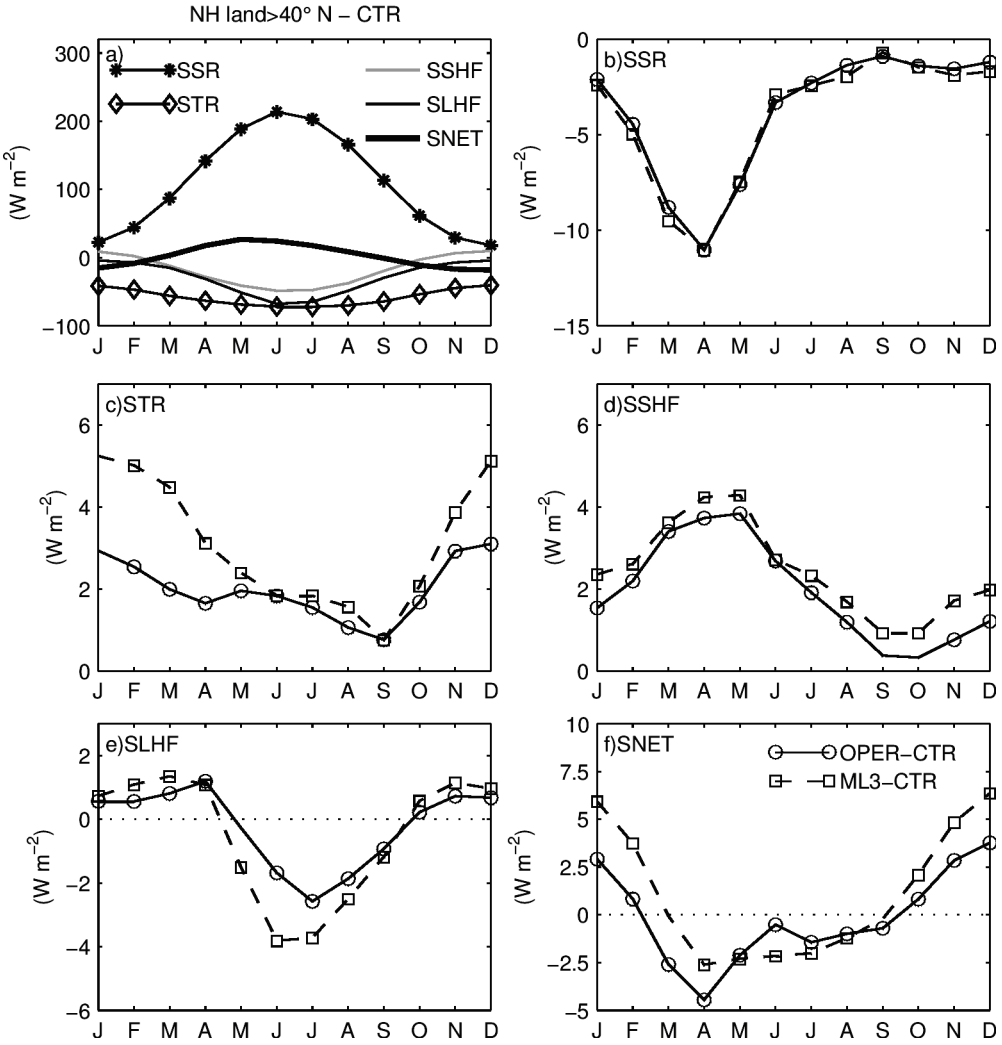

Figure 5.8. a) Mean annual cycle of the surface energy fluxes simulated by CTR averaged over the Northern Hemisphere land masses poleward of 40° N, excluding Greenland: surface solar radiation (SSR star symbol); surface thermal radiation (STR diamond symbol); surface sensible heat flux (SSHF gray line); surface latent heat flux (SLHF black line); and surface net energy (SNET tick black). The fluxes sign follow the model's convention: Positive – Incoming energy to the surface; Negative – Outgoing energy from the surface. Panels b) to f) represent the mean annual cycle of simulated differences between ML3-CTR (dashed) and OPER-CTR (solid) of SSR (b), STR (c), SSHF (d), SLHF (e), and SNET (f). The symbols mark if the monthly differences are significant at p<0.01 (two-tailed t-test) between ML3-CTR (squares) and OPER-CTR (circles).

The mean annual cycle of 2-meter (T2M, or air temperature), skin and soil temperature (surface to 7 cm depth) in Figure 5.9 are consistent with the changes in surface fluxes presented in Figure 5.8. The changes in surface fluxes, as well as temperature, are larger in ML3 than in OPER when compared with CTR. These changes are mainly due to the increased snow thermal insulation of the atmosphere from the underlying soil, much stronger in ML3. In CTR the atmosphere was being heated by the surface during winter, leading to colder soil temperatures and warmer air temperatures. OPER simulates lower snow densities (see DU10 for details), leading to a stronger insulation of the atmosphere from the soil. This effect is stronger in ML3 since the multi-layer snow scheme also accounts for the thermal insulation within the snowpack, i.e. the upper layer thermally insulates the lower layers.

The simulated T2M is compared against the CRU TS3.0 global dataset of monthly temperature [updated from Mitchell and Jones (2005)] for the period 1979 to 2006. Over NH40 (Figure 5.9 a) the T2M mean bias during winter was reduced from +2.2 K in CTR to 0.9 K in OPER and -0.1 K in ML3. The mean winter differences between CTR and CRU T2M (Figure 5.10 a) show a pronounced warm bias, reaching 8 K over snow covered regions. Both OPER and ML3 led to a significant cooling over snow covered regions. Over the Himalaya and Rockies CTR presents a negative T2M bias that was intensified in OPER and ML3. Part of the cold bias is associated with an overestimation of surface albedo (see Figure 5.4 and Figure 5.5). However, other factors such as excessive cloud cover (not shown) are also responsible for the cold biases over those mountainous regions.

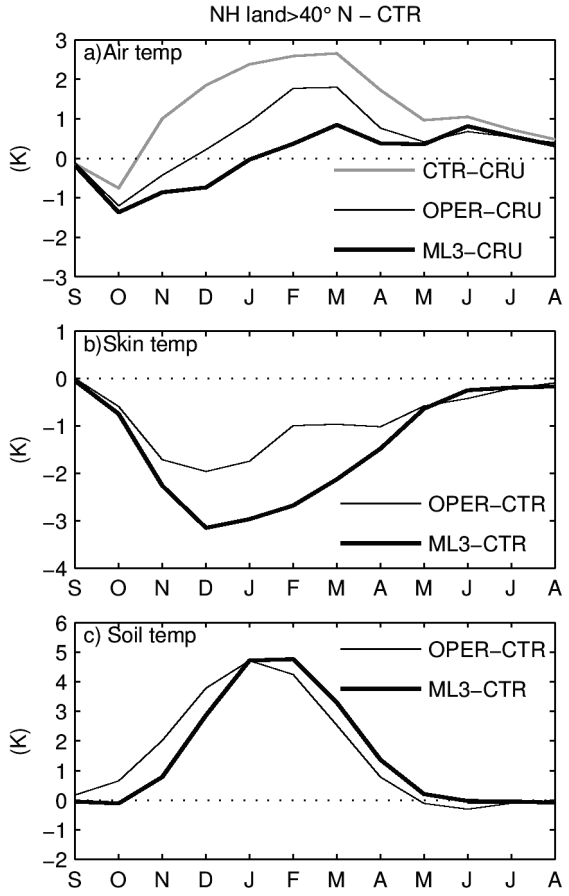

Figure 5.9. Mean annual cycle of simulated of 2-meter temperature (a - T2M), skin temperature (b) and soil temperature (c – first soil layer between 0 and 7 cm depth) averaged over the Northern Hemisphere land masses poleward of 40° N, excluding Greenland. T2M is represented as the differences between simulations and CRU, while skin and soil temperature are the differences of OPER and ML3 in respect to CTR. Note that the horizontal axis starts in September.

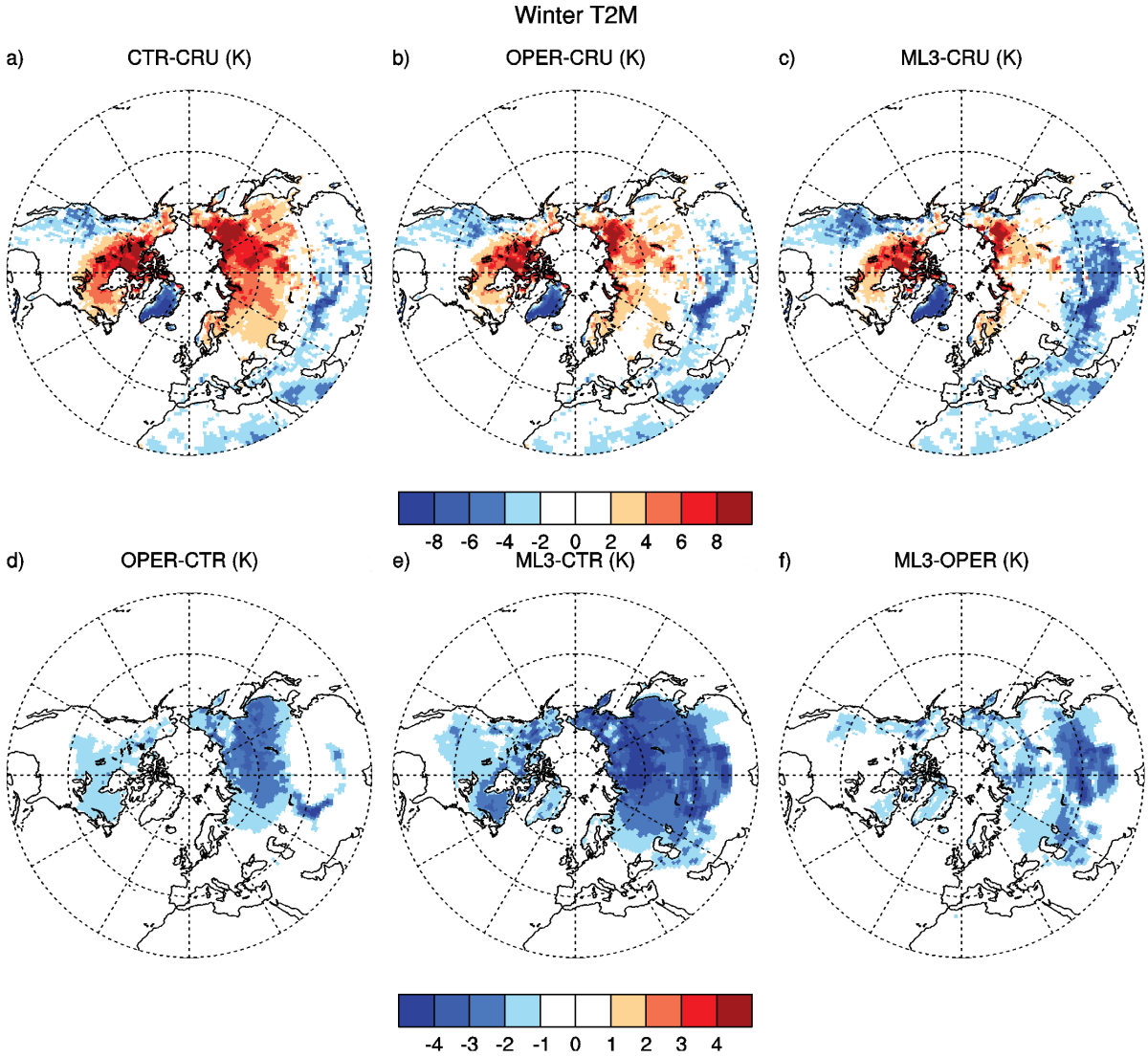

Figure 5.10. Simulated winter 2-meter temperature (K) biases of CTR (a), OPER (b) and ML3 (c) compared against CRU, and differences between OPER-CTR(d), ML3-CTR(e) and ML3-OPER (f). Only differences significant at p<0.05 are represented. Note the different color scales between the top and bottom panels.

5.4.4 Snow albedo feedback

The SAF can be quantified by the variation in net incoming shortwave radiation (Q) with surface air temperature (T_{air}) due to changes in surface albedo (α_s) (Cess and Potter 1988; Hall and Qu 2006):

$$\left(\frac{\partial Q}{\partial T_{air}}\right)_{SAF} = -I_t \frac{\partial \alpha_p}{\partial \alpha_s} \frac{\Delta \alpha_s}{\Delta T_{air}} \tag{5.1}$$

where α_p is the planetary albedo, I_t the incoming solar radiation at the top of the atmosphere, and the subscript SAF denotes that the partial derivative refers only to changes in Q with T_{air} due to changes in surface albedo (excluding all the other factors affecting solar radiation). The SAF is decomposed as the product of two terms in Eq. (5.1): (i) $(\partial\alpha_p / \partial\alpha_s)$ accounts for the attenuation effects of the atmosphere on anomalies in α_s (due to solar absorbers in the atmosphere, including clouds) and (ii)

($\Delta\alpha_s / \Delta T_{air}$) represents the changes of surface albedo induced by changes in surface air temperature, resulting from surface processes.

HQ06 proposed the calculation of ($\Delta\alpha_s / \Delta T_{air}$) in the seasonal cycle by taking climatological changes in the Northern Hemisphere from one month to another. They also estimated an observed ($\Delta\alpha_s / \Delta T_{air}$) in the seasonal cycle context taking changes from April to May values from the satellite-based International Satellite Cloud Climatology Project (ISCCP) and T_{air} from reanalysis data. In 17 climate models used for AR4 climate change experiments the ratio of ($\Delta\alpha_s / \Delta T_{air}$) evaluated as changes from present to future were very similar to the changes from April to May in present climate. The models showed a strong variability of the ratio ($\Delta\alpha_s / \Delta T_{air}$) with differences up to a factor of two when compared with the observational estimates. HQ06 also found that the intermodel variation of ($\partial\alpha_p / \partial \alpha_s$) was small due to the convergence of the models in representing the atmosphere's interaction with upwelling solar photons (Qu and Hall 2006).

The ($\Delta\alpha_s / \Delta T_{air}$) SAF component estimated from the EC-EARTH simulations and the observational estimates from HQ06 are presented in Table 5.2. CTR had a reduced sensitivity of surface albedo to surface temperature changes, almost 50% less than the estimates of HQ06. Both OPER and ML3 have similar SAF sensitivity values, closer to the HQ06 estimates. The increased values of OPER and ML3 when compared with CTR were mainly due to an increased change in surface albedo from April do May. This is due to the latter spring melting and to a stronger sensitivity of surface albedo to surface temperature changes in both OPER and ML3, when compared with CTR.

Table 5.2. Sensitivity of surface albedo to surface temperature changes from April do May ($\Delta\alpha_s / \Delta T_{air}$) averaged over the Northern Hemisphere land masses poleward of 30°N for the three simulations and the observational based estimates from Hall and Qu (2006) (HQ06). The values of surface albedo were weighted by April incoming insulation prior to averaging. The values between brackets represent the standard deviation of the mean for CTR, OPER and ML3 and the error estimate for HQ06.

	($\Delta\alpha_s / \Delta T_{air}$) **(% / K)**
CTR	-0.56 (+/-0.05)
OPER	-0.92 (+/-0.07)
ML3	-0.93 (+/-0.08)
HQ06	-1.07 (+/-0.07)

5.4.5 Upper air

The changes in upper air temperature and specific humidity of OPER and ML3 with respect to CTR are presented in Figure 5.11 as the mean annual cycle of time-pressure cross-section averaged of NH40. Both OPER and ML3 show a cooling of the lower troposphere up to 700 hPa during winter. During spring the cooling extends further in altitude reaching the 300 hPa. Although the surface cooling in OPER and ML3 has their strongest signal during winter, the vertical propagation is constrained by the strong stability of the planetary boundary layer. As for the surface temperature, the cooling in ML3 is stronger than in OPER (compare panels a-b of Figure 5.11).

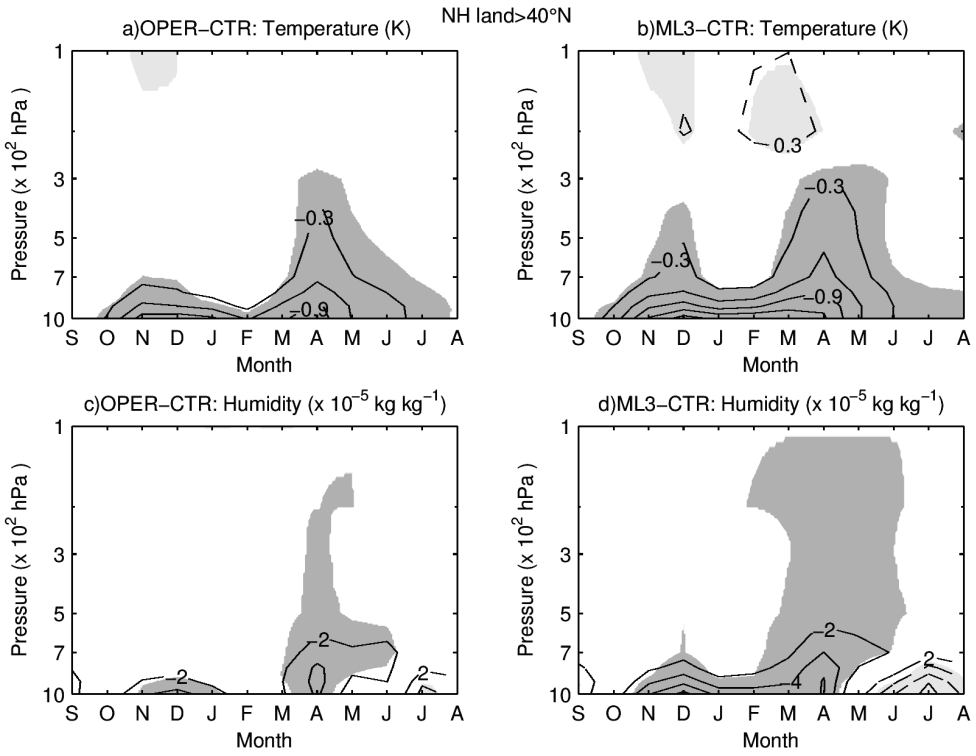

Figure 5.11. Mean annual cycle of time-pressure cross-section of temperature (a, b) and specific humidity (c, d) differences of OPER (a, c) and ML3 (b,d) in respect to CTR averaged over the Northern Hemisphere land masses poleward of 40° N, excluding Greenland. Solid (dashed) contours represent negative (positive) differences with an interval of 0.3 K and 2 x 10^{-5} kg kg^{-1} for temperature and specific humidity, respectively. Dark (light) shading indicates regions where the negative (positive) differences are significant at $p<0.05$.

The air temperature cooling has a direct impact on the reduction of the atmosphere water content at saturation. Both OPER and ML3 show a reduction of specific humidity in the lower troposphere during winter and spring (see Figure 5.11 c, d). In addition, the near-surface cooling in OPER and ML3 (in comparison with CTR) implies a reduction of moist convection, which in turn would reduce the moistening of the atmospheric column. However, during summer there is an increased of water availability in the lower troposphere from CTR to OPER and ML3, higher in the latter. This is coherent with the increased evapotranspiration (see Figure 5.6 c), that ultimately led to an increase of precipitation. The changes in upper air temperature and specific humidity in ML3 are stronger, both in spatial distribution and intensity, then in OPER when compared with CTR. This is consistent with the previous analysis to the surface water and energy fluxes, showing that the snow thermal insulation plays an important role in controlling the land-atmosphere coupling.

There is a reduction of the geopotencial height in OPER and ML3 as a result of the atmospheric cooling during winter and spring (not shown). The mean sea level pressure presents a positive anomaly (mainly over Siberia, not shown) in OPER and ML3 when compared with CTR, associated with the cooling of the atmosphere. However, the changes in mass distribution are difficult to analyze due to their reduced statistical significance. Further analysis of changes in local and/or hemispheric circulation patterns would require an increase of the ensemble size to proper disentangle the changes due the different snow schemes from those linked with atmospheric internal variability, which is out of the scope of the present study.

5.5 Conclusions

The offline simulations of the three snow schemes at Col de Porte and SNOWMIP2 sites, were evaluated as a validation to the ML3 snow scheme. ML3, the multi-layer version of OPER improved the snowpack simulations mainly over deep snowpack conditions. This was expected, since a bulk snowpack has a large thermal inertia, with difficulties in representing sporadic melting events during winter and early spring. On shallow snowpacks under high vegetation, ML3 had similar results to OPER. These results show that developments associated with the increased complexity of the snowpack vertical structure should also be accompanied by improvements on the representation of other processes such as sub-grid scale variability, radiative effects of the canopy, coupling with the atmosphere via the turbulent heat fluxes, among others. However, ML3 has a very simple vertical structure (only three layers with a minimum depth of 0.2 m in each layer). Although sharing a similar construction to other multi-layer snow scheme used within climate models (e.g.Boone and Etchevers 2001; Sun et al. 1999), but with a different vertical grid, there are more complex formulations for the vertical structure and physical process of the snowpack available in the literature (e.g. Anderson 1976; Brun et al. 1989). Nevertheless, the implementation and validation of such a complex snow scheme within EC-EARTH is beyond the scope of this study.

EC-EARTH climate simulations of snow cover and surface albedo were compared against remote sensing products. ML3 simulations of snow cover and surface albedo were analogous to OPER. This was foreseen, since both OPER and ML3 share the same parameterizations for snow cover fraction and snow albedo. The early spring snow melt in CTR associated with an underestimation of surface albedo was partially reduced with the OPER snow scheme. The improved performance of OPER over CTR was also found in offline simulations by DU10. The resemblance between the offline (DU10) and atmosphere coupled simulations highlight the reliability of the offline strategy to validate land surface models, and the important of the model physics in simulating snow cover. Over the Himalayan range and Rockies, OPER and ML3 overestimate snow cover and surface albedo during winter and spring (see Figure 5.3 and Figure 5.5). This bias was already present in CTR, but was intensified in OPER. Over those areas there is a cold bias of T2M (see Figure 5.10). Part of the bias can be directly associated with the excess snow cover and surface albedo that is reflecting part of the incoming solar radiation. However, other atmospheric process such has cloud cover can also be responsible for the cold bias. The sub-grid scale distribution of snow cover over complex terrain is not taken into account in EC-EARTH, with a significant impact on snow-cover evolution and associated energy and moisture fluxes (Liston 2004).

The increased snow thermal insulation from CTR to OPER and ML3 led to warmer soil temperatures during winter and spring. This reduced soil freezing, allowing snow melt and rainfall to infiltrate the soil instead of leaving the surface as surface runoff. The increased soil moisture content during late spring and summer is then responsible to higher evapotranspiration rates. This in turn, resulted in an increase of summer precipitation due to the increased moisture in the lower troposphere and an intensification of the soil-precipitation feedback. The sensitivity of surface albedo to surface temperature changes from April do May was strongly underestimated by CTR, while OPER and ML3 display similar values, closer to the estimates of HQ06. This chain of processes started during the cold season and ended during summer. This shows the importance of snow cover and of its representation in climate models both on the surface water and energy balances.

Furthermore, the increased snow thermal insulation in OPER and ML3 reduced the T2M warm bias over snow covered regions during winter and spring. Hazeleger et al. (2010) found similar improvements in coupled ocean-atmosphere simulations when running EC-EARTH with CTR and OPER snow schemes. Cook et al. (2008) reported similar results when investigating the sensitivity of surface climate to the treatment of snow thermal conductivity. In their experiments, high versus low insulation cases led to soil cooling of up to 20 K in winter and T2M warming of 6 K. Comparing with this study, CTR would be the low insulation case, OPER an intermediate case, and ML3 a high insulation. While Cook et al. (2008) demonstrated the importance of snow thermal conductivity by prescribing its value in a set of experiments, in this study we achieved similar results by using different snow schemes.

Acknowledgments

The authors are grateful for the valuable support of the EC-EARTH consortium. The National Snow and Ice Data Center is acknowledged for providing the snow cover data. We also thank the *MODIS* albedo science team and the Land Processes Distributed Active Archive Center (LP DAAC) for providing the MCD43C albedo data. The data from Col De Porte station was kindly provided by Meteo-France. We also thank Xin Qu for providing the SAF estimates. This work was supported by the Portuguese Foundation for Science and Technology (FCT) under project AMIC PTDC/AAC-CLI/109030/ 2008 cofinanced by the European Union under program FEDER. E. Dutra acknowledges the financial support of FCT under Grant FRH/BD/35789/2007 and ECMWF for travel support.

5.6 Appendix: Multi-layer snow scheme

The ML3 snow scheme is a multi-layer version of OPER for the energy and mass balance within the snowpack. ML3 has the same snow cover fraction, surface albedo and snow density parameterizations (see DU10 for further details), the latter evaluated for each snow layer separately. This multi-layer scheme follows closely the formulation of the ISBA-ES snow scheme (Boone and Etchevers 2001) with some adaptations required for HTESSEL, and with a different snow layering procedure.

The mass balance of the entire snowpack reads as

$$\frac{\partial S}{\partial t} = F + c_{sn}\left(F_l - E_{sn}\right) - R_{sn,N} \tag{5.2}$$

where S (kg m^{-2}) is the total mass in the snowpack (solid and liquid phases), c_{sn} is the grid-box snow cover fraction and F, F_l, E_{sn}, and $R_{sn,N}$ are the mass fluxes of snowfall, rainfall, snow sublimation and runoff from the N^{th} snow layer (N is the number of snow layers) at the interface with the soil (kg m^{-2} s^{-1}).

The liquid water content in each layer is a prognostic, differing from OPER that uses a diagnostic approach, following a bucket type formulation

$$\frac{\partial S_{l,i}}{\partial t} = R_{sn,i-1} - R_{sn,i} + Q_{sn,i} \big/ L_f \tag{5.3}$$

where $S_{l,i}$ is the liquid water content of the i^{th} layer (kg m^{-2}), L_f the latent heat of fusion (J kg^{-1}), $R_{sn,i}$ (kg m^{-2} s^{-1}) the flux of water at the bottom of layer i, and Q_{sn} (W m^{-2}) the energy released or absorbed due to water-ice phase changes. The top boundary condition, $R_{sn,0}$, is the rainfall interception ($c_{sn}F_l$).

Runoff is generated when the liquid water excess the snow liquid water capacity of the layer following Anderson (1976) (see also DU10 for definition).

The snow layers energy balance is given by

$$\left(\rho C\right)_{sn,i} D_{sn,i} \frac{\partial T_{sn,i}}{\partial t} = G_{sn,i-1} - G_{sn,i} - Q_{sn,i} \tag{5.4}$$

where $(\rho C)_{sn,i}$ is the snow layer volumetric heat capacity (J m^{-3} K^{-1}), $D_{sn,i}$ the snow layer depth (m), $T_{sn,i}$ the snow layer temperature (K) and G_{sn} the heat flux (W m^{-2}), representing the sum of the heat diffusion and the solar radiation. Snow thermal conductivity is calculated as in OPER, and the radiation flux follows Boone and Etchevers (2001). The top boundary condition, $G_{sn,0}$, is the result of the skin energy balance, accounting for the surface net solar and thermal radiation and turbulent heat fluxes. The bottom boundary condition, $G_{sn,N}$, is calculated as the basal heat flux in OPER.

The snow layering follows depth coordinates with an increased number of snow layers with increased depth up to a maximum of N layers given by

$$\begin{aligned}
D_{sn,1} &= \begin{cases} D_{sn}, & D_{sn} < 2D_{sn}^{MIN} \\ D_{sn}^{MIN}, & D_{sn} \geq 2D_{sn}^{MIN} \end{cases} \\
D_{\substack{sn,i \\ i=2,\ldots,N-1}} &= \begin{cases} 0 & , D_{sn} < iD_{sn}^{MIN} \\ \min\left(\dfrac{D_{sn} - D_{sn,1}}{N-1}, 3^{i-1} D_{sn}^{MIN} \right) & , D_{sn} \geq iD_{sn}^{MIN} \end{cases} \\
D_{sn,N} &= D_{sn} - \sum_{i=1}^{i=N-1} D_{sn,i}
\end{aligned} \tag{5.5}$$

where D_{sn} is the snowpack depth (m), and D_{sn}^{MIN} is the minimum snow layer depth. In the present study, N=3 and D_{sn}^{MIN}=0.2 were selected. This configuration was achieved after testing different configurations up to N=5 and D_{sn}^{MIN}=0.1 m in site simulations for CdP and SNOWMIP2. Three snow layers is a common number in the literature for snow schemes within numerical weather prediction or climate models (e.g. Boone and Etchevers 2001; Sun et al. 1999). The minimum snow layer depth was set to 0.2 m primarily to avoid numerical instabilities since both HTESSEL offline and EC-EARTH run with a time step of 1 hour, but also because the energy balance in HTESSEL is solved implicitly for the skin temperature, and not explicitly coupled to the snowpack energy balance. With the present configuration there is one snow layer up to D_{sn}< 0.4 m, two layers for 0.4≤ D_{sn} < 0.6 m, and the three layers are active for D_{sn} ≥0.6 m. The first layer is kept constant at 0.2 for D_{sn} ≥0.4 m and the second layer is limited to a maximum depth of 0.6 m. For 1 m depth the layering follows: 0.2, 0.4 and 0.4 m, while for 1.5 m depth: 0.2, 0.6, 0.7 m.

The adopted time step numerical procedure is the following:

1. Skin energy balance is solved to return the residual energy to the snowpack (HTESSEL component);
2. Updated SWE with snowfall and snow sublimation (first snow layer);
3. The energy balance for each layer is evaluated by solving the linearized system of equations simultaneously;

4. Water-ice phase changes are evaluated from the updated temperature profile. In the case of melting in the first layer, $T_{sn,1}$ is set to the freezing point, and point 3) is repeated again;
5. Phase changes, and layer runoff are evaluated to update the profiles of $T_{sn,i}$, $S_{i,}$ and $S_{l,i}$;
6. Snow density (for each layer) and surface snow albedo are updated;
7. Reset of vertical grid according to Eq. (5.5) for the depth of each layer, conserving mass and energy to obtain new profiles of $T_{sn,i}$, $S_{i,}$ $S_{l,i}$ and $\rho_{sn,i}$. This last point led, in some degree, to a vertical mixing of properties, especially during snow melt conditions.

6
Land-atmosphere coupling associated with snow cover*

Abstract

This study investigates the role of interannual snow cover variability in controlling the land-atmosphere coupling and its relation with near surface (T2M) and soil temperature (STL1). Global atmospheric simulations are carried out with the EC-EARTH climate model. Snow climatology, derived from a control run (COUP), is used to replace snow evolution in the snow-uncoupled simulation (UNCOUP). The snow cover and depth variability explains almost 60% of the winter T2M variability in predominantly snow-covered regions. During spring the differences in interannual variability of T2M are more restricted to the snow line regions. The variability of soil temperature is also damped in UNCOUP. However, there are regions with a pronounced signal in STL1 with no counterpart in T2M. These regions are characterized by a significant interannual variability in snow depth, rather than snow cover (almost fully snow covered during winter). These results highlight the importance of both snow cover and snow depth in decoupling the soil temperature evolution from the overlying atmosphere.

* Dutra, E.[1,2], C. Schar[2], P. Viterbo[3], and P. M. A. Miranda[1], 2011: Land-atmosphere coupling associated with snow cover. *Submitted to Geophysical Research Letters.*

[1] Centro de Geofísica da Universidade de Lisboa, Instituto Dom Luiz, University of Lisbon, Lisbon, Portugal.

[2] Institute for Atmospheric and Climate Science, ETH, Zurich, Switzerland.

[3] Institute of Meteorology, Lisbon, Portugal.

6.1 Introduction

Over the last few years, the land-atmosphere coupling and its associated feedbacks have been an active research topic on process oriented studies, climate change diagnostics and predictability exploration. One example is the role of soil moisture in controlling the land-atmosphere coupling via the soil-moisture-temperature feedback (Fischer et al. 2007; Lorenz et al. 2010; Seneviratne et al. 2006) or via the soil-moisture-precipitation feedback (Koster et al. 2004; Schar et al. 1999). Another known feedback is the snow-albedo feedback, evaluated either in observations (Flanner et al. 2011) or model simulations (Fletcher et al. 2009a; Qu and Hall 2006, 2007). The land surface hydrology, and its coupling with the atmosphere, is also recognized as a potential source for long-range atmospheric predictability (Dirmeyer 2005; Douville 2010; Peings et al. 2010).

Snow cover is known to play an important role in controlling some atmospheric circulation patterns and teleconnections (Allen and Zender 2010; Gong et al. 2007; Orsolini and Kvamsto 2009; Peings and Douville 2010; Sobolowski et al. 2010). Less attention has been given to the relation between snow cover and air and soil temperature in terms of interannual variability. This latter point is of particular interest as (potential changes in) interannual variability has an important impact upon the frequency of extremes (Katz and Brown 1992). More specifically, increasing greenhouse gas concentrations are expected to impact the interannual variability of temperature and precipitation (Räisänen 2002), and have for instance been investigated in relation to European summer temperature variability and heatwaves (Fischer and Schar 2009 ; Schar et al. 2004).

In this study we focus on the role of snow cover interannual variability in controlling the land-atmosphere coupling and its influence on near surface and soil temperature. This is achieved by carrying out simulations for present climate with the EC-EARTH model (Hazeleger et al. 2010), with and without prescribed snow evolution. The simulations setup is described in the next section followed by the results discussion in section 6.3. Section 6.4 summarizes the main conclusions of this study.

6.2 Simulations setup

The atmospheric component of EC-EARTH version 2 is based on ECMWF's Integrated Forecast System (IFS), cycle 31R1, also used in the current seasonal forecast system of ECMWF. The simulations were performed at TL159 horizontal spectral resolution (about 125 km on the grid point space) with 62 vertical levels extending up to 5 hPa. EC-EARTH also includes an ocean and sea ice components, but in this study atmosphere only runs were performed. The land surface component is the Hydrology Tiled ECMWF Scheme of Surface Exchanges over Land (HTESSEL, Balsamo et al. 2009), with an updated snow scheme (Dutra et al. 2010a). A general overview of EC-EARTH is given by Hazeleger et al. (2010). Chapter 5 describes its performance on simulating snow cover, surface albedo and near surface temperature.

The experiment consists of a 30-year-long climate run forced with climatological sea surface temperature and sea ice boundary conditions (coupled run – COUP). The boundary conditions are prescribed as the mean monthly annual cycle from 1979 to 2008 derived from the ECMWF reanalysis ERA-40 (Uppala et al. 2005) and ERA-Interim (Dee et al. 2011). With this setup only the internal

variability of the land-atmosphere system is considered. However, over high latitude regions most the of variability is induced by the chaotic atmospheric dynamics (Koster et al. 2000).

One additional simulation, uncoupled (UNCOUP), shares the same setup as COUP, except that its snow evolution at each time step is replaced with the climatology of COUP. For this purpose, three prognostic variables are replaced: snow mass (also referred as snow water equivalent – SWE), snow density and snow albedo. This removes the interannual variability of snow and uncouples the land surface from the atmosphere over snow covered regions. Snow temperature is left to evolve freely since it mainly responds to the synoptic conditions on shorter time scales (diurnal cycle) and its replacement could introduce strong discrepancies between the land surface and overlying atmospheric conditions. This strategy to decouple the land surface from the atmosphere was already applied both on general circulation models (GCM) (e.g. Koster et al. 2000) and regional climate models (e.g. Seneviratne et al. 2006) studies, but with a focus on the role of soil moisture rather than snow. In what concerns snow fields in GCMs, Douville (2010) forced the atmosphere with global re-analysis of snow, Orsolini and Kvamsto (2009) used observations of snow cover while Sobolowski et al. (2010) prescribed high- and low- snow cover forcings.

6.3 Results

We start the analysis by evaluating the winter and spring 2-meter temperature (T2M). Figure 6.1 displays the interannual winter and spring variability, represented as the standard deviation (σ), of T2M as simulated in the COUP and UNCOUP experiments. Over the oceans σ is reduced during winter and spring and its spatial patterns are very similar between COUP and UNCOUP. This is expected, since there is no interannual variability in the sea surface temperature. However, there is a south-north gradient in T2M σ that is mainly associated with known storm track dynamics (Chang et al. 2002). Moreover, the replacement of the snow evolution by its climatology in UNCOUP does not change the T2M variability over the oceans. Over land, the T2M interannual variability in COUP is higher over snow covered regions, especially during winter (Figure 6.1 a). This is a first sign of the snow induced land-atmosphere decoupling. Over snow covered regions the snow thermal insulation increases the near surface variability, explained by the boundary-layer decoupling of the surface from the atmospheric fluxes (Derbyshire 1999; Viterbo et al. 1999). The T2M variability signal is substantially weaker is spring than winter (Figure 6.1 a, d), and this largely follows the seasonal cycle of mid-latitude atmospheric variability.

The UNCOUP experiment displays a significant reduction of T2M interannual variability during winter and spring. The percentage of interannual variance of T2M explained by land-atmosphere coupling is estimated as $\Delta\sigma=(\sigma_{COUP}-\sigma_{UNCOUP})/\sigma_{COUP}$ (see Figure 6.1 c, f). This measure was also adopted by Seneviratne et al. (2006) using the variance instead of the standard deviation. During winter, Δσ T2M displays a large scale pattern throughout the North Eurasian and American continents. The regions with significant changes in variability are not restricted to the snow line areas (areas with an average snow cover between 25%-75%). This shows that not only the presence or absence of snow is important but also the amount of SWE, and its interannual variability. During spring, Δσ T2M has a lower amplitude than during winter, and is less spatially extended.

Snow cover variability is expected to play an important role in controlling the underlying soil temperatures (e. g. Lawrence and Slater 2010). This is confirmed in Figure 6.2 during winter and

spring, where the interannual σ of soil temperature in the uppermost layer (STL1 - 0 to 7 cm depth) exhibits a significant reduction in UNCOUP when compared with COUP. The spatial patterns of STL1 Δσ are similar to those of T2M. For example, over the Canadian prairies the damping of the interannual variability of snow cover in UNCOUP significantly reduces both T2M and STL1 variability. However, some regions appear with a significant signal in STL1 that was not present in T2M. Northeastern Eurasia is an example. In this region the interannual variability of T2M was not significantly controlled by snow cover whereas soil temperature is. During winter and spring Northeastern Eurasia has a reduced snow cover variability (since is mostly snow-covered, Figure 6.5) but a high snow depth interannual variability (Figure 6.6). This explains the strong reduction of STL1 variability in UNCOUP when compared with COUP.

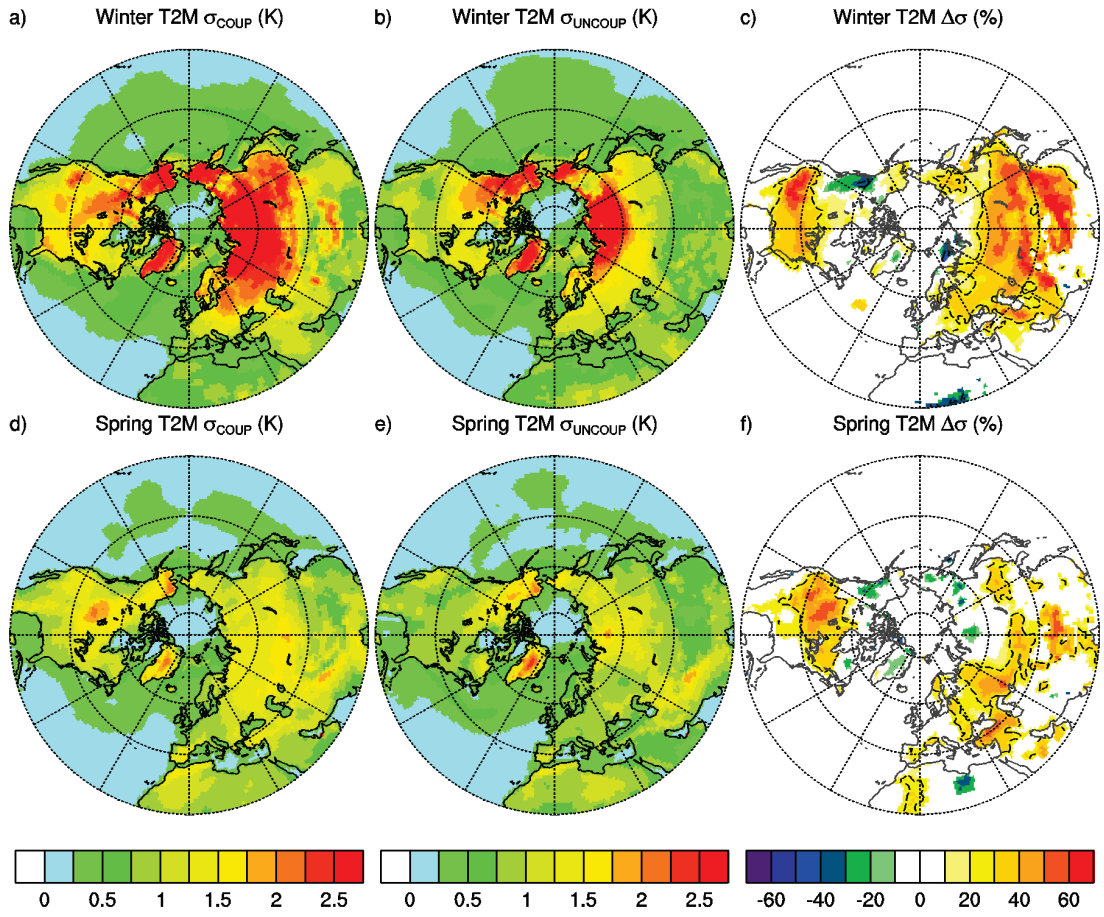

Figure 6.1. Standard deviation of winter (December-February) 2-meter temperature (T2M) in COUP (a) and UNCOUP (b), and spring T2M (March-May) in COUP (d) and UNCOUP (e). Percentage of interannual winter (c) and spring (f) T2M standard deviation due to land-atmosphere coupling associated with snow cover variability ($\Delta\sigma=(\sigma_{COUP}- \sigma_{UNOUP})/ \sigma_{COUP}$). In panels c and f the dashed lines enclose regions where the seasonal T2M variances of COUP and UNCOUP are significantly different at 90% following a F test *(Von Storch and Zwiers 1999).*

Additional analysis showed a significant damping of soil temperature variability up to one meter deep (Figure 6.7 and Figure 6.8) in UNCOUP. These findings further highlight the role of snow in controlling the land-atmosphere coupling with implications for the subsurface thermodynamics (Lesperance et al. 2010; Stieglitz and Smerdon 2007) and interpretation of borehole temperature profiles (Hu and Feng 2005). A significant reduction of the interannual variability of net surface

radiation (both solar and thermal) was also found over snow covered regions in UNCOUP (Figure 6.9 and Figure 6.10). This was a direct result of the prescribed snow cover and surface albedo in UNCOUP for solar radiation. The reduction of interannual variability of thermal radiation was due to the decrease of (i) air temperature variability, and (ii) surface emissivity variability. Changes in the surface turbulent heat fluxes were also observed, but weaker than those of the radiation fluxes. The surface water balance is not guaranteed in the UNCOUP simulation, due to the SWE replacement by the climatology, invalidating the assessment of changes in the surface hydrology variability.

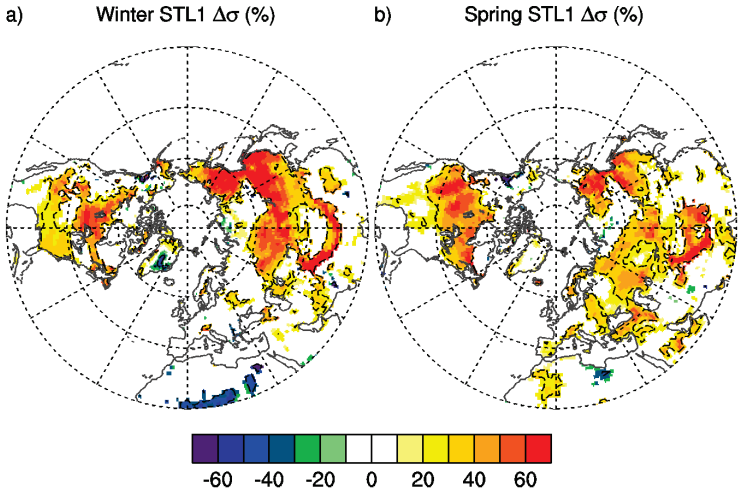

Figure 6.2. Percentage of interannual winter (a) and spring (b) soil temperature in the uppermost layer (STL1, 0 to 7 cm depth) standard deviation due to land-atmosphere coupling associated with snow cover variability ($\Delta\sigma=(\sigma_{COUP}- \sigma_{UNOUP})/ \sigma_{COUP}$). The dashed lines have the same meaning as in Figure 6.1.

We now focus on the evaluating of the land-atmosphere coupling over the transition regions between no snow and full snow cover during winter. Although SWE variability was found to play an import role in controlling the land-atmosphere coupling, the transition regions are more sensitive to changes in air temperature and precipitation induced by increasing greenhouse gas concentrations (Boer et al. 1992; Essery 1997). Figure 6.3 displays the differences in winter T2M and SLT1 σ as a function of the snow cover σ in COUP for all grid points with a mean snow cover between 1% and 75%. The regions with higher interannual variability of snow cover show a higher reduction of σ T2M in UNCOUP, with a correlation of 0.61. On the other hand, the interannual changes in STL1 have a low correlation with the snow cover variability. These results show that over the snow line transition regions snow cover variability plays an important role in controlling air temperature variability, while the impact on soil temperature is reduced.

Finally, a more detailed analysis is carried out over the Midwestern US (MWUS: 35°N < Latitude < 45°N; 100°W < Longitude < 80°W). This region was selected due to (i) its relatively homogeneous topography, (ii) reasonable combination between low and high vegetation cover, and (iii) its location over the winter snow line with a homogeneous latitudinal snow distribution and a meridional gradient of snow cover. Figure 6.4 represents T2M, STL1 and STL1-T2M averaged over MWUS as a function of snow depth for each one of the 30 winter seasons simulated in COUP and UNCOUP. The correlations in COUP between T2M and STL1 with snow depth are -0.82 and -0.59, respectively. The dumping of the interannual variability of T2M and STL1 is clearly shown in the estimated distributions (panels b and d of Figure 6.4).

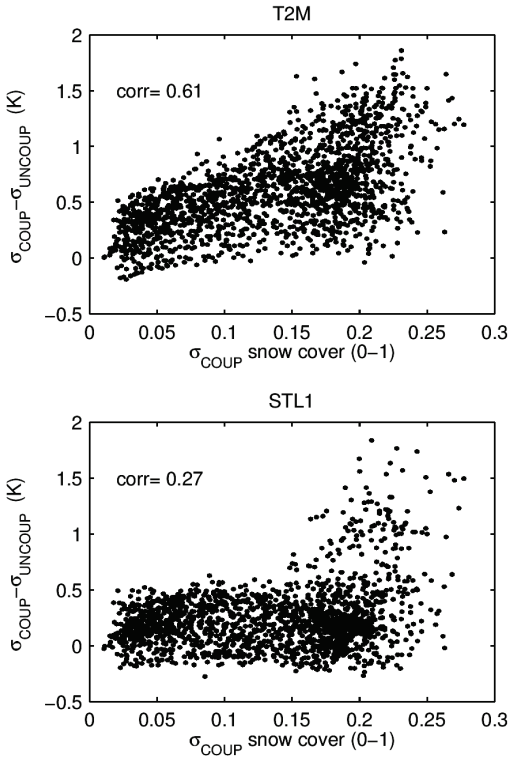

Figure 6.3. Grid point differences in winter interannual standard deviation between COUP-UNCOUP of T2M (a) and STL1 (b) as a function of snow cover standard deviation in COUP. The scatter plots encompass all grid points in the Northern Hemisphere with mean snow cover between 1% and 75% accounting for 23% of the Northern Hemisphere land regions.

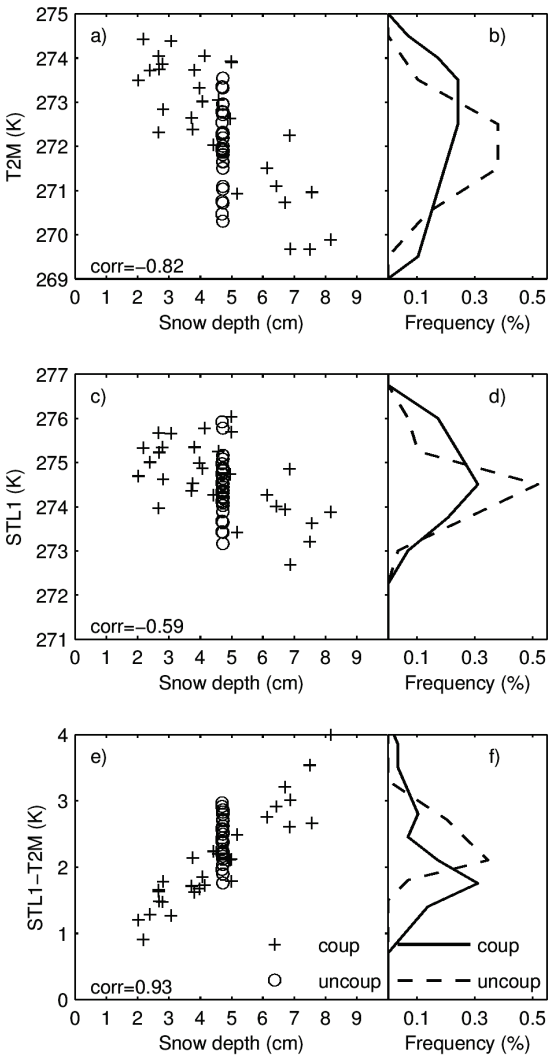

Figure 6.4. Scatter plots of mean T2M (a), STL1 (c) and STL1-T2M (e) as function of the mean snow depth averaged over Midwestern US (35°N < Latitude < 45°N; 100°W < Longitude < 80°W, about 15% of the US area) during winter as simulated by COUP (crosses) and UNCOUP (circles). The right panels represent the associated estimates of the distributions of T2M (b), STL1 (d) and STL1-T2M (f) simulated by COUP (solid line) and UNCOUP (dashed line).

An interesting finding is the high correlation between snow depth and STL1-T2M in COUP. It highlights the role of snow depth in decoupling the soil temperature evolution from the overlying atmosphere. Moreover, this relation is in close agreement with the work of Ge and Gong (2010). They found a similar relation between soil-air temperatures as function of snow depth by carrying out idealized simulation with a one-dimensional snowpack energy and mass balance model.

6.4 Conclusions

This study presents an evaluation of the snow cover interannual variability role in controlling the land-atmosphere coupling. Two experiments with coupled and uncoupled snow evolution using the EC-EARTH climate model were analyzed. In the UNCOUP experiment the snow evolution was replaced by the climatology derived from COUP. The replacement of the snow related prognostics (SWE, density and albedo) in UNCOUP has two effects: (i) the snow-cover season (from settling to melting) has the same evolution each year, i.e. no interannual variation, and (ii) no seasonal feedbacks related to snow cover are allowed. For example, if a positive temperature anomaly occurs during spring, the associated response of increased melting, that could led to an intensification of the temperature anomaly is not allowed in UNCOUP.

The interannual variability of snow cover and mass explains almost 60% of the winter T2M interannual variability over North Eurasian and American continents in regions that are predominantly snow-covered. During spring there is a reduction of the snow variability control on T2M. While in winter the signal was spread throughout the Northern latitudes, in spring is mainly constrained to the snow line regions, where the snow-albedo feedback plays an important role (Groisman et al. 1994b). The interannual variability of soil temperature is also damped in UNCOUP. The spatial patterns of STL1 $\Delta\sigma$ are similar to those of T2M. However, there are regions with a pronounced signal in STL1 $\Delta\sigma$ with no counterpart in T2M $\Delta\sigma$. Such regions are characterized by a significant interannual variability in snow depth, rather than snow cover (almost fully snow covered during winter). These findings further illustrate that not only the presence of snow in the ground controls the land-atmosphere coupling but also snow depth.

The results presented in this study are based only on EC-EARTH simulations and the question of their model dependency cannot be addressed. However, the increased decoupling between air and soil temperatures with increasing snow depth was also reported by Ge and Gong (2010) following a different simulation strategy and model from the ones used in this study (see Figure 6.4). Quantitatively the findings of this study are model dependent, but qualitatively point to the important role of interannual snow cover variability in controlling the land-atmosphere coupling with impact on the air and soil temperature variability. Further investigations integrating a multi-model approach could follow a similar procedure, and complement, the global land-atmosphere coupling experiment (GLACE) (Koster et al. 2006).

Acknowledgements

The authors are grateful for the valuable support of the EC-EARTH consortium members. This work was supported by the Portuguese Foundation for Science and Technology (FCT) under project AMIC PTDC/AAC-CLI/109030/2008 cofinanced by the European Union under program FEDER. E. Dutra acknowledges the financial support of FCT under Grant FRH/BD/35789/2007.

6.5 Appendix: Supplementary figures

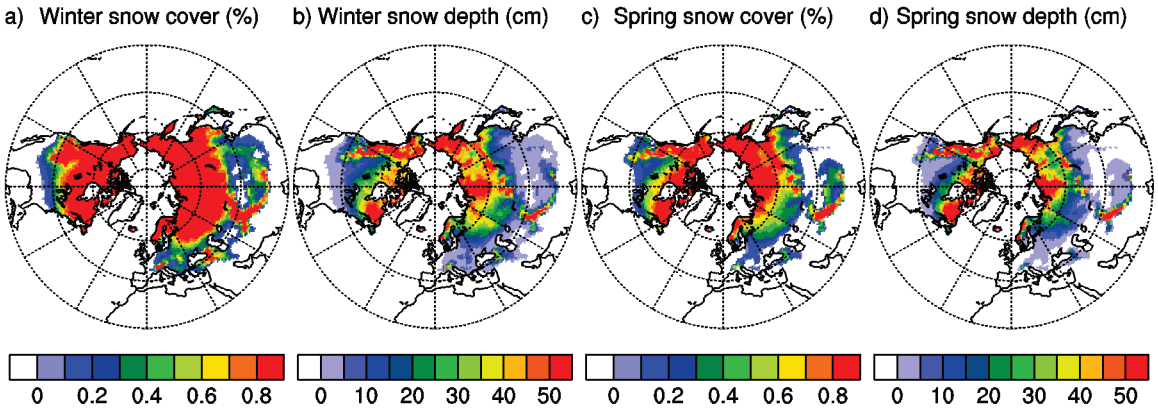

Figure 6.5. Mean winter (a, b) and spring (c, d) snow cover (a,c) and snow depth (b, d) simulated by COUP.

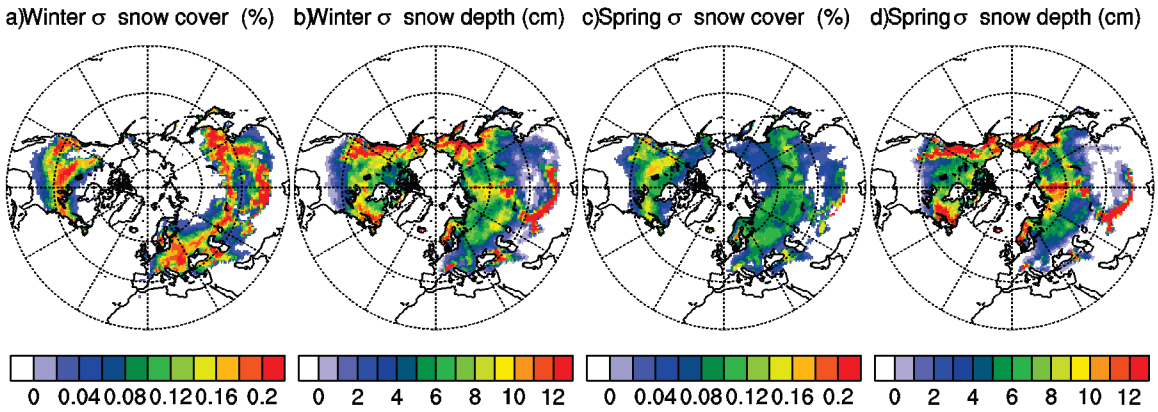

Figure 6.6. Standard deviation of winter (a, b) and spring (c, d) snow cover (a,c) and snow depth (b, d) simulated by COUP.

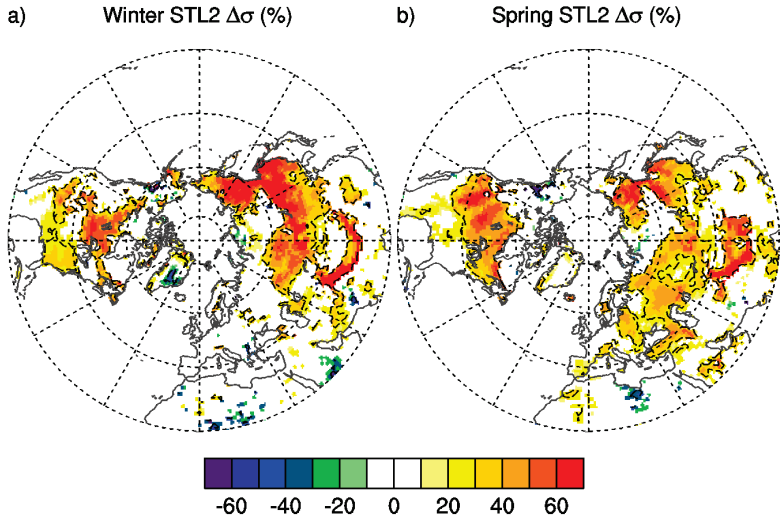

Figure 6.7. As Figure 6.2 but to soil temperature of layer 2 (7 to 21 cm depth)

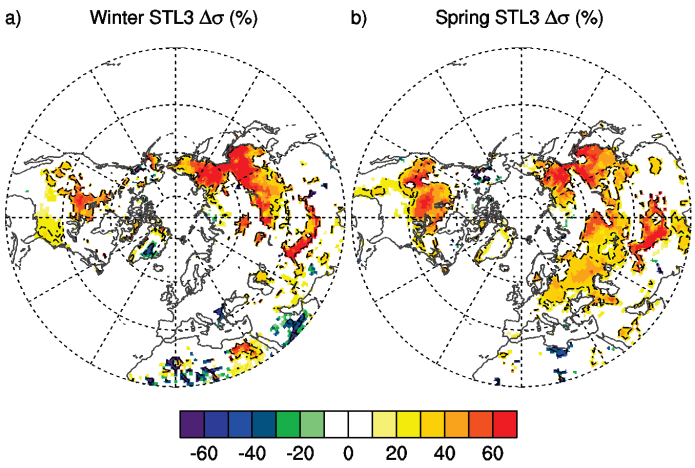

Figure 6.8. As Figure 6.2 but for soil temperature of layer 3 (21 to 100 cm depth).

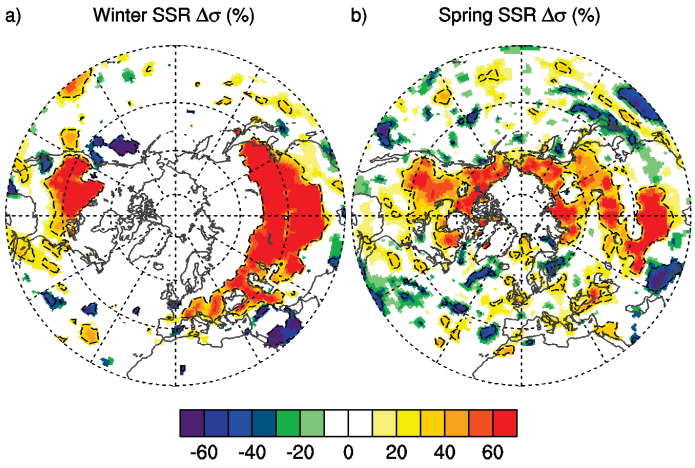

Figure 6.9. As Figure 6.2 but for surface solar radiation (downward minus upward).

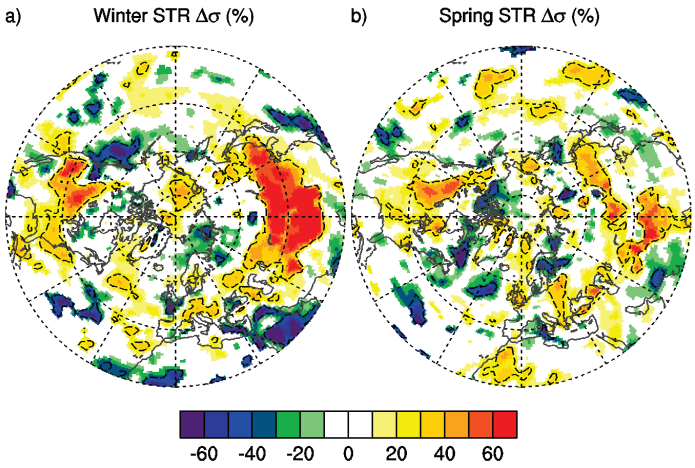

Figure 6.10. As Figure 6.2 but for surface thermal radiation (downward minus upward).

7 Overall conclusions

This dissertation presents an assessment of the role of cold processes, associated with snow cover, in controlling the land-atmosphere coupling. The work was based on model simulations, including offline simulations with the LSM HTESSEL, and coupled atmosphere simulations with the EC-EARTH climate model. Several limitations were found in the representation of snow in HTESSEL and EC-EARTH. This motivated the revision of the snow representation leading to the development and testing of a revised snow scheme in both models. The snow scheme became operational at the ECMWF integrated forecast system, and in the default configuration of EC-EARTH. The improved representation of the snowpack dynamics in HTESSEL was also followed by improvements in the near surface temperature simulations of EC-EARTH, and positive impacts in the IFS (Balsamo et al. 2011b). The new snow scheme development was complemented by a multi-layer version that showed potential benefits in modeling thick snowpacks. A key process was the better representation of snow thermal insulation, which led to significant improvements of the surface water and energy balance components. Similar findings were observed when coupling the snow scheme to lake ice, where lake ice duration was significantly improved. An assessment of the snow cover sensitivity to horizontal resolution, parameterizations and atmospheric forcing within HTESSEL highlighted the importance of accurate atmospheric forcing and snowpack parameterizations over flat terrain regions in detriment of horizontal resolution. A set of experiments with and without free snow evolution was carried out with EC-EARTH to assess how the interannual snow cover variability impacts near surface and soil temperatures. It was found that snow cover interannual variability explained up to 60% of the total interannual variability of near surface temperature over snow covered regions. Although these findings are model dependent, the results showed consistency with previously published works. Furthermore, the detailed evaluation of the snow dynamics simulation in HTESSEL and EC-EARTH guarantees consistency of the results. In the following paragraphs a brief overview of the main conclusions of each chapter is presented.

The second chapter of this dissertation described the implementation of the lake model FLake into HTESSEL. FLake is a numerical model describing the thermodynamic processes in a lake. The special issue of the journal *Boreal Environment Research* (volume 15 issue 2) reports the implementation and impact of FLake in several land surface models (Dutra et al. 2010b; Rooney and Jones 2010; Salgado and Le Moigne 2010). Offline simulations, forced by ERAI were performed to access the model's performance in simulating the lake surface water temperature and lake-ice duration. In spite of the limitations of the stand-alone simulation methodology (no feedback to the atmosphere), the model performed as expected, when compared with observations of both lake surface water temperature and lake-ice duration. The technical implementation of FLake into HTESSEL also allowed the representation of sub-grid scale lakes, embedded in the tile approach currently used in HTESSEL. This is of particular importance for climate applications, where at the typical horizontal resolutions (presently between 100 km and 200 km) most of the lakes are not resolved. In high-latitude regions the representation of sub-grid scale lakes changed the mean annual cycle of terrestrial energy storage, with increased storage during summer and subsequent release during autumn. This results from the higher

thermal capacity of water, when compared with soil. On the other hand, in equatorial regions, lakes changed the partition of energy fluxes to the atmosphere, with an increase of latent heat flux and a reduction of sensible heat flux. These findings highlighted the role of water bodies in controlling the land surface energy balance, which has been largely neglected in most land surface models.

In the scope of this dissertation, the thermal insulation of snow cover over lake ice was assessed by coupling the current snow scheme of HTESSEL to the lake ice. This improved the simulated lake ice duration over 429 water bodies in the Northern Hemisphere, when compared with available observations. A close relation between lake ice duration and frozen soil at nearby locations was also found. The effect of snow thermal insulation in controlling lake ice growth/breakup was reproduced by changing the lake ice albedo. However, the nature of underlying physical processes are different: 1) snow insulates the lake ice from the cold air temperatures, reducing its growth during the cold season; 2) without the snow thermal insulation, lake ice grows during the cold season and a reduction of its surface albedo during spring is necessary to accelerate the lake ice melt. The lack of lake ice depth observations constrains further assessments of the realism of these two approaches. Nevertheless, the present work showed that lakes significantly impact the surface energy fluxes. Global lake depths are required as the most important lake parameter. Balsamo et al. (2010) proposed an approach to derive an effective lake depth in order to overcome the lack of observational estimates, but also to account for the associated uncertainty in mapping real lake depths to a gridded lake cover. Besides lake depth, the lack of global data on other lake related parameters, such as optical characteristics of lake water, is still an impediment for further progress. Balsamo et al. (2011a) evaluated the performance of the ECMWF weather forecasts with FLake activated. The representation of sub-grid scale lakes brought a beneficial impact on weather forecasts over the Northern territories of Canada and over Scandinavia, particularly in spring and summer.

In the outcome of SnowMIP2 and the initial EC-EARTH simulations it was found that the representation of cold processes associated with seasonal snow cover in HTESSEL had some deficiencies. These limitations constrained further studies of the role of snow cover in controlling the land-atmosphere coupling. Therefore, a revision of the snow representation in HTESSEL was carried out, resulting in the development of a new snow scheme described in chapter 3. The new snow revision included four main processes: i) representation of liquid water content as a diagnostic; ii) new snow density parameterization; iii) revised snow cover fraction calculation; and iv) revision of exposed snow albedo and new forest albedo in presence of snow. The validation included offline simulations for several observational sites from SnowMIP2 and global simulations driven by the meteorological forcing from GSWP2 and ERAI. In the SnowMIP2 sites, the NEW snow scheme reduced the negative timing bias of snow depletion in forest plots from 21 to 13 days and positive bias in open plots from 10 to 2 days. Moreover, the simulated snow density was significantly improved, resulting in an augmented insulation effect of the snowpack. In 10 Northern Hemisphere basins, there was an average reduction of the monthly runoff RMSE from 0.75 to 0.51 mm day^{-1} from the old to the NEW snow scheme. These results illustrate the importance of snow insulation on the hydrological cycle, even at regional scales. There were also improvements of the surface albedo reducing the net shortwave radiation bias over the Northern Hemisphere. Simulated improvements of SWE in SnowMIP2 locations were mainly due to the snow liquid water representation on forest sites and to the new exposed albedo on open sites. The increased snow insulation effect, due to the new snow density parameterization, had an important role on the basin's water balance. Impacts of the new snow cover

fraction and exposed and shaded albedo parameterizations were evident when validating against remote sensing data. Sensitivity tests highlighted the role of the different components of the snow scheme, with the behavior conditioned by the climate and vegetation conditions of each site. Thus, a robust verification of a LSM model should include a variety of different (and independent) validation datasets.

Following the development of the snow scheme, the sensitivity of snow cover simulations to horizontal resolution, snowpack parameterization and atmospheric forcing was assessed in chapter 4. Offline simulations of HTESSEL were carried out, forced by the ECMWF deterministic weather forecasts from March 2006 to June 2010. The impact of horizontal resolution on snow cover was addressed by performing simulations at 25, 80 and 200 km. The impact of the atmospheric forcing on snow cover was assessed by forcing the model additionally with ERAI, at 80 km resolution. The snowpack parameterizations were analyzed by comparing simulations with the old snow scheme and NEW (described in chapter 3). The simulations were validated against four independent observational datasets. The horizontal resolution proved to play an important role on simulating snow cover in complex terrain regions, while its impact on flat terrain regions was reduced. In the latter regions, the accuracy of atmospheric forcing and model physics played a more important role. These results are model dependent and their generalization is not certain, especially concerning the model physics. However, the results show that developments in land surface models are strongly dependent on the quality of available forcing and validation datasets. The simulation setup framework presented can be also applied to investigate other land-atmosphere processes, especially alternative approaches to describe land surface sub-grid scale variability, which is a critical point in climate models.

The analysis presented in chapters 3 and 4 were based on offline simulations. However, the full impact of the snowpack parameterization can only be assessed in land-atmosphere coupled simulations. In Chapter 5 three different complexity snow schemes were evaluated within the EC-EARTH climate models. The snow schemes include CTR (standing for the old snow scheme) and OPER (NEW in chapter 3), and a multi-layer version of OPER (ML3). The ML3 snow scheme was validated with offline simulations, showing an improvement in representing a deep snowpack when compared with the other two single layer snow schemes. This was expected, since a bulk snowpack has large thermal inertia, with difficulties in representing sporadic melting events during winter and early spring. In the EC-EARTH climate simulations, the increased snow thermal insulation from CTR to OPER and ML3 led to warmer soil temperatures during winter and spring. This reduced the soil freezing allowing snow melt and rainfall to infiltrate to the soil instead of leaving the surface as surface runoff. The increased soil moisture content during late spring and summer was then responsible for higher evapotranspiration rates. This, in turn, resulted in an increase of summer precipitation due to the increased moisture in the lower troposphere and an intensification of the soil-precipitation feedback. This chain of processes started during the cold season and ended during summer. This showed the importance of snow cover, its representation in climate models, both on the surface water and energy balances. Furthermore, the increased snow thermal insulation in OPER and ML3 reduced the T2M warm bias over snow covered regions during winter and spring. The increased complexity of ML3 showed its potential in modeling thick snowpacks in open areas such as prairies or tundra in Northern Latitudes. Hazeleger et al. (2010) found similar improvements in coupled ocean-atmosphere simulations when running EC-EARTH with CTR and OPER snow schemes. Cook et al. (2008) reported similar results when investigating the sensitivity of surface climate to the treatment of snow

thermal conductivity. In their experiments, high versus low insulation cases led to soil cooling of up to 20 K in winter and T2M warming of 6 K. Comparing with this study, CTR would be the low insulation case, OPER an intermedium, and ML3 a high insulation. While Cook et al. (2008) demonstrated the importance of snow thermal conductivity by prescribing its value in a set of experiments, in this study similar results were found by using different snow schemes. The improved performance of OPER over CTR was also found in offline simulations (chapter 3 and 4). The resemblance between the offline and atmosphere coupled simulations highlights the reliability of the offline strategy to validate land surface models, and the importance of the model physics in simulating snow cover.

Following the advances achieved in the representation of snow related processes in HTESSEL and EC-EARTH, chapter 6 was focused in the land-atmosphere coupling in the presence of snow. For this purpose, global atmospheric simulations were carried out with the EC-EARTH climate model with and without interactive snow evolution. In the latter, snow evolution was replaced by a climatology derived from a control simulation. The interannual variability of snow cover and mass explained almost 60% of the winter T2M interannual variability over North Eurasian and American continents in regions that are predominantly snow-covered. During spring there was a reduction of the snow variability control on T2M. While in winter the signal was spread throughout the Northern latitudes, in spring it was mainly constrained to the snow line regions, where the snow-albedo feedback plays an important role. The interannual variability of soil temperature was also damped in UNCOUP. The spatial patterns of soil temperature variability changes are similar to those of air temperature. However, there are regions with a pronounced signal in soil temperature but no counterpart in air temperature. These regions are characterized by a significant interannual variability in snow depth rather than snow cover (almost fully snow covered during winter). These findings further that the land-atmosphere coupling is not only dependent on the presence of snow, but also on the snow depth.

This dissertation was organized in 7 chapters, where 5 of them (chapters 2-6) were presented as self-contained scientific papers, since they have been already published or submitted to publication. Although, each chapter focused on different subjects, they share a similar background in terms of modeling framework and scientific topic. The following points present an outlook and some of the remaining open questions in each one of the addressed topics:

- Lakes and climate: The offline experiments with interactive lakes showed significant impact in the surface water and energy balances. Further work could focus on the implementation and evaluation of lakes representation within EC-EARTH. This would also allow an integrated assessment of the role of snow thermal insulation in controlling lake ice evolution.
- Snow parameterizations: The new developed snow scheme and its multi-layer version were mainly focused on the thermal and mass balances of the snowpack. Processes associated with the interaction with the canopy and sub-grid scale variability were not addressed. Some results pointed to problems over high altitude complex terrain regions (namely the Himalaya and Rocky Mountains) reinforcing the need of addressing sub-grid scale variability, which is critical for climate modeling.
- Land-atmosphere coupling and snow: The snow thermal insulation proved to significantly control the land-atmosphere coupling. However, this process is poorly constrained, and strongly dependent on the model parameterizations. Furthermore, the interannual variability of

snow was also linked with near surface and soil temperature variability. An extension of the work could include additional simulation setups accounting for the model's uncertainty in representing land surface cold processes (for example a multi-model approach). The land-atmosphere coupling associated with snow cover could be further addressed by carrying out a large ensemble of simulations with free evolving snow. This would provide a mean snow evolution to be prescribed as a climatology (no interannual variability) and as the mean of the ensemble (no response to atmospheric variability). In addition, it would be interesting to compare the role of snow cover in controlling the land-atmosphere coupling with other boundary conditions like soil moisture, sea surface temperature and sea ice.

For some millions of years, snow and ice have played a major role in the definition of the mean global climate state, including the mean North-South temperature gradient, and the intensity and characteristics of the global circulation, but also of observed seasonal and interanual climate variability, and even of interglacial variability. A better understanding, and representation, of the physics involved in snow and ice processes at all scales is, clearly, a crucial step for the development of better Earth System models that are required to predict and manage climate change in the forthcoming decades.

References

Allen, R. J., and C. S. Zender, 2010: Effects of continental-scale snow albedo anomalies on the wintertime Arctic oscillation, *J. Geophys. Res.*, **115**(D23), D23105, doi: 10.1029/2010jd014490.

Anderson, E. A., 1976: A point energy and mass balance model of a snow cover, *NOAA Tech. Rep.* , NWQ 19, 150 pp.

Armstrong, R. L., and M. J. Brodzik, 2005: updated 2007, Northern Hemisphere EASE-Grid weekly snow cover and sea ice extent version 3. Boulder, Colorado USA: National Snow and Ice Data Center. Digital media.

Armstrong, R. L., and E. Brun, 2008: Snow and Climate. Physical processes, surface energy exchange and modeling. Cambridge University press, 222.

Baker, D. G., R. H. Skaggs, and D. L. Ruschy, 1991: Snow Depth Required to Mask the Underlying Surface, *J. Appl. Meteor.*, **30**(3), 387-392.

Balsamo, G., R. Salgado, E. Dutra, S. Boussetta, and T. Stockdale, 2011a: On the contribution of lakes in predicting near-surface temperature in a global weather forecasting model, *submitted to Tellus A*.

Balsamo, G., P. Viterbo, A. Beljaars, B. Van den Hurk, A. K. Betts, and K. Scipal, 2009: A revised hydrology for the ECMWF model: Verification from field site to terrestrial water storage and impact in the Integrated Forecast System, *J. Hydrometeor.*, **10**(3), 623-643 doi: 610.1175/2008JHM1068.1171.

Balsamo, G., E. Dutra, V. M. Stepanenko, P. Viterbo, P. M. A. Miranda, and D. Mironov, 2010: Deriving an effective lake depth from satellite lake surface temperature data: a feasibility study with MODIS data, *Boreal Environ. Res.*, **15**(2), 178-190.

Balsamo, G., S. Boussetta, E. Dutra, A. Beljaars, P. Viterbo, and B. Van den Hurk, 2011b: Evolution of land surface processes in the IFS, *ECMWF Newsletter*, **127**, 17-22.

Barenblatt, G. I., 1978: Self-Similar Distribution of Temperature and Salinity in Upper Thermocline, *Izvestiya Akademii Nauk Sssr Fizika Atmosfery I Okeana*, **14**(11), 1160-1166.

Bartlett, M. G., D. S. Chapman, and R. N. Harris, 2004: Snow and the ground temperature record of climate change, *J. Geophys. Res.*, **109**, F04008, doi: 10.1029/2004JF000224.

Bartlett, M. G., D. S. Chapman, and R. N. Harris, 2005: Snow effect on North American ground temperatures, 1950-2002, *J. Geophys. Res.*, **110**, F03008, doi: 10.1029/2005JF000293.

Belair, S., R. Brown, J. Mailhot, B. Bilodeau, and L. P. Crevier, 2003: Operational implementation of the ISBA land surface scheme in the Canadian regional weather forecast model. Part II: Cold season results, *J. Hydrometeor.*, **4**(2), 371-386.

Beniston, M., B. Uhlmann, S. Goyette, and J. I. Lopez-Moreno, 2011: Will snow-abundant winters still exist in the Swiss Alps in an enhanced greenhouse climate ?, *Int. J. Climatol.*, **31**, doi: 10.1002/joc.2151.

Benson, B., and J. Magnunson, 2007: Global lake and river ice phenology database. Boulder, Colorado USA: National Snow and Ice Data Center/World Data Center for Glaciology. Digital media.

Boer, G. J., N. A. McFarlane, and M. Lazare, 1992: Greenhouse Gas–induced Climate Change Simulated with the CCC Second-Generation General Circulation Model, *J. Climate*, **5**(10), 1045-1077, doi: 10.1175/1520-0442(1992)005<1045:GGCCSW>2.0.CO;2.

Bonan, G. B., 1995: Sensitivity of a Gcm Simulation to Inclusion of Inland Water Surfaces, *J. Climate*, **8**(11), 2691-2704.

Boone, A., and P. Etchevers, 2001: An intercomparison of three snow schemes of varying complexity coupled to the same land surface model: Local-scale evaluation at an Alpine site, *J. Hydrometeor.*, **2**(4), 374-394.

Boone, A., and Coauthors, 2004: The Rhone-aggregation land surface scheme intercomparison project: An overview, *J. Climate*, **17**(1), 187-208.

Bowling, L. C., and Coauthors, 2003: Simulation of high-latitude hydrological processes in the Torne-Kalix basin: PILPS phase 2(e) - 1: Experiment description and summary intercomparisons, *Global Planet. Change*, **38**(1-2), 1-30.

Brown, R., and R. L. Armstrong, 2008: Snow-cover data: measurement, products, and sources. *Snow and Climate*, R. L. Armstrong, and E. Brun, Eds., Cambridge University Press.

Brown, R., C. Derksen, and L. Wang, 2007: Assessment of spring snow cover duration variability over northern Canada from satellite datasets, *Remote Sens. Environ.*, **111**(2-3), 367-381, doi: DOI 10.1016/j.rse.2006.09.035.

Brubaker, K. L., R. T. Pinker, and E. Deviatova, 2005: Evaluation and comparison of MODIS and IMS snow-cover estimates for the continental United States using station data, *J. Hydrometeor.*, **6**(6), 1002-1017.

Brun, E., P. David, M. Sudul, and G. Brunot, 1992: A Numerical-Model to Simulate Snow-Cover Stratigraphy for Operational Avalanche Forecasting, *Journal of Glaciology*, **38**(128), 13-22.

Brun, E., Z. Yang, R. Essery, and J. Cohen, 2008: Snow-cover parameterization and modeling. *Snow and Climate*, R. L. Armstrong, and E. Brun, Eds., Cambridge University Press.

Brun, E., E. Martin, V. Simon, C. Gendre, and C. Coleou, 1989: An Energy and Mass Model of Snow Cover Suitable for Operational Avalanche Forecasting, *Journal of Glaciology*, **35**(121), 333-342.

Carrera, M. L., S. Bélair, V. Fortin, B. Bilodeau, D. Charpentier, and I. Doré, 2010: Evaluation of Snowpack Simulations over the Canadian Rockies with an Experimental Hydrometeorological Modeling System, *J. Hydrometeor.*, **11**(5), 1123-1140, doi: 10.1175/2010JHM1274.1

Cess, R. D., and G. L. Potter, 1988: A Methodology for Understanding and Intercomparing Atmospheric Climate Feedback Processes in General Circulation Models, *J. Geophys. Res.*, **93**(D7), 8305-8314, doi: 10.1029/JD093iD07p08305.

Chang, E. K. M., S. Lee, and K. L. Swanson, 2002: Storm Track Dynamics, *J. Climate*, **15**(16), 2163-2183, doi: 10.1175/1520-0442(2002)015<02163:STD>2.0.CO;2.

Choi, G., D. A. Robinson, and S. Kang, 2010: Changing Northern Hemisphere Snow Seasons, *J. Climate*, **23**(19), 5305-5310, doi: 10.1175/2010jcli3644.1.

Christensen, J. H., and O. B. Christensen, 2007: A summary of the PRUDENCE model projections of changes in European climate by the end of this century, *Climatic Change*, **81**, 7-30, doi: 10.1007/s10584-006-9210-7.

Cohen, J., M. Barlow, P. J. Kushner, and K. Saito, 2007: Stratosphere-troposphere coupling and links with Eurasian land surface variability, *J. Climate*, **20**(21), 5335-5343.

Cook, B. I., G. B. Bonan, S. Levis, and H. E. Epstein, 2008: The thermoinsulation effect of snow cover within a climate model, *Climate Dyn.*, **31**(1), 107-124.

Crosman, E. T., and J. D. Horel, 2009: MODIS-derived surface temperature of the Great Salt Lake, *Remote Sens. Environ.*, **113**(1), 73-81.

Dee, D. P., and Coauthors, 2011: The ERA-Interim reanalysis: configuration and performance of the data assimilation system, *Quart. J. Roy. Meteor. Soc.*, **137**(656), 553-597, doi: 10.1002/qj.828.

Derbyshire, S. H., 1999: Boundary-Layer Decoupling over Cold Surfaces as a Physical Boundary-Instability, *Bound-Lay Meteorol*, **90**(2), 297-325, doi: 10.1023/a:1001710014316.

Dirmeyer, P. A., 2005: The Land Surface Contribution to the Potential Predictability of Boreal Summer Season Climate, *J. Hydrometeor.*, **6**(5), 618-632, doi: 10.1175/JHM444.1.

Dirmeyer, P. A., A. J. Dolman, and N. Sato, 1999: The pilot phase of the Global Soil Wetness Project, *Bull. Amer. Meteor. Soc.*, **80**(5), 851-878.

Dirmeyer, P. A., X. Gao, and T. Oki, 2002: The second global soil wetness project science and implementation plan, *IGPO int. GEWEX Project Office Publ. Series*, **37**, 75.

Douville, H., 2010: Relative contribution of soil moisture and snow mass to seasonal climate predictability: a pilot study, *Climate Dyn.*, **34**(6), 797-818, doi: 10.1007/s00382-008-0508-1.

Douville, H., and J. F. Royer, 1996: Sensitivity of the Asian summer monsoon to an anomalous Eurasian snow cover within the Meteo-France GCM, *Climate Dyn.*, **12**(7), 449-466.

Douville, H., J. F. Royer, and J. F. Mahfouf, 1995: A New Snow Parameterization for the Meteo-France Climate Model .1. Validation in Stand-Alone Experiments, *Climate Dyn.*, **12**(1), 21-35.

Douville, H., P. Viterbo, J. F. Mahfouf, and A. C. M. Beljaars, 2000: Evaluation of the Optimum Interpolation and Nudging Techniques for Soil Moisture Analysis Using FIFE Data, *Monthly Weather Review*, **128**(6), 1733-1756.

Douville, H., F. Chauvin, S. Planton, J. F. Royer, D. Salas-Melia, and S. Tyteca, 2002: Sensitivity of the hydrological cycle to increasing amounts of greenhouse gases and aerosols, *Climate Dyn.*, **20**(1), 45-68.

Drusch, M., D. Vasiljevic, and P. Viterbo, 2004: ECMWF's global snow analysis: Assessment and revision based on satellite observations, *J. Appl. Meteor.*, **43**(9), 1282-1294.

Dutra, E., P. Viterbo, and P. M. A. Miranda, 2008: ERA-40 reanalysis hydrological applications in the characterization of regional drought, *Geophys. Res. Lett.*, **35**, L19402, doi:19410.11029/12008GL035381.

Dutra, E., G. Balsamo, P. Viterbo, P. M. A. Miranda, A. Beljaars, C. Schar, and K. Elder, 2010a: An Improved Snow Scheme for the ECMWF Land Surface Model: Description and Offline Validation, *J. Hydrometeor.*, **11**(4), 899-916, doi: 10.1175/2010jhm1249.1.

Dutra, E., V. M. Stepanenko, G. Balsamo, P. Viterbo, P. M. A. Miranda, D. Mironov, and C. Schar, 2010b: An offline study of the impact of lakes on the performance of the ECMWF surface scheme, *Boreal Environ. Res.*, **15**(2), 100-112.

Ebert, E. E., and J. A. Curry, 1993: An Intermediate One-Dimensional Thermodynamic Sea-Ice Model for Investigating Ice-Atmosphere Interactions, *J. Geophys. Res.*, **98**(C6), 10,085-010,109.

ECMWF, cited 2011: IFS Documentation CY28r1: IV Physical processes. [Available online at http://www.ecmwf.int/research/ifsdocs/CY28r1/Physics/index.html.]

Ehn, J. K., M. A. Granskog, T. Papakyriakou, R. Galley, and D. G. Barber, 2006: Surface albedo observations of Hudson Bay (Canada) landfast sea ice during the spring melt, *Ann. Glaciol.*, **44**, 23-29, doi: 10.3189/172756406781811376.

Esaias, W. E., and Coauthors, 1998: An overview of MODIS capabilities for ocean science observations, *Ieee T. Geosci. Remote*, **36**(4), 1250-1265.

Essery, R., 1997: Seasonal snow cover and climate change in the Hadley Centre GCM, *Ann. Glaciol.*, **25**, 362-366.

Essery, R., and Coauthors, 2009: SNOWMIP2: An Evaluation of Forest Snow Process Simulations, *Bull. Amer. Meteor. Soc.*, **90**(8), 1120-1135, doi: doi:10.1175/2009BAMS2629.1.

Etchevers, P., and Coauthors, 2004: Validation of the energy budget of an alpine snowpack simulated by several snow models (SnowMIP project), *Ann. Glaciol.*, **38**, 150-158, doi: 10.3189/172756404781814825.

Fischer, E. M., and C. Schar, 2009: Future changes in daily summer temperature variability: driving processes and role for temperature extremes, *Climate Dyn.*, **33**(7-8), 917-935, doi: 10.1007/s00382-008-0473-8.

Fischer, E. M., S. I. Seneviratne, D. Luthi, and C. Schar, 2007: Contribution of land-atmosphere coupling to recent European summer heat waves, *Geophys. Res. Lett.*, **34**, L06707, doi: 10.1029/2006GL029068.

Flanner, M. G., K. M. Shell, M. Barlage, D. K. Perovich, and M. A. Tschudi, 2011: Radiative forcing and albedo feedback from the Northern Hemisphere cryosphere between 1979 and 2008, *Nature Geosci*, **4**(3), 151-155, doi: 10.1038/ngeo1062.

Fletcher, C. G., P. J. Kushner, A. Hall, and X. Qu, 2009a: Circulation responses to snow albedo feedback in climate change, *Geophys. Res. Lett.*, **36**, L09702, doi: 10.1029/2009gl038011.

Fletcher, C. G., S. C. Hardiman, P. J. Kushner, and J. Cohen, 2009b: The Dynamical Response to Snow Cover Perturbations in a Large Ensemble of Atmospheric GCM Integrations, *J. Climate*, **22**(5), 1208-1222, doi: 10.1175/2008JCLI2505.1.

Foppa, N., A. Stoffel, and R. Meister, 2007: Synergy of in situ and space borne observation for snow depth mapping in the Swiss Alps, *International Journal of Applied Earth Observation and Geoinformation*, **9**(3), 294-310, doi: DOI: 10.1016/j.jag.2006.10.001.

Frei, A., R. Brown, J. A. Miller, and D. A. Robinson, 2005: Snow mass over North America: Observations and results from the second phase of the atmospheric model intercomparison project, *J. Hydrometeor.*, **6**(5), 681-695.

Gao, X., P. A. Dirmeyer, and T. Oki, 2004: Update on the second global soil wetness project (GSWP-2), *GEWEX Newsletter*, **14,**, 10.

Ge, Y., and G. Gong, 2010: Land surface insulation response to snow depth variability, *J. Geophys. Res.*, **115**, D08107, doi: 10.1029/2009JD012798.

Giorgi, F., R. Francisco, and J. Pal, 2003: Effects of a subgrid-scale topography and land use scheme on the simulation of surface climate and hydrology. Part I: Effects of temperature and water vapor disaggregation, *J. Hydrometeor.*, **4**(2), 317-333.

Gong, G., J. Cohen, D. Entekhabi, and Y. Ge, 2007: Hemispheric-scale climate response to Northern Eurasia land surface characteristics and snow anomalies, *Global Planet. Change*, **56**(3-4), 359-370, doi: 10.1016/j.gloplacha.2006.07.025.

Grippa, M., L. Kergoat, T. Le Toan, N. M. Mognard, N. Delbart, J. L'Hermitte, and S. M. Vicente-Serrano, 2005: The impact of snow depth and snowmelt on the vegetation variability over central Siberia, *Geophys. Res. Lett.*, **32**, L21412, doi:21410.21029/22005GL024286.

Groisman, P. Y., T. R. Karl, and R. W. Knight, 1994a: Observed Impact of Snow Cover on the Heat-Balance and the Rise of Continental Spring Temperatures, *Science*, **263**(5144), 198-200.

Groisman, P. Y., T. R. Karl, R. W. Knight, and G. L. Stenchikov, 1994b: Changes of Snow Cover, Temperature, and Radiative Heat-Balance over the Northern-Hemisphere, *J. Climate*, **7**(11), 1633-1656, doi: 10.1175/1520-0442(1994)007<1633:COSCTA>2.0.CO;2.

Groisman, P. Y., R. W. Knight, T. R. Karl, D. R. Easterling, B. M. Sun, and J. H. Lawrimore, 2004: Contemporary changes of the hydrological cycle over the contiguous United States: Trends derived from in situ observations, *J. Hydrometeor.*, **5**(1), 64-85.

Hall, A., and X. Qu, 2006: Using the current seasonal cycle to constrain snow albedo feedback in future climate change, *Geophys. Res. Lett.*, **33**, L03502, doi: 10.1029/2005gl025127.

Hazeleger, W., and Coauthors, 2010: EC-Earth: A Seamless Earth-System Prediction Approach in Action, *Bull. Amer. Meteor. Soc.*, **91**(10), 1357-1363, doi: 10.1175/2010BAMS2877.1.

Helfrich, S. R., D. McNamara, B. H. Ramsay, T. Baldwin, and T. Kasheta, 2007: Enhancements to, and forthcoming developments in the Interactive Multisensor Snow and Ice Mapping System (IMS), *Hydrol. Processes*, **21**(12), 1576-1586.

Hirschi, M., S. I. Seneviratne, and C. Schar, 2006: Seasonal variations in terrestrial water storage for major midlatitude river basins, *J. Hydrometeor.*, **7**(1), 39-60.

Hirschi, M., and Coauthors, 2011: Observational evidence for soil-moisture impact on hot extremes in southeastern Europe, *Nature Geosci*, **4**(1), 17-21, doi: 10.1038/ngeo1032.

Hogewind, F., and P. Bissolli, 2010: Operational Maps of Monthly Mean Temperature for WMO Region VI (Europe and Middle East), *submitted to Időjárás*

Hostetler, S. W., F. Giorgi, G. T. Bates, and P. J. Bartlein, 1994: Lake-Atmosphere Feedbacks Associated with Paleolakes Bonneville and Lahontan, *Science*, **263**(5147), 665-668.

Hu, Q., and S. Feng, 2005: How have soil temperatures been affected by the surface temperature and precipitation in the Eurasian continent?, *Geophys. Res. Lett.*, **32**(14), L14711, doi: 10.1029/2005gl023469.

Im, E. S., E. Coppola, F. Giorgi, and X. Bi, 2010: Validation of a High-Resolution Regional Climate Model for the Alpine Region and Effects of a Subgrid-Scale Topography and Land Use Representation, *J. Climate*, **23**(7), 1854-1873, doi: 10.1175/2009jcli3262.1.

Immerzeel, W. W., L. P. H. van Beek, and M. F. P. Bierkens, 2010: Climate Change Will Affect the Asian Water Towers, *Science*, **328**(5984), 1382-1385, doi: 10.1126/science.1183188.

Jarlan, L., G. Balsamo, S. Lafont, A. Beljaars, J. C. Calvet, and E. Mougin, 2008: Analysis of leaf area index in the ECMWF land surface model and impact on latent heat and carbon fluxes: Application to West Africa, *J. Geophys. Res.*, **113**, D24117, doi:24110.21029/22007JD009370.

Jonas, T., C. Marty, and J. Magnusson, 2009: Estimating the snow water equivalent from snow depth measurements in the Swiss Alps, *J Hydrol*, **378**(1-2), 161-167, doi: DOI: 10.1016/j.jhydrol.2009.09.021.

Jordan, R., 1991: A one-dimensional temperature model for snow cover, *CRREL special Rep. 91-b, Cold Regions Research and Engeneering Laboratory, Hanover*, 49 pp.

Jung, T., and Coauthors, 2010: The ECMWF model climate: recent progress through improved physical parametrizations, *Quart. J. Roy. Meteor. Soc.*, **136**(650), 1145-1160, doi: 10.1002/qj.634.

Katz, R. W., and B. G. Brown, 1992: Extreme events in a changing climate: Variability is more important than averages, *Climatic Change*, **21**(3), 289-302, doi: 10.1007/bf00139728.

Kitaigorodski, S. A., and M. Yu.Z, 1970: On Theory of Open Ocean Active Layer, *Izvestiya Akademii Nauk Sssr, Fizika Atmosfery i Okeana* **6**, 178-188.

Koster, R. D., M. J. Suarez, and M. Heiser, 2000: Variance and Predictability of Precipitation at Seasonal-to-Interannual Timescales, *J. Hydrometeor.*, **1**(1), 26-46, doi: 10.1175/1525-7541(2000)001<0026:VAPOPA>2.0.CO;2.

Koster, R. D., and Coauthors, 2004: Regions of strong coupling between soil moisture and precipitation, *Science*, **305**(5687), 1138-1140, doi: 10.1126/science.1100217.

Koster, R. D., and Coauthors, 2006: GLACE: The Global Land–Atmosphere Coupling Experiment. Part I: Overview, *J. Hydrometeor.*, **7**(4), 590-610, doi: 10.1175/JHM510.1.

Kotlarski, S., F. Paul, and D. Jacob, 2010: Forcing a Distributed Glacier Mass Balance Model with the Regional Climate Model REMO. Part I: Climate Model Evaluation, *J. Climate*, **23**(6), 1589-1606, doi: doi:10.1175/2009JCLI2711.1.

Krinner, G., 2003: Impact of lakes and wetlands on boreal climate, *J. Geophys. Res.*, **108**(D16), 4520, doi:4510.1029/2002JD002597.

Laternser, M., and M. Schneebeli, 2003: Long-term snow climate trends of the Swiss Alps (1931–99), *Int. J. Climatol.*, **23**(7), 733-750, doi: 10.1002/joc.912.

Lawrence, D. M., and A. G. Slater, 2010: The contribution of snow condition trends to future ground climate, *Climate Dyn.*, **34**(7-8), 969-981, doi: 10.1007/s00382-009-0537-4.

Lehner, B., and P. Doll, 2004: Development and validation of a global database of lakes, reservoirs and wetlands, *J Hydrol*, **296**(1-4), 1-22.

Lesperance, M., J. E. Smerdon, and H. Beltrami, 2010: Propagation of linear surface air temperature trends into the terrestrial subsurface, *J. Geophys. Res.*, **115**, D21115, doi: 10.1029/2010JD014377.

Liston, G. E., 2004: Representing subgrid snow cover heterogeneities in regional and global models, *J. Climate*, **17**(6), 1381-1397.

Liu, X. D., and M. Yanai, 2002: Influence of Eurasian spring snow cover on Asian summer rainfall, *Int. J. Climatol.*, **22**(9), 1075-1089.

Livneh, B., Y. L. Xia, K. E. Mitchell, M. B. Ek, and D. P. Lettenmaier, 2010: Noah LSM Snow Model Diagnostics and Enhancements, *J. Hydrometeor.*, **11**(3), 721-738, doi: 10.1175/2009jhm1174.1.

Lofgren, B. M., 1997: Simulated effects of idealized Laurentian Great Lakes on regional and large-scale climate, *J. Climate*, **10**(11), 2847-2858.

Long, Z., W. Perrie, J. Gyakum, D. Caya, and R. Laprise, 2007: Northern lake impacts on local seasonal climate, *J. Hydrometeor.*, **8**(4), 881-896.

Lorenz, R., E. B. Jaeger, and S. I. Seneviratne, 2010: Persistence of heat waves and its link to soil moisture memory, *Geophys. Res. Lett.*, **37**(9), L09703, doi: 10.1029/2010gl042764.

Los, S. O., and Coauthors, 2000: A global 9-yr biophysical land surface dataset from NOAA AVHRR data, *J. Hydrometeor.*, **1**(2), 183-199.

Loth, B., H. F. Graf, and J. M. Oberhuber, 1993: Snow Cover Model for Global Climate Simulations, *J. Geophys. Res.*, **98**(D6), 10451-10464.

Loveland, T. R., B. C. Reed, J. F. Brown, D. O. Ohlen, Z. Zhu, L. Yang, and J. W. Merchant, 2000: Development of a global land cover characteristics database and IGBP DISCover from 1 km AVHRR data, *Int. J. Remote Sens.*, **21**(6-7), 1303-1330.

Lynch-Stieglitz, M., 1994: The Development and Validation of a Simple Snow Model for the Giss Gcm, *J. Climate*, **7**(12), 1842-1855.

Magnuson, J. J., and Coauthors, 2000: Historical trends in lake and river ice cover in the Northern Hemisphere, *Science*, **289**(5485), 1743-1746.

Marks, D., M. Reba, J. Pomeroy, T. Link, A. Winstral, G. Flerchinger, and K. Elder, 2008: Comparing Simulated and Measured Sensible and Latent Heat Fluxes over Snow under a Pine Canopy to Improve an Energy Balance Snowmelt Model, *J. Hydrometeor.*, **9**(6), 1506-1522.

Mironov, D., 2008: Parameterization of lakes in numerical weather prediction. Description of a lake modelCOSMO Technical Report, No. 11, Deutscher Wetterdienst, Offenbach am Main, Germany, 41 pp.

Mironov, D., G. Kirillin, E. Heise, S. Golosov, A. Terzhevik, and I. Zverev, 2003: Parameterization of lakes in numerical models for environmental applications. *Proc. 7th Workshop on Physical Processes in Natural Waters*, Russian Academy of Sciences, Petrozavodsk, Karelia, Russia, 135-143.

Mironov, D. V., S. Golosov, S. S. Zilitinkevich, K. D. Kreiman, and A. Terzhevik, 1991: Seasonal changes of temperature and mixing conditions in a lake. *Modelling Air–Lake Interaction: Physical Background*, Springer-Verlag, Ed.

Mironov, D. V., E. Heise, E. Kourzeneva, B. Ritter, N. Schneider, and A. Terzhevik, 2010: Implementation of the lake parameterisation scheme FLake into numerical weather prediction model COSMO, *Boreal Environ. Res.*, **15**, 218-230.

Mitchell, T. D., and P. D. Jones, 2005: An improved method of constructing a database of monthly climate observations and associated high-resolution grids, *Int. J. Climatol.*, **25**(6), 693-712.

Molders, N., H. Luijting, and K. Sassen, 2008: Use of atmospheric radiation measurement program data from Barrow, Alaska, for evaluation and development of snow-albedo parameterizations, *Meteorology and Atmospheric Physics*, **99**(3-4), 199-219.

Molini, A., G. G. Katul, and A. Porporato, 2011: Maximum discharge from snowmelt in a changing climate, *Geophys. Res. Lett.*, **38**(5), L05402, doi: 10.1029/2010gl046477.

Moody, E. G., M. D. King, C. B. Schaaf, D. K. Hall, and S. Platnick, 2007: Northern Hemisphere five-year average (2000-2004) spectral albedos of surfaces in the presence of snow: Statistics computed from Terra MODIS land products, *Remote Sens. Environ.*, **111**(2-3), 337-345.

Nijssen, B., and Coauthors, 2003: Simulation of high latitude hydrological processes in the Torne-Kalix basin: PILPS phase 2(e) - 2: Comparison of model results with observations, *Global Planet. Change*, **38**(1-2), 31-53.

NOAA/NESDIS/OSDPD/SSD, 2004, updated 2006: IMS daily Northern Hemisphere snow and ice analysis at 4 km and 24 km resolution. Boulder, CO: National Snow and Ice Data Center. Digital media. [Available online at: http://nsidc.org/data/g02156.html].

Orsolini, Y. J., and N. G. Kvamsto, 2009: Role of Eurasian snow cover in wintertime circulation: Decadal simulations forced with satellite observations, *J. Geophys. Res.*, **114**, D19108, doi: 10.1029/2009jd012253.

Pappenberger, F., H. L. Cloke, G. Balsamo, T. Ngo-Duc, and T. Oki, 2010: Global runoff routing with the hydrological component of the ECMWF NWP system, *Int. J. Climatol.*, **30**, 2155-2174, doi: 10.1002/joc.2028.

Pedersen, C. A., and J. G. Winther, 2005: Intercomparison and validation of snow albedo parameterization schemes in climate models, *Climate Dyn.*, **25**(4), 351-362.

Peings, Y., and H. Douville, 2010: Influence of the Eurasian snow cover on the Indian summer monsoon variability in observed climatologies and CMIP3 simulations, *Climate Dyn.*, **34**(5), 643-660, doi: 10.1007/s00382-009-0565-0.

Peings, Y., H. Douville, R. Alkama, and B. Decharme, 2010: Snow contribution to springtime atmospheric predictability over the second half of the twentieth century, *Climate Dyn.*, 1-20, doi: 10.1007/s00382-010-0884-1.

Qu, X., and A. Hall, 2006: Assessing snow albedo feedback in simulated climate change, *J. Climate*, **19**(11), 2617-2630, doi: 10.1175/JCLI3750.1.

Qu, X., and A. Hall, 2007: What controls the strength of snow-albedo feedback?, *J. Climate*, **20**(15), 3971-3981, doi: 10.1175/Jcli4186.1.

Räisänen, J., 2002: CO2-Induced Changes in Interannual Temperature and Precipitation Variability in 19 CMIP2 Experiments, *J. Climate*, **15**(17), 2395-2411, doi: 10.1175/1520-0442(2002)015<2395:CICIIT>2.0.CO;2.

Ramsay, B. H., 1998: The interactive multisensor snow and ice mapping system, *Hydrol. Processes*, **12**(10-11), 1537-1546.

Rangwala, I., J. R. Miller, G. L. Russell, and M. Xu, 2010: Using a global climate model to evaluate the influences of water vapor, snow cover and atmospheric aerosol on warming in the Tibetan Plateau during the twenty-first century, *Climate Dyn.*, **34**(6), 859-872, doi: 10.1007/s00382-009-0564-1.

Rauscher, S. A., E. Coppola, C. Piani, and F. Giorgi, 2010: Resolution effects on regional climate model simulations of seasonal precipitation over Europe, *Climate Dyn.*, **35**(4), 685-711, doi: 10.1007/s00382-009-0607-7.

Robock, A., M. Q. Mu, K. Vinnikov, and D. Robinson, 2003: Land surface conditions over Eurasia and Indian summer monsoon rainfall, *J. Geophys. Res.*, **108**(D4), -, doi: 10.1029/2002jd002286.

Roesch, A., 2006: Evaluation of surface albedo and snow cover in AR4 coupled climate models, *J. Geophys. Res.*, **111**(D15), D15111, doi: 10.1029/2005jd006473.

Roesch, A., and E. Roeckner, 2006: Assessment of snow cover and surface albedo in the ECHAM5 general circulation model, *J. Climate*, **19**(16), 3828-3843.

Roman, M. O., and Coauthors, 2009: The MODIS (Collection V005) BRDF/albedo product: Assessment of spatial representativeness over forested landscapes, *Remote Sens. Environ.*, **113**(11), 2476-2498.

Rooney, G. G., and I. D. Jones, 2010: Coupling the 1-D lake model FLake to the community land-surface model JULES, *Boreal Environ. Res.*, **15**(5), 501-512.

Rouse, W. R., and Coauthors, 2005: The role of northern lakes in a regional energy balance, *J. Hydrometeor.*, **6**(3), 291-305.

Rutter, N., D. Cline, and L. Li, 2008: Evaluation of the NOHRSC snow model (NSM) in a one-dimensional mode, *J. Hydrometeor.*, **9**(4), 695-711.

Rutter, N., and Coauthors, 2009: Evaluation of forest snow processes models (SnowMIP2), *J. Geophys. Res.*, **114**, D06111, doi: 10.1029/2008JD011063.

Salgado, R., and P. Le Moigne, 2010: Coupling of the FLake model to the Surfex externalized surface model, *Boreal Environ. Res.*, **15**(2), 231-244.

Salomon, J. G., C. B. Schaaf, A. H. Strahler, F. Gao, and Y. F. Jin, 2006: Validation of the MODIS Bidirectional Reflectance Distribution Function and Albedo retrievals using combined observations from the Aqua and Terra platforms, *Ieee T. Geosci. Remote*, **44**(6), 1555-1565.

Schar, C., D. Luthi, U. Beyerle, and E. Heise, 1999: The soil-precipitation feedback: A process study with a regional climate model, *J. Climate*, **12**(3), 722-741, doi: 10.1175/1520-0442(1999)012<0722:TSPFAP>2.0.CO;2.

Schar, C., P. L. Vidale, D. Luthi, C. Frei, C. Haberli, M. A. Liniger, and C. Appenzeller, 2004: The role of increasing temperature variability in European summer heatwaves, *Nature*, **427**(6972), 332-336.

Schär, C., L. Vasilina, F. Pertziger, and S. Dirren, 2004: Seasonal Runoff Forecasting Using Precipitation from Meteorological Data Assimilation Systems, *J. Hydrometeor.*, **5**(5), 959-973, doi: doi:10.1175/1525-7541(2004)005<0959:SRFUPF>2.0.CO;2.

Seager, R., Y. Kushnir, J. Nakamura, M. Ting, and N. Naik, 2010: Northern Hemisphere winter snow anomalies: ENSO, NAO and the winter of 2009/10, *Geophys. Res. Lett.*, **37**, L14703, doi: 10.1029/2010gl043830.

Sellers, P. J., S. O. Los, C. J. Tucker, C. O. Justice, D. A. Dazlich, G. J. Collatz, and D. A. Randall, 1996: A revised land surface parameterization (SiB2) for atmospheric GCMs .2. The generation of global fields of terrestrial biophysical parameters from satellite data, *J. Climate*, **9**(4), 706-737.

Seneviratne, S. I., P. Viterbo, D. Luthi, and C. Schar, 2004: Inferring changes in terrestrial water storage using ERA-40 reanalysis data: The Mississippi River basin, *J. Climate*, **17**(11), 2039-2057.

Seneviratne, S. I., D. Luthi, M. Litschi, and C. Schar, 2006: Land-atmosphere coupling and climate change in Europe, *Nature*, **443**(7108), 205-209, doi: 10.1038/nature05095.

Sheffield, J., and Coauthors, 2003: Snow process modeling in the North American Land Data Assimilation System (NLDAS): 1. Evaluation of model-simulated snow cover extent, *J. Geophys. Res.*, **108**(D22), 8849, doi:8810.1029/2002JD003274.

Shuai, Y. M., C. B. Schaaf, A. H. Strahler, J. C. Liu, and Z. T. Jiao, 2008: Quality assessment of BRDF/albedo retrievals in MODIS operational system, *Geophys. Res. Lett.*, **35**(5), L05407, doi:05410.01029/02007GL032568.

Slater, A. G., A. J. Pitman, and C. E. Desborough, 1998: The validation of a snow parameterization designed for use in general circulation models, *Int. J. Climatol.*, **18**(6), 595-617.

Sobolowski, S., G. Gong, and M. F. Ting, 2010: Modeled Climate State and Dynamic Responses to Anomalous North American Snow Cover, *J. Climate*, **23**(3), 785-799, doi: 10.1175/2009jcli3219.1.

Stieglitz, M., and J. E. Smerdon, 2007: Characterizing land-atmosphere coupling and the implications for subsurface thermodynamics, *J. Climate*, **20**(1), 21-37, doi: 10.1175/Jcli3982.1.

Stroeve, J., J. E. Box, F. Gao, S. L. Liang, A. Nolin, and C. Schaaf, 2005: Accuracy assessment of the MODIS 16-day albedo product for snow: comparisons with Greenland in situ measurements, *Remote Sens. Environ.*, **94**(1), 46-60.

Sun, S. F., J. M. Jin, and Y. K. Xue, 1999: A simple snow-atmosphere-soil transfer model, *J. Geophys. Res.*, **104**(D16), 19587-19597.

Sverdrup, H. U., 1935: Scientific Results of the Norwegian-Swedish Spitsbergen Expedition in 1934. Part IV. The ablation on Ischsen's Plateau and on the 14th of July Glacier., *Geogr. Ann.*, **17**, 145-218.

Tamsalu, R., and K. Myrberg, 1998: A theoretical and experimental study of the self-similarity concept, *MERI, Report Series of the Finnish Institute of Marine Research*, **37**, 3-13.

Tribbeck, M. J., R. J. Gurney, and E. M. Morris, 2006: The radiative effect of a fir canopy on a snowpack, *J. Hydrometeor.*, **7**(5), 880-895.

Uppala, S. M., and Coauthors, 2005: The ERA-40 re-analysis, *Quart. J. Roy. Meteor. Soc.*, **131**(612), 2961-3012, doi: 10.1256/qj.04.176.

Van den Hurk, B., and P. Viterbo, 2003: The Torne-Kalix PILPS 2(e) experiment as a test bed for modifications to the ECMWF land surface scheme, *Global Planet. Change*, **38**(1-2), 165-173.

Van den Hurk, B., P. Viterbo, A. C. M. Beljaars, and A. K. Betts, 2000: Offline validation of the ERA40 surface scheme, *ECMWF Tech. Memo.*, **295**, 42 pp.

Verseghy, D. L., 1991: Class-a Canadian Land Surface Scheme for Gcms .1. Soil Model, *Int. J. Climatol.*, **11**(2), 111-133.

Viterbo, P., and A. C. M. Beljaars, 1995: An Improved Land-Surface Parameterization Scheme in the Ecmwf Model and Its Validation, *J. Climate*, **8**(11), 2716-2748.

Viterbo, P., and A. K. Betts, 1999: Impact on ECMWF forecasts of changes to the albedo of the boreal forests in the presence of snow, *J. Geophys. Res.*, **104**(D22), 27803-27810.

Viterbo, P., A. Beljaars, J. F. Mahfouf, and J. Teixeira, 1999: The representation of soil moisture freezing and its impact on the stable boundary layer, *Quart. J. Roy. Meteor. Soc.*, **125**(559), 2401-2426, doi: 10.1002/qj.49712555904.

Von Storch, H., and F. W. Zwiers, 1999: *Statistical Analysis in Climate Research.* Cambrige University Press, 484 pp.

Wang, Z., and X. B. Zeng, 2010: Evaluation of Snow Albedo in Land Models for Weather and Climate Studies, *J Appl. Meteorol. Clim.*, **49**(3), 363-380, doi: 10.1175/2009jamc2134.1.

Wang, Z., X. Zeng, and M. Decker, 2010: Improving snow processes in the Noah land model, *J. Geophys. Res.*, **115**, D20108, doi: 10.1029/2009JD013761

Wild, M., A. Ohmura, H. Gilgen, and E. Roeckner, 1995: Validation of General-Circulation Model Radiative Fluxes Using Surface Observations, *J. Climate*, **8**(5), 1309-1324.

Wilks, D., S., 2006: *Statistical Methods in the Atmospheric Sciences.* Academic Press, 648 pp.

Williams, J., 1975: The Influence of Snowcover on the Atmospheric Circulation and Its Role in Climatic Change: An Analysis Based on Results from the NCAR Global Circulation Model, *J. Appl. Meteor.*, **14**(2), 137-152, doi: 10.1175/1520-0450(1975)014<0137:TIOSOT>2.0.CO;2.

Yang, Z. L., R. E. Dickinson, A. Robock, and K. Y. Vinnikov, 1997: Validation of the snow submodel of the biosphere-atmosphere transfer scheme with Russian snow cover and meteorological observational data, *J. Climate*, **10**(2), 353-373.

Zhou, L., and Coauthors, 2003: Comparison of seasonal and spatial variations of albedos from Moderate-Resolution Imaging Spectroradiometer (MODIS) and Common Land Model, *J. Geophys. Res.*, **108**(D15), 4488, doi: 10.1029/2002jd003326.

Zilitinkevich, S. S., and D. V. Mironov, 1992: Theoretical-Model of the Thermocline in a Fresh-Water Basin, *J Phys Oceanogr*, **22**(9), 988-996.